Alonso Madrigal Sánchez

Multi-scale modelling of waves propagation on the Norwegian Coast

Master of Science in
Marine and Coastal Systems

Work performed under the supervision of:
Hans Bihs
José Jacob

UNIVERSIDADE DO ALGARVE
FACULDADE DE CIÊNCIAS E TECNOLOGIA
2018

UNIVERSIDADE DO ALGARVE
FACULDADE DE CIÊNCIAS E TECNOLOGIA
2018

Multi-scale modelling of waves propagation on the Norwegian Coast

A Thesis
submitted to the Faculty of Sciences and Technology
at the University of Algarve
in partial fulfilment of the requirements for the degree of

Master of Science in Marine and Coastal Systems

Supervisors:
Hans Bihs
José Jacob

Candidate:
Alonso Madrigal Sánchez

Multi-scale modelling of waves propagation on the Norwegian Coast.

Declaration of authorship of work

I declare to be the author of this work, which is original and unpublished. Authors and works consulted are duly cited in the text and are included in the list of references.

Abstract

Fjords coastlines are attributed to glaciers as the main agent of erosion. Thus, fjords are characterised by an irregular coastline configuration and rapid changes in their deep and steep slopes. These features generate a unique behaviour on the ocean wave propagation and on the water hydrodynamics. Norwegian coastline has environmental conditions to support diverse aquaculture developments along the coast. Therefore, aquaculture in Norway is considered a growing field with an enormous potential especially in offshore locations. The development of numerical tools, such as wave models, will produce a huge improvement on the different technologies used nowadays. To achieve this huge engineering challenge a simulation of the ocean waves reaching the Norwegian fjords will be analysed using coupled numerical models. This study proposed a combined use of two different numerical models, cascade of wave models, to utilise the strengths of the models while reducing their disadvantages. For example, spectral wave model such as STWAVE is fast in open ocean but not able to capture the diffraction phenomenon, shallow water model such as REEF3D::SFLOW is able to capture most wave transformation phenomenon but limited by water depth; Computational Fluid Dynamic (CFD) model such as REEF3D::CFD captures three-dimensional details of water wave but is computationally costly. The results obtained from the large domain and coarse grid model will serve as the input to the next region with middle resolution and a refined grid size. This is carried on until the results for the area of interest are obtained. A first step validating the reliability of REEF3D::SFLOW was carried out through the use of a submerged bar case. During the process of testing the feasibility of the cascade of wave models methodology, different models were evaluated for specific domain and topography. As a result, only two models were applied on the final simulation: STWAVE and REEF3D::CFD. Thus, the combined methodology resulted useful to obtain a rough estimation of the wave propagation and transformation outside the fjords and its potential effects over Flatøya fish farm development. It can be also an important input for their fish cage design.

Keywords: Norwegian coast; numerical models; 3D simulations; wave model validation

Resumo

As zonas costeiras dos fiordes são moldadas pelos glaciares como o principal agente de erosão. Assim, os fiordes são caracterizados por uma configuração irregular da sua linha de costa e por variações abruptas nas suas vertentes profundas e íngremes. Estas características são responsáveis por um comportamento único na propagação de ondas oceânicas e na hidrodinâmica das suas águas. O litoral norueguês tem condições ambientais que permitem apoiar o desenvolvimento de diversas aquiculturas diversificadas ao longo da costa. Por esse motivo, a aquicultura na Noruega é considerada uma área em crescimento e com um enorme potencial, especialmente em locais ao largo, próximo das suas costas. O desenvolvimento de ferramentas numéricas, como os modelos de ondas, é responsável pela enorme melhoria nas diferentes tecnologias usadas hoje em dia. Para alcançar este enorme desafio colocado à engenharia, é analisada a simulação das ondas que atingem e se propagam nos fiordes noruegueses usando modelos numéricos acoplados. Neste estudo propôs-se a utilização combinada de dois modelos numéricos diferentes, ou cascata de modelos de ondas, para aproveitar as vantagens dos modelos e reduzir as suas desvantagens. Por exemplo, um modelo espectral de ondas, como o STWAVE, é rápido em oceano aberto mas não consegue resolver o fenómeno da difração, um modelo de águas pouco profundas, como o REEF3D::SFLOW, é capaz de reproduzir a maioria dos fenómenos de transformação de ondas, mas está limitado pela profundidade da água. Um modelo de Dinâmica de Fluidos Computacional (CFD), como o REEF3D::CFD, captura detalhes tridimensionais das ondas de superfície, mas é dispendioso em termos computacionais. Assim, modelos diferentes devem ser avaliados em domínios e topografias específicos. Os resultados obtidos a partir do modelo aplicado ao domínio com dimensões maiores e malha menos refinada servirão como dados de entrada para a região seguinte com resolução intermediária e uma malha mais refinada. Este processo é executado até que se obtenham os resultados para a área de interesse. Um primeiro passo para validar o modelo REEF3D :: SFLOW e aferir a exatidão e confiança na sua aplicação foi realizado através do uso do caso de uma barra submersa realizado em laboratório. No estudo da viabilidade da metodologia de cascata de modelos de ondas foram avaliados diferentes modelos em domínios e topografia específicos. Como resultado deste estudo, apenas foram aplicados dois modelos na simulao final: STWAVE e REEF3D

:: CFD. Assim, a metodologia combinada mostrou ser útil para obter uma estimativa aproximada da propagação e transformação das ondas fora dos fiordes e seus efeitos potenciais sobre o desenvolvimento da piscicultura de Flatoya. Os resultados obtidos também podem ser bastante úteis na concepção das gaiolas flutuantes para o peixe.

Para mis familias

Madrigal Sánchez
Madrigal Rick
Madrigal Preciado

Muchas gracias por todo el apoyo
y el amor desde la distancia.

Acknowledgments

This thesis work is done to accomplish the requirement for a graduate student in the two years of Master program: Marine and Coastal Systems (MaCS- SIMCO).

First, I would like to thank my main supervisor Hans Bihs for giving me the opportunity to be part of this project. I would like to thank my co-supervisors Arun Kamath and Professor José Jacob for their advice and guidance. An especially thank to my co-supervisor Weizhi Wang for his guidance and patience in dealing with all my doubts during the time of this project. Also big thank to him for all his assistance and the time to correct this document. Gratitude to Onno Musch and Athul Sasikumar from Norconsult, for their advice and to allow me to use the data needed to accomplish this project. I would like to extend my gratitude to all my professors part of the MaCS program within the Universidade do Algarve. Finally, the last but not the less, I would like to thank to all my MaCS classmates for the good times and support during the last two years. [ADA] [MH]

Contents

List of Figures

List of Tables

List of Symbols

a	Wave amplitude
C	Phase velocity
C_0, A_{ij}, B_{ij}	Coefficients
CFL	Time-step
c_x, c_y	Velocities on x and y axis
c_g	Group velocity
d	Still water depth
$\vec{D}_{ij}$	Mean velocity deformation tensor
D/Dt	Total derivative
dx	Grid cell size
g	Acceleration due to gravity
H	Wave height
He	Total energy head
i, j, k	vectors along the x, y and z-direction
k	Wave number
$\vec{K}$	Kinetic energy of the turbulence fluctuations
L	Spatial discretization
N	Spectrum
P	Pressure
P_k	Production rate

q	Unit discharge
S	Net effect of sources
$\|S\|$	Mean strain rate
S_{nl}	Non-linear interactions / Non-linear wave-wave interactions
S_{tot}	Net source function
T	Wave period
t	time
u	Velocity averaged over time / Horizontal velocity
v	Kinematic viscosity
w	Vertical velocity
z	Elevation of a point in the flow field
Z	Bed elevation
	Greek symbols
α	Wave direction
γ	Relative wave height
δ	Direction of the current
δ_{ij}	Kronecker delta
ε	Wave steepness
η	Free surface elevation
θ	Wave angle
θ_s	Angle of free surface streamline
Λ	Longitude
λ	Wavelength
μ	Wave ray
ρ	Fluid density

σ	Space
c_σ	Propagation velocity
Φ	Velocity potential
ϕ	Level set function
φ	Latitude
ω	Angular frequency

Chapter 1

Introduction

1.1 Norwegian Coastline

The Norwegian landscape has unique features carved over very long-time spans as a consequence of geological processes. Its dramatic landscape was mainly formed by surface processes occurred during the Quaternary period [24]. Additional processes such as global and regional environmental changes over the last 2-3 million years, had produced advance and retreat effects on glaciers presence in Norway coast. Thus, these processes have as a result geological formations well known as fjords.
Fjord's coastlines are attributed to the constant action of ice sheets and glaciers, thus, they are considered one of the most powerful agents of erosion. Therefore, as Fig. 1.1 (a) shows, fjords are geomorphological features with an unique configuration, including U-shape valleys and very steep slopes on the shoreline. Fjords are also narrow and deep inlets characterised by an irregular coastline configuration and rapid changes in depth [50] [66]. These features generate an unique behaviour on the ocean wave propagation and transformation, as well as, on the water hydrodynamics occurring within the fjords. Interest on understanding the fjords dynamics has been considered since the World War II [59].
Fjords are considered a transitional water system from the terrestrial to the marine environment [32]. They can be also categorised as coastal embayments and semi-closed water systems with a seasonality water circulation pattern isolated from the open ocean most of the time and a type of estuary too [23][33]. Fjords are typically with entrance sills separating their deep waters from the adjacent coastal waters which restrict water circulation as it is showen in Fig. 1.1 (b). Moreover, fjords as a semi-closed water system with restricted water circulation, present a strong stratification on the water column [66][23] [73] [40] [12]. Thus, it results in a high time residency of the water masses within fjords, producing increments on pollutants and increasing the concentration of organic matter. As a result, these systems can be easily affected

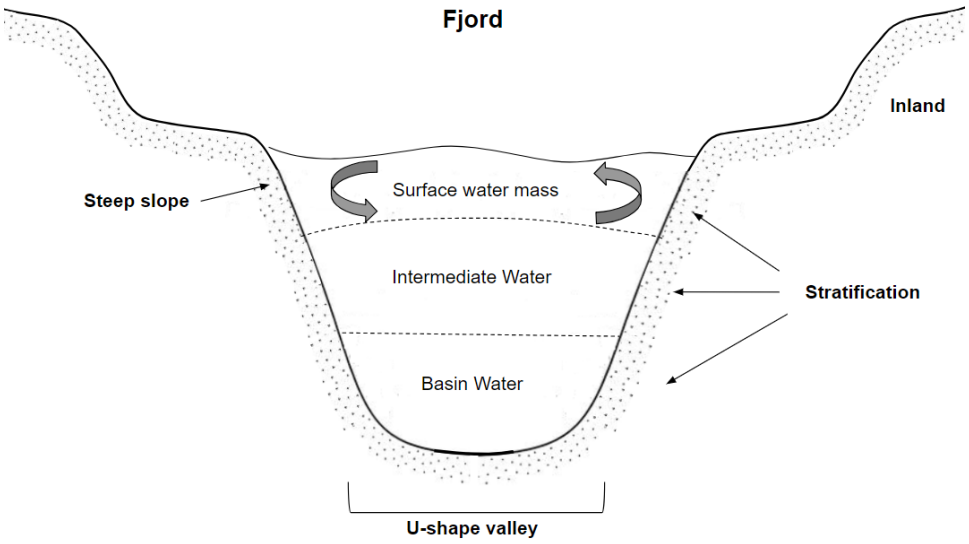

(a)

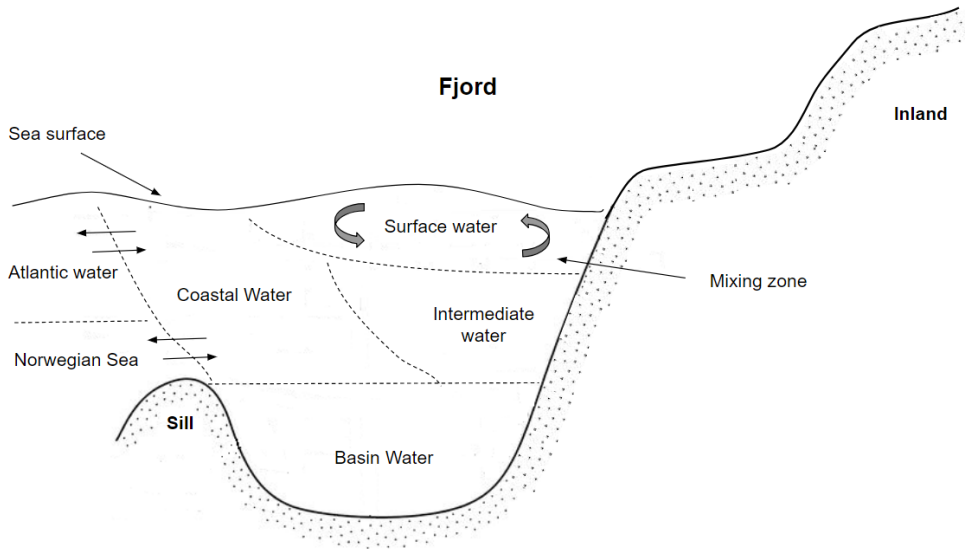

(b)

Figure 1.1: Fjord scheme: (a) Cross section of the inner part a fjord with stratification patterns; (b) Fjord entrance configuration and the different water masses. Adapted from [66]

by anthropogenic activities such as run-off from urban, industrial and agricultural activities [23] [33].
Marine aquaculture industry has expanded significantly and is facing an intensification of their activities during the last decades. The rough ocean conditions in the offshore Norwegian coastline, pushed marine aquaculture industry to be mainly located inside the fjords. As a consequence of the massive production and the amount of waste from the industry, aquaculture is having a huge ecological impact on those fragile environments [6]. Some studies have shown that the most important factor to consider while determining the level of environmental affection coming from aquaculture, is the fish farm locations rather than the fish production itself. Therefore, they reported that the best location of the fish farms was found to be near the mouth of the fjord where the water exchange with the coast is the largest [63].
In accordance with the Directorate of Fisheries, (http://www.fiskeridir.no/) Norwegian fish farms have produced in average 1,000,000 tons per year during the last decade. Aquaculture industry passed from producing 50,000 ton in 1985 to 600,000 in 2006, equivalent to 1.7 billion Euro. Information reported highlighted the economical relevance of fish farm industry in the national economy.
Nowadays, Norwegian authorities are pushing aquaculture industry to place their fish farms offshore the fjords to reduce the pollution within the fjords. Those new developments will deal with a high frequency of extreme ocean conditions never faced on the industry before. Therefore, detailed studies of the wave conditions surrounding those new developments have a high relevance.

1.2 Numerical Wave Models

Wave predictions were for the first time studied during the World War II by Sverdrup and Munk [68] [49]. In the last 80 years diverse studies understanding the wave propagation and transformation had been developed. On the early 50's, Pierson [54] introduced the concept of wave spectrum, followed by the development of the first generation of numerical wave models in 1958 [53]. The advances on numerical modelling has been facing great improvements in developments as well as periods of consolidation of those new models.
During the last decades numerical models have been raising as one of the most powerful tools to study sea surface waves. However, the random nature of sea surface waves makes it one of the most complicated phenomena to be studied [70]. Sverdrup and Munk's wave prediction technique, was based only on the statistical values of significant wave height [70]. In the beginning these models were only used in predictions with coarse grids, applicable for deep waters. Therefore, accurate modelling of wave propagation in coastal regions with fine grids became essencial [70][72].

Accurate numerical simulations provide a great understanding of the physical ocean processes. Between the different ocean characteristics, nonlinear interactions are considered one of the most solid piece of information in wave simulations [16]. Numerical models proved their importance as an engineering tool in the planning and construction of coastal infrastructure, by forescasting and hindcasting ocean and meteorological conditions. On the other hand, during the study of waves interacting with the coastline and coastal engineering structures, numerical models are a useful tool helping to understand sediment transport processes and to identify regions with an amount of wave energy that can be harnessed. The identification of regions with high wave energy potential could lead to the development of renewable wave energy field [70].

Caetano and Innocentini in 2003 [14], compiled and briefly described the three types of numerical models applied to ocean wave simulations. These models are classified in first, second and third generation. In first generation models, also known as decoupled models, a two-dimensional wave spectrum (frequency-direction) evolves when the wind forcing reaches a saturation level defined by an universal equilibrium distribution. Each spectral component propagates with its own group velocity; thus, they do not consider non-linear interactions among distinct frequencies. In second-generation models, the nonlinear interactions are parameterised to a certain spectral distribution of energy. These are known as parametrical models, where the swell is explicitly represented by the spectrum and the wind sea by parameters[14]. Previous experiences with wave interactions and a high complexity in bathymetric configurations pushed the research community to develop a new third generation of numerical model with non-linear interactions [70] [72]. Since then, many other wave models initially based on the WAM model (WAve Modeling), have appeared, being the most notable SWAN and WAVEWATCH III [11][26].

This master thesis attempts to validate the combined use of two different wave models. Spectral wave models, such as SWAN, are widely applied to simulated wave propagation in different ocean conditions. However, spectral wave models cannot account accurately for diffraction and sudden changes in water depth. Additionally, a wave model solving the Non-Hydrostatic Shallow Water Equations (NHSWEs) was proposed for this study. These wave model types have limitations from intermediate to shallow waters. Thus, a third wave model was proposed, CFD model from the open source REEF3D [8] [37]. As Wang et al., (2017) [72] mentioned, CFD models are becoming an alternative to modelling in coastal engineering. However, its high demand on computational resource produce a limitated use due to time-consuming and high cost [72].

Each of the models proposed (SWAN/STWAVE, REEF3D::SFLOW and REEF3D::CFD) has advantages and disadvantages, thus, a combined use of them could provide a great understanding of wave physical processes such as refraction, shoaling,

diffraction and reflection effects. This is a methodology known as a 'Cascade of wave models', it will provide a better understanding of the unique conditions on the Norwegian coast.

1.3 Objectives of the study

The approach of this study will help, through different simulations, to understand the wave propagation and transformation on the Norwegian coastline characterised by fjords configuration. Accurate information regarding the behaviour of the waves interacting on the Norwegian shoreline can be useful to Norwegian aquaculture industry as valuable data to contribute to the locations and design of the fish cage. Therefore, the objective of this study is to simulate the wave propagation and transformation in a Norwegian fjord by using a combination of two different models, the spectral model STWAVE, and the open source REEF3::CFD approach wave model. Limitations on the different numerical models guides us to apply a cascade of wave models methodology combining the above mentioned wave models. Additionally, the results obtained from this projects are planned to be applied on a fish farm located on Flatøya on the North West of Trondheim.

Chapter 2

Numerical Models

Engineering problems can be solved by two different approaches: through the use of experimental models; and with mathematical models. Within the use of mathematical models is possible to find the applying numerical models [43]. Thereby, due to the characteristic geomorphology of the Norwegian coast previously mentioned, numerical models are considered the most suitable approach to be applied during this project. This chapter attends to briefly describe the basic concepts of the wave models suggested for this project such as STWAVE, SFLOW and CFD. The two last wave models are part of the open source REEF3D.

2.1 Spectral Wave Models

The need of a better resolution on the wave models in coast regions lead to the development of the third generation numerical models [26]. As mentioned on section 1.2, since the first wave model - Sea Waves Modeling Project [26] - was developed on the 80's, different third generation numerical wave models have been developed to study the wave spectrum evolution [26]. Within all those wave models based on different theories, a classification of the third generation of numerical models considered two types of wave models:

- Phase resolving wave models describe the sea surface as a function of space and time. This type of models are taking into account physical phenomena such as refraction, diffraction and quadruplets wave-wave interactions. Additionally, dissipation effects such as bottom friction and breaking effects induced by changes on depth are also considered. This family of models has a subclassification in accordance with the different equations applied: Hamiltonians equations [47]; Boussinesq equations [16][17][9][39][44]; and, Mild-slope equation [7]. One important aspect while applying those type of wave models is that they do not consider wind as a wave generation process [4] [52].

- Phase averaging models are used to represent the sea surface through a spectral description for applications on large scale. In these wave models two methods can be applied: Lagrangian approach; and Eulerian approach. On the first method, waves are propagated independently from deep to shallow waters by transporting the wave energy along wave rays. Lagrangian models are numerically inefficient when non-linear effects such as wave breaking or wave-wave interactions are considered. Second approach, Eulerian method formulated the wave transformation on a grid and every grid point has the information of the whole spectrum. Reason why it is a more efficient approach than Lagrangian method. Eulerian method used to simulate wind waves is also efficient dealing with wave generation, dissipation and non-linear interaction processes. However, disadvantages of Eulerian method in coastal waters are due to the absence of diffraction and the use of linear wave theory for wave propagation. Limitations due to diffraction effects lies in the fact that the study area should be few wavelengths away from obstacles with rapid changes on depth or vertical walls. Contrary to the phase resolving models, Eulerian methods do not compute all the physical processes for finite-depth waters, therefore, dissipation effects such as bottom friction and breaking effects induced by changes on depth are not well represented.

Limitations on the third generation wave prediction model WAM and the parametrization of the non-linear interactions S_{nl} discrete interaction approximation (DIA) from Hasselmann [30], triggered the development of spectral wave models such as SWAN [26][11][10][69] and STWAVE [25] [46]. DIA resulted a great improvement successfully describing the essential features of a developing wave spectrum with quadruplets wave-wave interactions [11][56]. However, DIA has some limitations, as many other theories have, with poor approximation when the model is dealing with long-crested waves and with some frequency resolutions. Unfortunately, it is a fundamental limitation affecting many third generation wave models.
Another feature of the third generation of wave models is that, they might be applied using two types of schemes regarding the grid size. Explicit scheme is used on WAM model with an efficiency solving large computational problems such as tsunamis and the subsequent flooding events [74]. It is more suitable for shallow water due to the small grid sizes applied and a high resolution, however, due to its fine grid size it cannot be applied on oceanic scales. As a contrast, SWAN and STWAVE employs an implicit schemes with coarse grid size. This coarse grid offer less resolution of the spectral in comparison with the explicit scheme, but with less cost on the shallow water, providing realistic estimates of the most relevant wave parameters. They can also be divided into generation models such as WAM [26], and transformation models such as SWAN and STWAVE [25]. Therefore, SWAN does not represent well the

wave propagation and transformation near the shoreline [11].
Models as SWAN, based on the phase averaging and using the Eulerian approach, have an advantage efficiently representing the effects of spatial propagation and all physical processes of generation, shoaling and refraction due to bottom variations, dissipation by breaking and whitecapping, and nonlinear wave-wave interactions [69][11][56][57]. On the particular case of SWAN considered one of the most used wave models on coastal waters, it gives good results in terms of predicting energy spectrum and significant wave height, however, its applications are limited to coastal regions [15]. Thus, SWAN also can simulate the wave transformation from deep to shallow waters. It might be run as either stationary or non-stationary and using either Cartesian or spherical coordinates [11][56].
As a comparison STWAVE is a simple steady-state, finite difference, spectral model based on the wave action balance equation, with a high similitude with the more complex SWAN model [25]. It is a simpler model developed by US Army Corps of Engineers [64] that takes into account the main coastal processes: depth-induced wave refraction and shoaling, current-induced refraction and shoaling, depth-induced wave breaking, diffraction, parametric wave growth because of wind input, and wave-wave interaction and whitecapping that redistribute and dissipate energy in a growing wave field [25].
STWAVE has the aim to provide an easy-to-apply, flexible, and robust model for nearshore wind-wave growth and propagation. It might also deal with wave-current interaction and steepness-induced wave breaking. In addition to its simplicity, Gonçalves et al. (2012) [25] reported that the main advantage of STWAVE over SWAN is that almost no boundary conditions effects are introduced. This is the result of a zero flux condition on the lateral boundaries that provides better boundary conditions.
The STWAVE model uses the governing equation for steady-state conservation of spectral wave action along a wave ray:

$$(C_g)\,\frac{\partial}{\partial x_i}\left(CC_g cos(\mu-\alpha)\right)N = \frac{S}{\sigma} \tag{2.1}$$

where, C represents the absolute phase velocity defined as:

$$C = C_r + U\cos(\delta-\alpha) \tag{2.2}$$

with the relative phase velocity defined using the standard formulation $C_r = \sigma/k$, δ is the direction of the current relative to the x-axis and α is the wave direction relative to the same x-axis. The absolute group velocity vector defines the direction of the wave ray (μ):

$$\mu = \tan^{-1}\left[\frac{C_{gr}\sin\alpha + U\sin\delta}{C_{gr}\cos\alpha + U\cos\delta}\right] \tag{2.3}$$

However, due to the restriction on time and the amount of simulations on different wave models required to accomplish the objectives of this study, STWAVE lies as the most suitable option for this study to get accurate and reliable wave data from open ocean.
As aforementioned, as many of the third generation wave models, STWAVE presents some limitations nearshore due to physical phenomena like wave diffraction which can not be well represented [55]. Due to the necessity of detailing the full wave propagation in the fjords a high-resolution phase-resolved numerical model is needed to reflect detailed wave phenomena in the fjords [72].

2.1.1 Wave Action Balance Equation

The Eulerian form of the balance equation describes the evolution of the wave spectrum in time, geographical and spectral spaces by

$$\frac{DN}{Dt} = \frac{S}{\sigma} \tag{2.4}$$

where, D/Dt represents the total derivative and S represents the net effect of sources and sinks for the spectrum N. The left-hand also represents their kinematic part.
The evolution of the wave spectrum is described by the spectral action balance equation Eq. [2.5], for Cartesian coordinates, [29]. This equation represents the effects of spatial propagation, refraction, shoaling, generation, dissipation and nonlinear wave-wave interactions.

$$\frac{\partial N}{\partial t} + \frac{\partial c_x N}{\partial x} + \frac{\partial c_y N}{\partial y} + \frac{\partial c_\sigma N}{\partial \sigma} + \frac{\partial c_\theta N}{\partial \theta} = \frac{S_{tot}}{\sigma} \tag{2.5}$$

where, left-hand side is identified as the kinematic part of the equation. The first term represents the local rate of change of action density in time. The second and third term represent propagation of action in geographical space (with propagation velocities c_x and c_y in x and y space, respectively). The fourth term represents shifting of the relative frequency due to variations in depths and currents (with propagation velocity c_σ in σ space). The fifth term represents depth and current induced refraction (with propagation velocity c_θ in θ space). The term $S[= S(cr, \theta)]$ at the right-hand side of the action balance equation is the source term in terms of energy density, representing the effects of generation, dissipation, and nonlinear wave-wave interactions.

$$c_x = c_{g,x} + U_x, c_y = c_{g,y} + U_y \tag{2.6}$$

where, c_g is the group velocity component for x and y directions.
Regarding ocean large scales using spherical or curvilinear coordinate, the Eq. [2.5] takes the form given by Eq. [2.7]

$$\frac{\partial N}{\partial t} + \frac{\partial c_\Lambda N}{\partial \Lambda} + cos^{-1}\varphi \frac{\partial c_\varphi cos\varphi N}{\partial \varphi} + \frac{\partial c_\sigma N}{\partial \sigma} + \frac{\partial c_\theta N}{\partial \theta} = \frac{S_{tot}}{\sigma} \tag{2.7}$$

with longitude, Λ and latitude φ.
In deep waters, the net source function S_{tot} contains normally three parts, a wind-wave interaction term S_{in}, a non-linear wave-wave interactions term S_{nl} and a dissipation (white-capping) term S_{ds}. In some cases linear wind-input S_{ln} can also be considered. In shallow waters, additional processes have to be considered, most notably wave-bottom interactions S_{bot}. In extremely shallow water, depth-induced breaking S_{db} and triad wave-wave interactions S_{tr} become also important. So, the net source function is defined by

$$S_{tot} = S_{ln} + S_{in} + S_{nl} + S_{ds} + S_{bot} + S_{db} + S_{tr} \tag{2.8}$$

As mentioned above, on the absence of currents SWAN applies the energy balance equation instead of the action balance equation [11].
I must be note that the normal symbol used to represent longitude is λ. However, due to wavelength is also expressed with the same symbol, thus, in this document longitude will be found as Λ.

2.2 Computational Fluid Dynamics (CFD)

Computational Fluid Dynamics (CFD) models are becoming the new alternative for modelling in coastal engineering, due to its capability to incorporate most of the complexity in the flow field with few assumptions. These type of models could describe in detail the flow phenomena, too. CFD models such as REEF3D::CFD, are focused on wave hydrodynamics by solving the incompressible Navier-Stokes equations [2] [72]. But, its high accurate rate and high resolution give it a disadvantage. Therefore, limitation regarding its application to coastal engineering leads towards a high demand on the computational resources. However, new technologies can offer a new solution to improve super computer infrastructure and parallel computation technology [72]. Currently, CFD models may be computed using several different approaches. However, as described below two main approaches can be distinguished among all: Models solving the Reynolds-averaged Navier-Stokes equations (RANS) or models computing the dynamic of the fluid directly [65].

Reynolds-Averaged Navier-Stokes (RANS) Models

- Eddy-viscosity models (EVM): One assumes that the turbulent stress is proportional to the mean rate of strain. Further more eddy viscosity is derived from turbulent transport equations (usually k + one other quantity).

- Non-linear eddy-viscosity models (NLEVM): Turbulent stress is modelled as a non-linear function of mean velocity gradients. Turbulent scales are determined by solving transport equations (usually k + one other quantity). Model is set to mimic response of turbulence to certain important types of strain.
- Differential stress models (DSM): This category consists of Reynolds-stress transport models (RSTM) or second-order closure models (SOC). One is required to solve transport equations for all turbulent stresses.

Computation of fluctuating quantities (CFQ)

- Large-eddy simulation (LES) One computes time-varying flow, but models sub-grid-scale motions.
- Direct numerical simulation (DNS) No modelling whatsoever is applied. One is required to resolve the smallest scales of the flow as well.

Models computing fluctuation quantities resolve shorter length scales than models solving RANS equations. On a scale of providing good results DNS model is considered the most advanced, followed by LES model and RANS models provide the less accurate results. However, DNS and LES models have a huge computational demand in comparison with those models applying RANS methods [65].

2.3 SFLOW - Numerical model

Traditionally, Boussinesq-type wave model approximations are applied to solve the hydrostatic pressure effects. On the other hand, effects of non-hydrostatic pressure could be included too, through adding higher order derivative terms to the Non-linear Shallow Water equations. However, the approximations involved may not guarantee that the Boussinesq-type wave models can predict the onset of wave breaking and its energy losses correctly [77]. Therefore, the development of Non-hydrostatic models has became a popular tool on many modelling activities including open ocean and coastal regions.
During this study REEF3D::SFLOW approach - part of the open-source hydrodynamic model REEF3D - a depth-averaged model solving the non-hydrostatic shallow water equations was used. Models as REEF3D::SFLOW solving the non-hydrostatic pressure incorporate the entire vertical momentum equation. The vertical momentum equation is also part of Newton's second law (later explained on section 3.1). REEF3D::SFLOW is a two-dimensions model using the solution of incompressible Navier-Stokes equations.
REEF3D::SFLOW approach is able to track the free surface motion using a single-valued function of the horizontal plane and requires much fewer grid cells in the

vertical direction by applying the Level Set Method later explained on section 3.4 [77][34], and helping to obtain simulations of wave transformation in coastal waters much more feasible and efficient. Unfortunately, as was the case of the spectral wave models, REEF3D::SFLOW has also limitations due to rapid changes in depth. Limits are attributed to the fundamentals of the shallow water equations.
A projection method solving the time-discretized equations stepwise is used. Therefore, in each time step, an auxiliary system is first solved by disregarding a divergence constraint. The resulting intermediate momentum is then corrected by the solution of a Poisson equation - Eq. 3.21 - to be in compliance with the divergence constraint. To apply the non-hydrostatic extension for shallow water equations the pressure was decomposed in two components, hydrostatic and non-hydrostatic. Together with the Projection Method, developed by Chorin in 1968 [18], this splitting has the advantage that the solver for the non-hydrostatic equation sets can resort to the solver for the shallow water equations. Still, this extension requires the solution of an additional Poisson equation in each time step [34][76].
For steady two-dimensions flow in a Cartesian coordinate system, the depth-averaged energy equation may be written as

$$H_e = \frac{1}{q}\int_Z^\eta \left(\frac{u^2+w^2}{2g} + \frac{p}{\rho g} + \vartheta\right) u dz \tag{2.9}$$

where He denotes the total energy head; u is the velocity in the streamwise x-direction; w is the vertical velocity; η is the free-surface elevation; q is the unit discharge; g is acceleration due to gravity; ρ is the density of the fluid; p is the pressure; $\vartheta = (z-Z)cos^2\theta_s + Z$; z is the elevation of a point in the flow field; Z is the bed elevation; and θ_s is the angle of the free-surface streamline (denoted by the subscript s) with the horizontal. Eq. 2.9 describes the depth-averaged total energy, determined between the free-surface and bed streamlines for an incompressible and non-viscous fluid [76].

2.4 NSEWAVE - Numerical Model

REEF3D::NSEWAVE model as the previous REEF3D::SFLOW approach, solves the non-hydrostatic Navier-Stokes equations. REEF3D::NSEWAVE is able to simulate in three-dimensions, however, it differs from REEF3D::SFLOW approach due to the fact that REEF3D::NSEWAVE does not apply the shallow water equations.
As a part of the open-source REEF3D, REEF3D::NSEWAVE approach implement a free surface tracking algorithm - for single-valued - using the divergence of the depth integrated flow velocities. It is also based on the governing equation explained on section 3.1 solving the incompressible Reynolds-Averaged Navier-Stokes

(RANS). The governing free surface equation is solved on a fixed mesh, avoiding remeshing and some of the known inaccuracies of the σ-coordinate grid method. This σ-coordinate method applied on this approach, is similar to the one used by some large scale ocean and atmospheric models. REEF3D::NSEWAVE as well as the previous model REEF3D::SFLOW, solves the Navier-Stokes equations by using the Projection Method [18].
The non-hydrostatic flow model used is based on a compact difference scheme that takes into account the effect of the non-hydrostatic pressure with a very small number of vertical grid points [78].
A two-equation turbulence model $k-\omega$, is used in REEF3D::NSEWAVE model. The free surface is also obtained using the Level Set Method, previously mentioned, where the zero level set of a signed distance function, $\phi(\vec{x};t)$ is used to represent the interface between air and water.
In REEF3D::NSEWAVE approach the Poisson pressure equation is solved iteratively with the algorithms available from the high performance solver library HYPRE. Projection method together with the library $HYPRE$ used in NSEWAVE model are briefly described on section 3.7.
Additionally, as the REEF3D::CFD approach, REEF3D::NSEWAVE also uses a fifth-order conservative finite difference Weighted Essentially Non-Oscillatory (WENO) scheme. The third-Order Total Variance Diminishing (TVD) Range-Kutta Scheme is employed for time advancement of the level set function and the reinitialisation equation. Both schemes are described on section 3.2.1 and section 3.3, respectively.
In order to reduce the computational cost in the RANS framework, the free surface can be evaluated in a different manner. During REEF3D::NSEWAVE simulations, the horizontal velocity component is integrated over the entire water column. The flux between each neighbouring column is calculated and then the continuity equation is applied to obtain the free surface.

$$\frac{\partial \eta}{\partial t} + \frac{\partial}{\partial x}\int_{-d}^{\eta} u dz + \frac{\partial}{\partial y}\int_{-d}^{\eta} v dz = 0 \tag{2.10}$$

where, η represents the free surface elevation, u is the time averaged velocity, v is the kinematic viscosity, and d the still water depth [34].

2.5 Combine Numerical Wave Models

Another major development in the numerical wave modelling is the coupling of different types of models together to obtain improvements on the results and a better understanding of the ocean physical processes. Currently, research using coupling numerical models has been increasing due to the improvements on the accuracy of the

measurements [70]. Through this section few different cases successfully combining wave models were pointed out, as well as their contribution to the wave propagation and the hydrodynamic fields.

During the use of any numerical wave model different errors appear as a consequence of the limitations and theories of each model. Babovic et al. (2005) [3], developed an algorithm able to efficiently correct the error inherent to the different models and their application in ocean wave prediction by using a third generation wave model known as WAve Model (WAM). Inaccuracies and uncertainties could accumulate to produce poor model results. Errors in the model parameterisation may contribute significantly to the overall error in a numerical model. The results demonstrate significant increase in accuracy of a resulting hybrid model (combining a deterministic model with the stochastic local model).

Thomas and Dwarakish in 2015 [70], carried out simulations in the Jakarta harbour, Indonesia, using the spectral phase-averaging model SWAN and the phase-resolving model Optimized Variational Boussinesq Model (OVBM). They reported that SWAN was a helpful tool to obtain a realistic wave data to use it as an input in OVBM. Moreover, from the comparison of wave disturbance both models show, in general, similar behaviour, except for reflection and diffraction effects. Phase resolving models are mostly used in the case of ports simulations since effect of diffraction is predominant near the entrance of ports.

Regarding wave simulations in fjords, Wang et al. (2017) [72], considered the use of two numerical models, SWAN and REEEF3D::CFD. On the process of the large-scale waves approaching the shorelines of the Norwegian coast, fjords produce a significant effect on wave properties. Therefore, a spectral wave model, SWAN, is used to get the wave properties from the offshore wave data, before shoaling occurs, to have a reasonable wave input into the REEF3D::CFD model. On the other hand, REEF3D::CFD model simulated the wave propagation, finding a rather steady pattern inside the fjords, hence, this phenomenon was found well defined on the results. REEF3D::CFD models can be effectively applied on large scale wave simulations in Norwegian fjords and CFD approach shows satisfying capacity of carrying out such simulations. The combination of SWAN and REEF3D::CFD reduces the cost on time and computational resources tremendously and its coupling shows a promising potential [72]. Moreover, they suggested a future development of a coupled numerical model considering a spectral wave model (SWAN), a Boussinesq-type model and a CFD model.

Chapter 3

Numerical Methodology

In the particular case of the open-source REEF3D, a RANS base model, was developed with a focus on free surface flows in hydraulic engineering at the Department of Civil and Transport Engineering, NTNU [35]. It solves the governing equations on a structured Cartesian grid and is able to implement high-order schemes with the finite difference method. REEF3D is also able to apply various wave theories, such as linear wave theory, second and fifth-order Navier-Stokes wave theory, solitary wave theory and irregular wave theories, among others. The equations to describe the waves include the velocities in the horizontal and vertical direction u and w and the level set function for the surface elevation [72]. REEF3D, can be applied through three different approaches: REEF3D::SFLOW; REEF3D::NSEWAVE; and, REEF3D::CFD. Is possible to use those models in a wide range of engineering applications like: numerical wave tanks simulations; wave forces, including wave propagation and transformation; floating bodies; semi-closed water bodies such as fjords and open channels flow; sediment transport; and, engineering structures such as breakwaters.
REEF3D::CFD approach was for the first time applied in to a large scale CFD wave modelling at the Norwegian coastline, by [72]. The increase on computational resources and improved CFD tools, above mentioned, enhance its application to large domain simulations of wave propagation in Norwegian fjords. Additionally, the authors reported that wave propagation is rather steady inside the fjord. The different wave transformation phenomena are well presented in the simulation results. Therefore, REEF3D::CFD simulation has a prominent advantage in comparison to the phase-averaged models where only the significant wave height contours are presented. Concluding, that REEF3D::CFD has a great potential when it is combined with SWAN, reducing enormously the time-consuming and the computational resources cost. Bihs et al. (2016) [8] described a successful case study using REEF3D::CFD model as a numerical wave tank. This study was focused on setting a numerical wave tank and comparing it with experimental measurements from the NTNU wave tank. The results achieved a good agreement representing accurately the physics of

the wave propagation and hydrodynamics.
For more information regarding the wave theories, reader could find more details on section 4.

3.1 Governing Equations

Governing equations are the key of fluid dynamics, thus, Reynolds Average Navier-Stokes (RANS) equations are used as the governing equations of any CFD model. The fundamental of CFD models describing the physics of any fluid are contained on: continuity, momentum and energy equations. Governing equations are at the same time based on three fundamental principles

- Mass is conserved
- $F = ma$ (Newton's second law)
- Energy is conserved

Therefore, RANS equations are able to describe the behaviour of a viscous and incompressible fluid basing their formulation on the momentum conservation principle. Conservation laws are considered fundamental principles of physics, where a fluid is governed by the mass and momentum conservation laws.

- Conservation of Mass: The equation for conservation of mass is given by

$$\frac{\partial \rho}{\partial t} + \nabla.(\rho U) = 0 \tag{3.1}$$

  With the assumption of incompressibility, the density is a conservative parameters without changes on space or time. Thus, the term with the derivative of the density disappears and the equation for incompressible flows reduces to

$$\frac{\partial u_i}{\partial x_i} = 0 \tag{3.2}$$

  This equation is also known as the equation of continuity.

- Conservation of Momentum: The momentum conservation arises from Newton's second law. Hence, once it is applied on a fluid, momentum equation can be written as

$$\frac{\partial u_i}{\partial t} + \frac{\partial u_i u_j}{\partial x_j} = \frac{\partial}{\partial x_j}\left(\mu \frac{\partial u_i}{\partial x_j}\right) - \frac{1}{\rho}\frac{\partial p}{\partial x_i} \tag{3.3}$$

Using the equation of continuity Eq.3.2 with the above equation, the Navier Stokes equation can be formed and is written as

$$\frac{\partial u_i}{\partial t} + u_j \frac{\partial u_i}{\partial x_j} = -\frac{1}{\rho}\frac{\partial p}{\partial x_i} + \frac{\partial}{\partial x_j}\left[\nu\left(\frac{\partial u_i}{\partial x_j} + \frac{\partial u_j}{\partial x_i}\right)\right] + g_i \tag{3.4}$$

where, u is the velocity averaged over time t, ρ the fluid density, p the pressure, v is the kinematic viscosity and g is the acceleration due to gravity.

3.2 Discretization Methods

Application of numerical methods demands to solve partial differential equations (PDE) to numerically determine the fluid flow. Thus, the governing equations have to be discretized. Within the diversity of methods containing different non-linear coefficients, time-dependence of the coefficients or the higher-order of the equations, is possible to mention three main numerical methods.

- Finite volume methods
- Finite element methods
- Finite difference methods

Finite volume methods calculate the values of conserved quantities, mass and momentum, averaged over a control volume. The values of the conserved quantities are considered within the control volume. Finite element methods approximate continuous quantities as a set of discrete quantities at discrete points. For simulations with complex topography finite difference represent the most common method used by solving PDE and is the method applied during this study. There are three different ways to define the discrete points of the domain in accordance with the number of dimensions on the simulation: a set of points in a line (one-dimension); on a mesh (two-dimensions); and on a grid (three-dimensions). This way of defining the domain is called as spatial discretization. Due to the features of a three-dimensions domain the Cartesian staggered method was applied. This method consist on a grid where the unknown variables are not located at the same grid points.

3.2.1 Convection Discretization

The convective term of the RANS equations needs to be discretized to numerically solve the equations. Therefore, a fifth-order of the Weighted Essentially Non-Oscillatory (WENO) scheme is used [27].

- Weighted Essentially Non- Oscillatory (WENO) Scheme

$$\phi_x = \begin{cases} \phi_x^- & if\ U_1 > 0 \\ \phi_x^+ & if\ U_1 < 0 \\ 0 & if\ U_1 = 0 \end{cases} \tag{3.5}$$

The WENO approximation for $\phi_x^{\pm}$, where ϕ is a given level set function, is a convex combination of the three possible ENO approximations:

$$\phi_x^{\pm} = \omega_1^{\pm}\phi_x^{1\pm} + \omega_2^{\pm}\phi_x^{2\pm} + \omega_3^{\pm}\phi_x^{3\pm} \tag{3.6}$$

The three ENO stencils defined for ϕ are

$$\begin{aligned} \phi_x^{1\pm} &= \frac{q_1^{\pm}}{3} - \frac{7q_2^{\pm}}{6} + \frac{11q_3^{\pm}}{6} \\ \phi_x^{2\pm} &= -\frac{q_2^{\pm}}{6} + \frac{5q_3^{\pm}}{6} + \frac{q_4^{\pm}}{3} \\ \phi_x^{3\pm} &= \frac{q_3^{\pm}}{3} + \frac{5q_4^{\pm}}{6} - \frac{q_5^{\pm}}{6} \end{aligned} \tag{3.7}$$

with,

$$\begin{aligned} q_1^- &= \frac{\phi_{i-2} - \phi_{i-3}}{\Delta x},\ q_2^- = \frac{\phi_{i-1} - \phi_{i-2}}{\Delta x},\ q_3^- = \frac{\phi_i - \phi_{i-1}}{\Delta x}, \\ q_4^- &= \frac{\phi_{i+1} - \phi_i}{\Delta x},\ q_5^- = \frac{\phi_{i+2} - \phi_{i+1}}{\Delta x} \end{aligned} \tag{3.8}$$

and

$$\begin{aligned} q_1^+ &= \frac{\phi_{i+3} - \phi_{i+2}}{\Delta x},\ q_2^+ = \frac{\phi_{i+2} - \phi_{i+1}}{\Delta x},\ q_3^+ = \frac{\phi_{i+1} - \phi_i}{\Delta x}, \\ q_4^+ &= \frac{\phi_i - \phi_{i-1}}{\Delta x},\ q_5^+ = \frac{\phi_{i-1} - \phi_{i-2}}{\Delta x} \end{aligned} \tag{3.9}$$

the weights are written as:

$$\omega_1^{\pm} = \frac{\alpha_1^{\pm}}{\alpha_1^{\pm} + \alpha_2^{\pm} + \alpha_3^{\pm}},\ \ \omega_2^{\pm} = \frac{\alpha_2^{\pm}}{\alpha_1^{\pm} + \alpha_2^{\pm} + \alpha_3^{\pm}},\ \ \omega_3^{\pm} = \frac{\alpha_3^{\pm}}{\alpha_1^{\pm} + \alpha_2^{\pm} + \alpha_3^{\pm}}, \tag{3.10}$$

and

$$\alpha_1^{\pm} = \frac{1}{10}\frac{1}{\left(\widetilde{\epsilon} + IS_1^{\pm}\right)^2}, \quad \alpha_2^{\pm} = \frac{6}{10}\frac{1}{\left(\widetilde{\epsilon} + IS_2^{\pm}\right)^2}, \quad \alpha_3^{\pm} = \frac{3}{10}\frac{1}{\left(\widetilde{\epsilon} + IS_3^{\pm}\right)^2} \tag{3.11}$$

with the regularization parameter $\widetilde{\epsilon} = 10^{-6}$ in order to avoid division by zero and the following smoothness indicators:

$$\begin{aligned} IS_1^{\pm} &= \frac{13}{12}\left(q_1 - 2q_2 + q_3\right)^2 + \frac{1}{4}\left(q_1 - 4q_2 + 3q_3\right)^2, \\ IS_2^{\pm} &= \frac{13}{12}\left(q_2 - 2q_3 + q_4\right)^2 + \frac{1}{4}\left(q_2 - q_4\right)^2, \\ IS_3^{\pm} &= \frac{13}{12}\left(q_3 - 2q_4 + q_5\right)^2 + \frac{1}{4}\left(3q_3 - 4q_4 + q_5\right)^2 \end{aligned} \tag{3.12}$$

3.3 Time Discretization

REEF3D models can be run in several different explicit time schemes to project method for the pressure algorithm. Within the different options available, during this study only two were implemented: Second-Order Adam-Bashforth Scheme; and, Third-Order Total Variance Diminishing (TVD) Range-Kutta Scheme.

- Second-Order Adam-Bashforth Scheme
  It is an explicit second-order scheme that employs the values from two previous time steps. An application of the scheme to the level set function is:

$$\phi^{n+1} = \phi^n + \frac{\Delta t_n}{2}\left(\frac{\Delta t_n + 2\Delta t_{n-1}}{\Delta t_{n-1}} L\left(\phi^n\right) - \frac{\Delta t_n}{\Delta t_{n-1}} L\left(\phi^n\right)\right) \tag{3.13}$$

  where term L represents the spatial discretization.

- Third-Order TVD Range-Kutta Scheme
  This is an explicit third-order scheme able to express a high order accuracy in smooth regions without oscillations that could be caused due to the presence of discontinuities [28]. An example of such an implementation is the third order TVD Runge Kutta scheme [61]:

$$\begin{aligned} \phi^{(1)} &= \phi^n + \Delta t L\left(\phi^n\right) \\ \phi^{(2)} &= \frac{3}{4}\phi^n + \frac{1}{4}\phi^{(1)} + \frac{1}{4}\Delta t L\left(\phi^{(1)}\right) \\ \phi^{n+1} &= \frac{1}{3}\phi^n + \frac{2}{3}\phi^{(2)} + \frac{2}{3}\Delta t L\left(\phi^{(2)}\right) \end{aligned} \tag{3.14}$$

where ϕ is expressed as a generic variable.

3.4 Modelling the Free Surface

The interface between two different fluids represents a challenge for engineers on fluid dynamics. This challenge arises from the large difference in the densities of a gas and a liquid, e.g. ocean water and air. Therefore, the free surface has to be modelled by tracking the free moving two phase flow between both, water and air. Several methods have been developed to achieve the proper modelling of the free surface between the two different media. Some of those methods consider a Lagrangian approach, while others are based on Eulerian approach [31] [75]. However, few methods are using a combination of Lagrangian and Eulerian approach [20]. Few of those methods available are:

- Marker and Cell (MAC) approach
- Volume of Fluids (VOF) Method
- Particle Level Set Method
- Level Set Method (LSM)

3.4.1 Level Set Method

Level Set Method (LSM) was the method chosen to be applied on REEF3D with an Eulerian approach. This means that it can perform numerical computations considering curves and surfaces on a fixed Cartesian grid, without having to parameterise those features. In other words, it is focusing on what is happening on space on each individual grid cell as time passes. LSM uses a signed distance function, known as level set function $\phi(\vec{x}, t)$, with a $\phi(\vec{x}, t) = 0$ at the interface. This function is able to capture the free surface. LSM approach is able to deal with problems in multiple space dimensions where the bottom features are changing during the simulation [1]. Thus, the function is defined as

$$\phi(\vec{x}, t) \begin{cases} > 0 & if\ \vec{x}\ is\ in\ phase\ 1 \\ = 0 & if\ \vec{x}\ is\ at\ the\ interface \\ < 0 & if\ \vec{x}\ is\ in\ phase\ 2 \end{cases} \tag{3.15}$$

The movement of the interface is characterized by the convection of the level set function determined by

$$\frac{\partial \phi}{\partial t} + \vec{u}\nabla\phi = 0 \tag{3.16}$$

3.5 Numerical Wave Tank

A numerical wave tank (NWT) constitutes an essential tool used as a part of a numerical model for design and analysis in the ocean and coastal engineering field. The different NWT applied on a numerical model are an alternative to physical modeling, however, their reliability has to be proven with validation cases e.g. a submerged bar reported by Beji and Battjes (1993) [5]. This specific case has been used several times to validate different new numerical model.
A numerical wave tank has the capability to simulate wave-structures interactions with regular waves, solitary waves, and irregular waves with different wave spectrum like Pierson-Moskowitz and JONSWAP. Moreover, numerical wave tanks can incorporate different bottom characteristics, as well as they can work with real bathymetric features and physical obstacles such as island, and diverse coastal engineering structures [45]. There are different approaches where numerical wave tanks can be based on:

- Potential theory with finite element discretization;
- RANS equations with free surface description by VoF method;
- RANS equations with free surface description by Level Set Method:
- Combination of Potential theory and RANS equations.

With the increasing power and efficiency of computational resources, RANS models in numerical wave tanks are experiencing a growing demand. They also could permit a detailed analysis of the flow physics accounting for turbulence effects, and diminish the higher computational costs.
Fig.3.1 represents a numerical tank composed by six boundaries. Hence, the boundary conditions are considered as follows: velocity inlet (1) and outlet (4). These two boundaries might be also considered as inflow and outflow, respectively. The front (3), back (2) and bottom (5) boundaries are considered as wall boundaries or symmetry planes (here normal velocity components are set to be zero). On the upper part of the numerical tank the atmospheric pressure is applied (6).

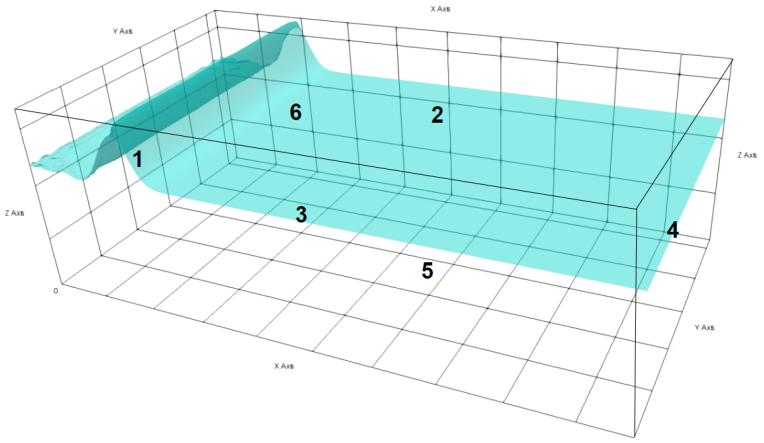

Figure 3.1: Scheme representing the different boundaries considered in a 3D Numerical Wave Tank.

3.6 Wave Generation and Absorption

Numerical wave tanks are an essential part of a numerical model established with a wave generation and a wave absorption zone, on the opposite side.
Wave generation zone, as the name itself says, is the area where the waves had been generated on the numerical model. On the other hand, wave absorption zone is set up to dissipate the wave energy, to prevent the reflection of the waves and the subsequent physical issues produced. Fig. 3.2 represents a wave tank divided in three sections: ZONE 1, wave generation; ZONE 2, working area; and ZONE 3, wave absorption. Each zone is associated with a specific relaxation function.
As on the majority of the components of a numerical model, wave absorption can be applied using different methods too. The combined use of an analytical solution followed by a computational solution is known as the relaxation method. Therefore, the wave generation and the beach zones on a numerical model can be usually called relaxation zones. During this study a Dirichlet type method was applied. It consist on inlet boundaries for free surface flows, by solving ODE and PDE, where the fluid will have zero velocity relative to the boundary. To generate waves using this method, two variables for each time step are required. The first variable is the free surface level at the generation boundary and the second one is the velocity in both components, horizontal and vertical.
REEF3D open source is able to run simulations with several wave types following different wave theories such as small amplitude wave theory, Stokes and Cnoidal wave theories with different orders and solitary wave theory, among others. Bases of some wave theories are explained on section 4.

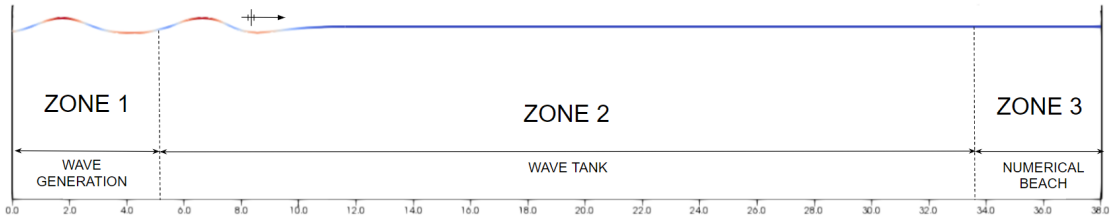

Figure 3.2: Sections of a Numerical Wave Tank

Through the relaxation method, generated waves are moderated after every time step with an analytical solution [42]. The relaxation method in zone 1 is obtained using following rules for pressure and velocity.

$$\begin{aligned} u_{relaxed} &= \Gamma(x)u_{analytical} + (1-\Gamma(x))u_{computational} \\ p_{relaxed} &= \Gamma(x)p_{analytical} + (1-\Gamma(x))p_{computational} \end{aligned} \tag{3.17}$$

Meanwhile, relaxation method in zone 3 is obtained using the following rules for pressure and velocity.

$$\begin{aligned} u_{relaxed} &= \Gamma(x)u_{computational} + (1-\Gamma(x))u_{analytical} \\ p_{relaxed} &= \Gamma(x)p_{computational} + (1-\Gamma(x))p_{analytical} \end{aligned} \tag{3.18}$$

3.7 Solution to Navier-Stokes Equations

Navier-Stokes equations represent a challenge to solve completely, due to the presence of non-linear terms on Eq.(3.4). Neither possible to solve them directly. Hence, to completely solve RANS the pressure term included in the momentum equation has to be calculated.
As mentioned before, during this study the hydrodynamic model REEF3D had been used. This numerical model offers different algorithms to solve the pressure term.

- Projection Method (PJM)
- Semi Implicit Method for Pressure Linked Equation (SIMPLE)
- SIMPLEC (SIMPLE-Consistent)
- SIMPLER (SIMPLE-Revised)
- PISO (Pressure Implicit with Split Operator)

Chorin in 1968 [18] developed the Projection method, which is considered, the most relevant method used on CFD models. It is also the method applied during this study. PJM method has the capability to solve the Navier-Stoke equations Eq.3.4, through solving numerically the time-dependent incompressible fluid flow problems. Moreover, this method offers the advantage of decoupling the velocity and pressure fields. First, the intermediate velocity field U_i^* is computed by ignoring pressure gradients by the transient equation.

$$\frac{\partial(u^* - u_i^n)}{\partial t} + u_j^n \frac{\partial u_i^n}{\partial x_j} = \frac{\partial}{\partial x_j}\left[v(\phi^n)\left(\frac{\partial u U_i^n}{\partial x_j} + \frac{\partial u_j^n}{\partial x_i}\right)\right] + g_i \tag{3.19}$$

Then, through a projection step it is possible to calculate the velocity in the next time-step, $n+1$, for pressure.

$$\frac{\partial(u_i^{n+1} - u_i^*)}{\partial t} + \frac{1}{\rho(\phi^n)}\frac{\partial p^{n+1}}{\partial x_i} = 0 \tag{3.20}$$

The equation obtained is called Poisson pressure equation.

$$\frac{\partial}{\partial x_i}\left(\frac{1}{\rho(\phi^n)}\frac{\partial P}{\partial x_i}\right) = -\frac{1}{\Delta t}\frac{\partial U_i^*}{\partial x_i} \tag{3.21}$$

3.7.1 Iterative Solver

Poisson pressure equation Eq. (3.21) may be solved through two different schemes:

- Direct Eliminations Methods.
  Method based on the standard Gauss Elimination technique, which systematically applies row operations to transform the original system of equations into a form that is easier to solve. Unfortunately, they have a high computational demand.

- Iterative Methods.
  Preferred methods used for non-linear systems due to their accuracy and efficiency to deal with those type of systems. They are also applied for huge systems, solving more than 300 equations [71]

Within the different methods available on REEF3D the Bi-Conjugate Gradient Stabilized (BiCGstab) method was applied to this work. This is an Iterative method applied through the use of $HYPRE$ solver library. $HYPRE$ is a software implementing the BiCGstab method for scalar applications and rectangular grids. Therefore, $HYPRE$ library solves the Poisson pressure equation.

Chapter 4

Wave Theory

One of the bases on coastal engineering field lies over wave theories such as Linear Wave Theory, Non-linear Wave Theory and, Solitary Wave Theory.

4.1 Linear Wave Theory

George B. Airy developed (1845) a theory describing the wave kinematics and dynamics through a first-order equation for surface gravity waves. Nowadays, this theory is known as small amplitude or linear wave theory. It's strictly only applied to conditions in which the wave height is small compared to the wavelength and the water depth [41]. Therefore, there are few limitations which have to be considered while applying it.

- The fluid is homogeneous and incompressible; therefore, the density ρ is a constant.
- Surface tension can be neglected
- Coriolis effect due to the earth's rotation can be neglected.
- The fluid is ideal or inviscid (lacks viscosity).
- The particular wave being considered does not interact with any other water motions. The flow is irrotational so that water particles do not rotate (only normal forces are important and shearing forces are negligible).

  If the velocity potential, Φ, is introduced on continuity equation (Eq. (4.2) right term), then it can be expressed as Laplace equation (left term of Eq. (4.2)).

$$\frac{\partial^2 \Phi}{\partial x^2} + \frac{\partial^2 \Phi}{\partial z^2} = 0 = \frac{\partial u}{\partial x} + \frac{\partial w}{\partial z} \tag{4.1}$$

thus, Φ must satisfy Laplace equation

$$\frac{\partial^2 \Phi}{\partial x^2} + \frac{\partial^2 \Phi}{\partial z^2} = 0 \tag{4.2}$$

and, horizontal and vertical components are represented by u and w, respectively.

$$u = \frac{\partial \Phi}{\partial x}, w = \frac{\partial \Phi}{\partial z} \tag{4.3}$$

- The bed is a horizontal, fixed, impermeable boundary, which implies that the vertical velocity at the bed is zero.

$$w = \frac{\partial \Phi}{\partial z} = 0 \tag{4.4}$$

when $z = -h$

- Pressure (p) at the free surface is uniform and constant. Assuming that $u^2 + w^2 = 0$ and $p/\rho = 0$, then

$$\eta = \frac{1}{g}\frac{\partial \Phi}{\partial t} \tag{4.5}$$

when $z = \eta$

- The wave amplitude is small and the wave shape is not variant in time and space.

  when η is very small, then Eq. (4.5) is $z = 0$

- Waves are plane or long-crested (two-dimensional).

By the use of small amplitude theory it is possible to get a rough and fast estimation of wave characteristics and their potential effects. Wave amplitude, a, can be expressed as $a = (H/2)$, where H is defined as the wave height.
Moreover, the first three assumptions might be valid for almost all coastal engineering problems. However, subsequent assumptions might be considered in accordance with the wave conditions and the objectives of each case study.
Then, water surface profile is given by

$$\eta = \left(\frac{H}{2}\right) cos(\omega t - kx) \tag{4.6}$$

Other wave parameters include $\omega = 2\pi/T$ the angular frequency and T wave period, the wave number $k = 2\pi/\lambda$ and wavelength λ, the phase velocity or wave celerity

$C = \lambda/T = \omega/k$, the wave steepness $\varepsilon = H/\lambda$, the relative depth or shallowness term d/λ, and the relative wave height H/d.
The linear wave theory is based on the two fundamental equations (the mass and momentum balance Eq. (3.2) and (3.4), respectively), along with linearised kinematic and dynamic boundary conditions (more details on section 3.1).
With a small amplitude approximation, the kinematic boundary condition is linearised and reduced at mean water level to

$$\frac{\partial \eta(x,t)}{\partial t} = w(x,0,t) \tag{4.7}$$

where $\eta(x,t)$ is the free surface elevation and t the time.
The dynamic boundary condition, too, is simplified to yield the linearised dynamic condition at the mean water level:

$$\frac{\partial \Phi(x,0,t)}{\partial t} + g\eta(x,t) = 0 \tag{4.8}$$

The linear wave theory, thus, defines η,Φ,u,w and the dispersion relation as

$$\eta = a\ sin(\omega t - kx) \tag{4.9}$$

$$\Phi = \frac{ag}{\omega}\frac{cosh\ (k(z+d))}{cosh\ (kd)}cos(\omega t - kx) \tag{4.10}$$

where Eq. (4.9) is considered for a regular wave.
The velocity potential obtained by Eq. (4.10) can be used to find the velocities in u and w components.

$$u = \frac{\partial \Phi}{\partial x} = \omega a\frac{cosh\ (k(z+d))}{sinh(kd)}sin(\omega t - kx) \tag{4.11}$$

$$w = \frac{\partial \Phi}{\partial z} = \omega a\frac{sinh\ (k(z+d))}{sinh(kd)}cos(\omega t - kx) \tag{4.12}$$

Solving Eq. (4.10), we obtain the dispersion relation

$$\omega^2 = gk\ tanh\ (kd) \tag{4.13}$$

It can also be referred as frequency dispersion, and it means that waves of different wavelength travel at different phase speed. Since wave celerity, C, is defined as $C = \lambda/T = \omega/k$, from Eq. (4.13) it is possible to get

$$C = \frac{gT}{2\pi}tanh\left(\frac{2\pi d}{\lambda}\right) \tag{4.14}$$

and

$$\lambda = \frac{gT^2}{2\pi} tanh\left(\frac{2\pi d}{\lambda}\right) \tag{4.15}$$

Eq. (4.15) is an implicit relationship by virtue of the wavelength λ.
If the water depth d is larger than about half the wavelength, λ, the water is deep (as the waves are considered) and may be used the simplified relation $\omega^2 = gk$. If we apply period and λ, we obtain

$$\lambda = \frac{g}{2\pi} T^2 \tag{4.16}$$

that is,

$$\lambda[m] = 1.56T^2, \tag{4.17}$$

where T is measured in seconds. Thus, a simple e.g. of a wave period of 10 s in deep water has a wavelength of 156 m. On the contrary if $d < \lambda/25$, the water is shallow as far as the waves are concerned. Then,

$$\omega = \sqrt{gd}k \tag{4.18}$$

and we obtain

$$\lambda[m] = 3.13\sqrt{d}T \tag{4.19}$$

In shallow water the wavelength is thus proportional to the wave period.

4.2 Non-linear Wave Theories

4.2.1 Second-Order Stokes Wave Theory

As mentioned before a first-order equation for surface gravity waves can be solved and described through the linear wave theory. However, when the wave amplitude, a, is higher or finite compared to the ratio of wavelength and the water depth (ratio < 1), then the linear wave theory is no longer valid. For this reason, the development of higher-order approximations was necessary [43].
Stokes (1847) was the first who developed a second-order approximation to address problems with finite amplitude waves; known as the non-linear wave theory or second-order Stokes wave theory. Non-linear theory uses the perturbation method to take into account the non-linear terms. This method consists to present the solution as an expansion series of the wave steepness, $\varepsilon = H/\lambda < 1$. Where H and λ, still defined

as wave height and wavelength, respectively.
Non-linear wave presents a relationship between the potential flow and the pressure exerted by the water waves. Maatoug and Ayadi in 2016 [43], mentioned that the difficulty of non-linear wave problems lies not only on the fact that the kinematic and dynamic conditions are non-linear in relation to the velocity potential, but especially because they are applied at an unknown and variable free surface. To overcome this difficulty, Stokes used an approach consisting of perturbations series around the still water level to develop the non-linear theory.
The second-order Stokes boundary value problem is governed by the Laplace Eq. 4.2 within the flow domain together with the kinematic and dynamic boundary conditions. Both boundaries, consider the free surface and the condition of zero vertical velocity at the bottom in addition to the lateral boundary conditions and initial conditions.
Wave steepness is no longer used in shallow waters, to characterise the non-linearity of the waves. Therefore, the theory is applicable in deep waters and some range of intermediate waters. It formulates the wave characteristics in form of a power series of H/λ. The non-dimensional factor used in the power series are known as the perturbation factor. Here, η, Φ, u and w are:

$$\eta = a\ cos(kx - \omega t) + \frac{\pi H}{8}\frac{H}{L}\frac{cosh\ kd(2 + cosh\ 2kd)}{sinh^3\ kd} cos\ 2(kx - \omega t) \tag{4.20}$$

$$\Phi = \frac{ag}{\omega}\frac{cosh\ k(d+z)}{cosh\ kd} sin\ (kx - \omega t) + \frac{3\pi CH}{16}\frac{H}{\lambda}\frac{cosh\ 2k(d+z)}{sinh^4\ kd} sin\ 2(kx - \omega t) \tag{4.21}$$

$$u = \frac{\partial \Phi}{\partial x} = \omega a \frac{cosh\ k(z+d)}{sinhkd} sin(kx - \omega t) + \frac{H}{\lambda}\frac{3\pi^2 H\ cosh(2k(d+z))}{4T\ sinh^4(kd)} cos2(kx - \omega t) \tag{4.22}$$

$$w = \frac{\partial \Phi}{\partial x} = \omega a \frac{cosh\ k(z+d)}{sinhkd} sin(kx - \omega t) + \frac{H}{\lambda}\frac{3\pi^2 H\ sinh(2k(d+z))}{4T\ sinh^4(kd)} sin2(kx - \omega t) \tag{4.23}$$

While a wave is approaching shallow water new problems arise, thus, a cnoidal wave theory often could provides better periodic-wave approximations. This theory is known as the Fenton's theory or fifth-order Stoke wave theory. It will be explained on the subsequent subsection.

4.2.2 Fifth-Order Stokes Wave Theory

The importance of the Linear wave theory between different features and assumptions lies on waves travelling over a horizontal bottom in any depth of water and its simplicity to be applied (section4.1). Additionally, Stokes presented a second-order approximation for waves of finite height (section 4.2.1). Then, Skjelbreia and

Hendrickson in 1960 [62] first aim the results of the fifth-order theory and values of various coefficients as a function of the parameter $d = \lambda$, section 4.1. This theory also worked on the expansion of a and k as a term ak. Where k is set-up as the wave number - $k = 2\pi/\lambda$ - and a has no physical significance other than that of being a length scale which is equal to the amplitude of the wave at lowest order. Thus, choosing ak as expansion parameter means that convergence for very steep waves cannot be achieved [62]. After more than two decades, Fenton in 1985 [22], developed a fifth-order Stokes wave theory based around an expansion term $kH/2$ instead of the expansion ak. However, it was necessary to use convergence-enhancement procedures to obtain accurate results for steep waves. Thus, Fenton's fifth-order theory demonstrated that it is more efficient and accurate than original fifth-order wave theory and suitable for shallow and deep waters [22]. It can also be described as a steady periodic water wave theory designed to be used for long waves in shallow water.
Fenton postulates a formula for fluid velocities based on a Fourier series expansion about the term H/d. He also discovered that much better results could be obtained by expanding the parameter d/λ also called as shallowness parameter [21].
Assuming that the wave train data supplied are d, H and T, then k must be computed before the theory can be applied. This is done by solving Eq. 4.13 in terms of k, using Newton's method. Once k is known, a number of coefficients are calculated and these are used in power series expansions to find the surface profile and wave kinematics [21].
With an increase in wave height, it becomes essential to evaluate higher order perturbations to obtain a good representation of the wave. Fenton's theory [22] for the analytical solution for this order is used in this work. The Taylor expansion with the perturbation factor here, $\pi H/\lambda$, is evaluated till the fifth power. Thus, the relations for η,Φ,u and w here are

$$\eta = \frac{1}{k}\sum_{n=1}^{5} \epsilon^n b_n \; cos(n\theta) \tag{4.24}$$

where

$$\begin{aligned} b_1 &= 1 + \epsilon^2 B_{31} - \epsilon^4 (B_{53} + B_{55}) \\ b_2 &= B_{22} + \epsilon^2 B_{42} \\ b_3 &= -B_{31} + \epsilon^2 B_{53} \\ b_4 &= B_{44} \\ b_5 &= B_{55} \end{aligned} \tag{4.25}$$

$$\Phi = C_0 \sqrt{\frac{g}{k^3}} \sum_{n=1}^{5} \epsilon^n a^n cosh(nkz) sin(n\theta) \tag{4.26}$$

where

$$\begin{aligned} a_1 &= A_{11} + \epsilon^2 A_{31} + \epsilon^4 A_{51} \\ a_2 &= A_{22} + \epsilon^2 A_{42} \\ a_3 &= A_{33} + \epsilon^2 A_{53} \\ a_4 &= A_{44} \\ a_5 &= A_{55} \end{aligned} \tag{4.27}$$

$$u = C_0 \sqrt{\frac{g}{k}} \sum_{n=1}^{5} \epsilon^n \; n \; a_n cosh(nkz) cos(n\theta) \tag{4.28}$$

$$w = C_0 \sqrt{\frac{g}{k}} \sum_{n=1}^{5} \epsilon^n \; n \; a_n sinh(nkz) sin(n\theta) \tag{4.29}$$

Where u and w are the horizontal and vertical components, respectively, and the coefficients C_0, A_{ij}, B_{ij} are dimensionless functions of the water depth d and wavelength λ.
For a detailed explanation of the fifth-order theory reader might be interested to find out the original papers [22] and [21].

4.3 Solitary Wave theory

Airy wave theory is also a good approximation for solitary waves such as a tsunami wave in the ocean, before they steepen near the coast. Solitary wave consists of a single crest non-linear wave with infinite length, therefore, it is long enough that almost every part of the ocean waters could be considered shallow waters. A solitary wave is not only transmitting energy it is also displacing the water particles from their original position toward the direction of the wave. It means they displace energy and water mass [48].
During the first approximation of the solitary wave theory the Boussinesq approach was considered. It was based on observations from the Russell's work previously described few decades before. Russell's work consists of a report of observations of a free surface isolated wave propagating in a canal [58]. In the other hand, Kortewegde Vries (KdV) equation, as well as being a notable integrable equation, was also a valid model for solitary waves in a wide variety of physical contexts
Stokes theories briefly described above, contain λ parameter in the two fundamental terms previously described: the relative depth (d/λ) and the wave steepness (H/λ). In comparison with those previous theories, the solitary wave theory on the other hand, contains a fundamental parameter that is independent of wave length, known as the relative wave height (wave height/depth, H/d).

Relative wave height is part of the significant non-dimensional parameters, where the non-dimensional coordinates are described as

$$X = \frac{x}{d}, Z = \frac{z}{d} \tag{4.30}$$

where the relative elevation of the free surface is

$$\mu = \frac{\eta}{d} \tag{4.31}$$

and the relative wave height

$$\gamma = \frac{H}{d} \tag{4.32}$$

At the bottom $Z = 0$, at the crest of the wave $Z = 1 + \gamma$. The non-dimensional components of horizontal and vertical orbital velocity are

$$U = \frac{u}{C}, W = \frac{w}{C}. \tag{4.33}$$

with the wave velocity described as C.
Boussinesq approach, is based on the equation of motion for irrational , non-divergent flow. The solution is based on the expansion of the velocity potential in a power series

$$\Phi = \sum_{n=o}^{\infty} \Phi_n z^n. \tag{4.34}$$

Wave velocity is described as follow

$$C = \sqrt{g(d+H)} = \sqrt{gd(1+\gamma)}, \tag{4.35}$$

and for the wave profile we have

$$\mu = \gamma sech^2 \left(\sqrt{\frac{3\gamma}{4}} X \right). \tag{4.36}$$

Volume and mass transport are given by

$$\bar{u} = \frac{4d}{T} \sqrt{\frac{\gamma}{3}}, \tag{4.37}$$

where γ is the relative wave height
The energy contained in a solitary wave, between $-\infty$ and $+\infty$, is calculate through

$$E = \frac{8}{3} \rho g d^3 \gamma \sqrt{\frac{\gamma}{3}}. \tag{4.38}$$

Particles displacement and trajectories are parameters considered to evaluate the displacement of energy and water mass, as was mentioned before. Knowing this parameters is possible to calculate the amount of energy and water mass approaching the shoreline.

4.4 Wave Transformation

Ocean waves parameters can be modified during their transition from offshore zones to coastal areas by physical objects such as islands, bays and coastal engineering structures among other. This modifications fall into three physical phenomena: refraction, reflection and diffraction. Basic concepts of these wave physical phenomena are described on the subsequent subsections.

4.4.1 Refraction

During the trajectory of the waves approaching the coastline the physical objects spread around on the ocean bottom together with changes on depth will affect the initial wave parameters; e.g., H, T, C, λ and wave incidence angle θ. Refraction is defined as the changes on wave direction, wave height and wave velocity when the waves pass from one media to another with differences on depth. In this process the waves start feeling the ocean bottom and together with the friction effect, the waves will tend to line-up itself paralleled to the coastline [19]. Therefore, determining the refraction effect is essential in coastal engineering.
The velocity of a single wave crest is directly proportional to the depth where it propagates. This means that the velocity of the wave will decrease when the water depth diminish too. The direction of propagation of a wave, also know as wave angle, can be determined by a line crossing perpendicularly the wave crest. This line is known as orthogonal and it can be calculated with manual methods or by applying numerical models [19].
As mentioned before, wave refraction coupled with shoaling effect will determine the height of the ocean waves, as well as, changes of the wave propagation angle on the different segments of a single wave. Variations on the wave angle of each segment will determine if the energy contained on the wave converge or diverge on a specific point on the coast. Thus, it determines how much energy contained on a wave will impact on a specific point. This process has a huge impact on the natural sediment transport pattern, which contributes to the alteration of bottom topography [49].

4.4.2 Reflection

Reflection phenomena are described as the changes in direction of an ocean wave passing between two different media. The wave can be either partially of totally reflected from a physical object including natural or engineering structures. The energy reflected might returns in an angle with an opposite propagation to the one the original wave came from [19]. The portion of the wave reflected will also produced a wave interference with the subsequent wave set approaching the coast. When two waves with opposite angle of propagation coincide in phase, it magnify their wave height - in a total sum of both wave heights - during an instant.
During a harbour development wave reflection becomes a relevant factor regarding the protected area inside the harbour. If the energy contained on a wave is not totally dissipated and the energy reminded propagate inside a harbour it can results in a build-up of energy as a consequence of a multiple reflection in the absence of a media able to sufficient dissipate this energy. Therefore, if the reflection is not properly approached surface fluctuations within the harbours may cause excessive water motion.
The amount of wave energy reflected from a media depends on the slope, roughness, and permeability of the beach or structure involved. Wave steepness and the angle of wave approximation play also an important role determining the quantity of energy reflected [19].

4.4.3 Diffraction

Ocean wave diffraction is described as the lateral transfer of energy along a wave crest. It can occur when a set of waves encounter surface obstacles, such as island or breakwaters. Therefore, when a wave passes over a physical obstacle and the energy is transferred laterally through the wave crest, this energy will be carried out into the shadow zone of the obstacle [19]. Due to the amount of energy that is spread along a longer area, the wave intensity on the shadow zone is much less than on the front of the obstacle. Even though wave diffraction may be found offshore, its relevancy is reduced to coastal areas.
Calculation of diffraction effects, as on the wave reflection phenomena, is essential on the planning process of coastal engineering developments. Specially in the particular case of a harbour development. The proper distribution and orientation of the breakwaters, groynes and entrance of a harbour will reduce then the lateral transfer of energy into the shadow zone.

Chapter 5

Validation and Discussions

The validation of any new numerical model is a primordial step to find the reliability of any new model. Through a validation it is possible to analyse both the propagation characteristics and the physical processes of generation and dissipation of the model. The result obtained has to be compared with results that previously proved its reliability [60]. Thus, the comparison must be carried out using any of the three different data sets potentially available: laboratory observations, field observations and previous model validations results.
Sargent in 2013 [60], mentioned that the cost and time used to determine that a model is absolutely valid over the complete domain is normally high. As a result, tests can be performed until sufficient confidence is obtained that a model can be considered valid for its intended application.
This section describes a validation case used to check the reliability of REEF3D::SFLOW numerical model. As mentioned before, this numerical wave model belong to the open-source REEF3D. Therefore, several simulations with different wave parameters were carried out to find the water depth, grid size and time step limits of the model. As the last part of this section and to cover the main objective of this project, a methodology containing two different wave models was applied. It was used on a fish farm located in the Southern-East coastline of Flatøya island, Norway. As well as, the results and discussions of the different cases are located on this same section. A brief description of the numerical wave tank testing was included on this chapter too.

5.1 SFLOW

5.1.1 Testing of the Numerical Wave Tank

Simulations were run on the numerical tank without any obstacle and slope, to observe only the response of the wave tanks to the wave propagation. Bunnik and Huijsmans

in 2005 [13], enhanced the importance of testing and validate the numerical wave tank used on the different wave models. This process of validation and testing will provide important information of the accuracy and reliability of the full wave model. As mentioned in section 3.6, the wave generation method used during the different simulations was Dirichlet. On the opposite side of the generation zone, there is the numerical beach or relaxation ZONE 3 - Fig. 3.2. To test the reliability of the absorption system applied, simulations with different depths were applied too. It is also known as a convergence study.
The dimensions of the tank were set-up as equal as the wave tank used for the benchmark validation case. The benchmark case is explained below in section 5.1.3. The configuration of the tank used here includes the same wave gauges locations too.

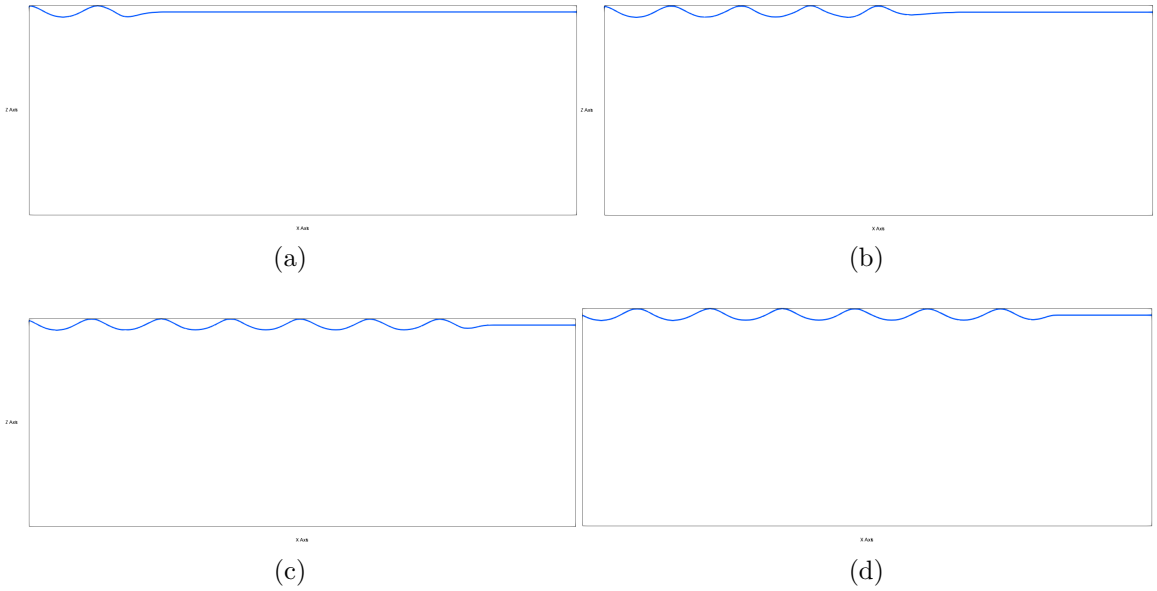

Figure 5.1: Water wave evolution on a numerical wave tank without any obstacle. (a) Wave propagation after t=100 s; (b) Wave propagation after t=200 s; (c) Wave propagation after t=500 s; and, (d) Wave propagation after t=1200 s

After several simulations only focused on the numerical wave tank performances, without any obstacle, the results obtained are showed on Fig. 5.1. The results shows that relaxation ZONE 1, explained on section 3.6, has a good representation of the wave conditions previously set-up. Fig. 5.1 shows a sequence of waves propagating around the wave tank until they reach the numerical beach. The waves generated conserved their parameters along all the numerical tank and during all the simulation. Thus, it is not possible to observe any modification and transformation of the wave profile through the simulation. Therefore, any anomaly due to the numerical wave tank was dismissed.

Simulations were run for 1200 s to observe if there is any change on the wave absorption pattern related with long simulations. As a result, it was not possible to observe any energy of the wave reflected by the numerical beach or absorption system. Also, the wave energy is smoothly dissipated through the numerical beach. Therefore, it is assumed that the numerical beach produces ideal results regarding the dissipation of the wave energy.

5.1.2 Convergence studies

Convergence studies are a simple but efficient method used to determine the limits of a specific parameter used within a numerical model. The method consists of comparing different simulations where only one parameter is modified at the time between each simulation, keeping the rest of the variables with the same value as stated on Table 5.1. Through this method is easier to identify the limits of the wave model regarding the parameter of interest. The geometry of the wave tank used during the convergence studies is the same one as the one described on section 5.1.3.
Within the different parameter considered during setting up a simulation, two deserved an special attention: grid size (dx); and, time-step (CFL) of the simulation. The CFL number is expressed from Courant-Friedrichs-Levy condition and represents the quotient between the time interval and time residency within a finite volume. CFL is used to solve differential equations and partial derivatives and in this case it is calculated as $velocity \cdot time - step/dx$.
This factor is used when determining the time step size based on the CFL criterion for adaptive time-stepping. On the other hand, grid size will determine how much detail is expected to be obtained for a certain simulation. Smaller the grid size greater the detail of the simulation, however, a small grid size will also represent a greater computational demand.
As mentioned above, several simulations were performed to identify the limits of the model regarding the grid size and time-step. Mesh size was considered a priority variable, thus, it was first performed. Nine different grid sizes were selected: 0.005, 0.01, 0.015, 0.02, 0.03, 0.05, 0.07, 0.09 and 0.1 m. A smaller grid size - $dx = 0.005$ m - increase the computational demand resulting in a simulation crashing. On the other hand, dx greater than 0.05 m gave also not satisfactory results. Therefore, only five different grid sizes were kept for the mesh size convergence study - 0.01, 0.015, 0.02, 0.03 and 0.05 m - as they can be observed on Fig. 5.2.

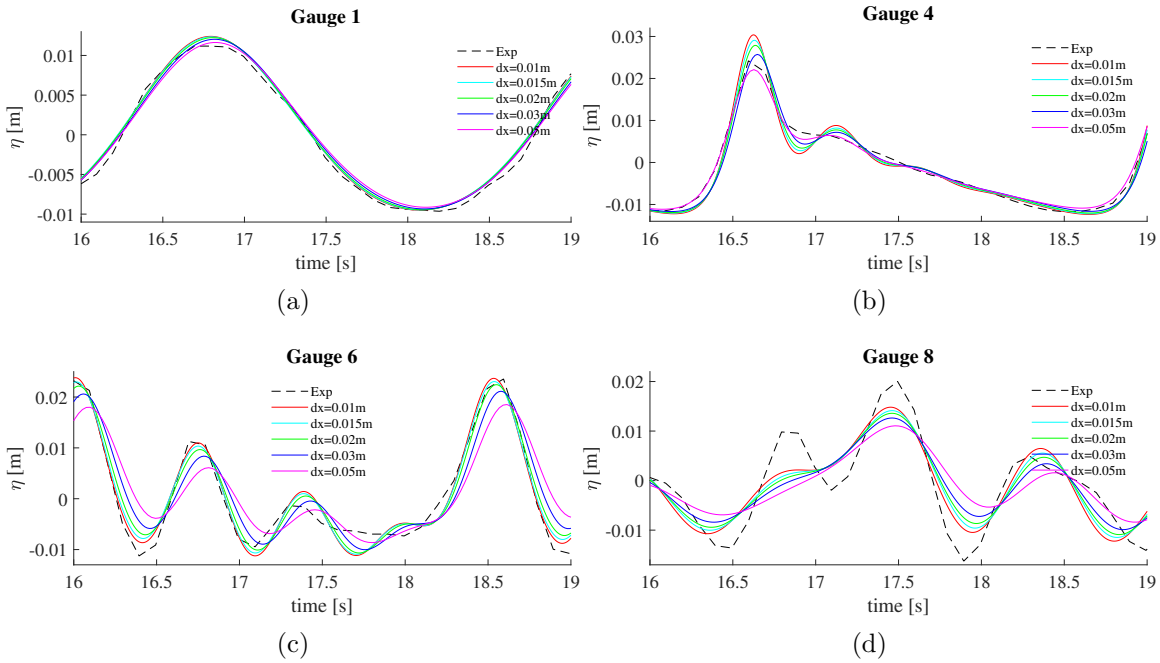

Figure 5.2: Mesh size convergence study with second-order Stoke waves, H =0.022 m and CFL=0.5. Experimental data - Exp - is represented by the dash line. Five different grid sizes - dx - were simulated. (a)Waves without transformation due to the obstacle. (b)Waves already transformed due to the obstacle, located on the higher and flat part of the obstacle. (c) Waves loosing height due to the presence of the lee slope. (d) Wave front completely transformed due to the obstacle.

Kamath et al. in 2017 [36], reported the use of five different dx compared with the experimental data reported by Beji and Battjes (1993) [5]. Results obtained during this study were also compared with the experimental data [5] having a good agreement as the one founded by [36]. The results presented in Fig. 5.2 plotted four Wave Gauges - WG - showing the evolution of the waves and the differences of the five dx used. Experimental data is represented by the dash line. Analysing carefully the six different profiles, it is possible to observe that in general all free surface elevations converge with the experimental data showing some differences on wave amplitude. Those wave amplitude differences occur manly after the waves were completely transformed due to the lee slope of the submerged bar. It was also observed that there are some differences on amplitude and waveform between the profiles not only with the experimental data profile, but also between the profiles obtained from REEF3D::SFLOW. On the other hand, there are two grid sizes that show a closer approximation to the experimental profile. As is expected the smaller the grid - dx= 0.01 m - the greater the resolution and better approximation to the experimental profile. However, the bigger grid size - dx= 0.05 m - also presents a good approximation to the experimental data (dash

line).
During this study the smaller grid - dx= 0.01 m - was selected as the most suitable to the experimental data profile. As an alternative of a simulation with less computational demand and less time consume, dx= 0.05 m could also offer a good approximation to the data profile.
Based on the results of Fig. 5.2, dx= 0.01 m together with the wave variables - H=0.022 m and T=2.5 s - were used as fixed parameters to perform the CFL convergence study. Five different CFL values were applied - 0.1, 0.2, 0.25, 0.3 and 0.5 - during the simulations to obtain Fig. 5.3. Contrary to the mesh size study, all the profiles show similar profile with minimum differences on amplitudes on the highest and lowest points of the profiles. However, CFL= 0.5 showed the closest approximation to the experimental data.

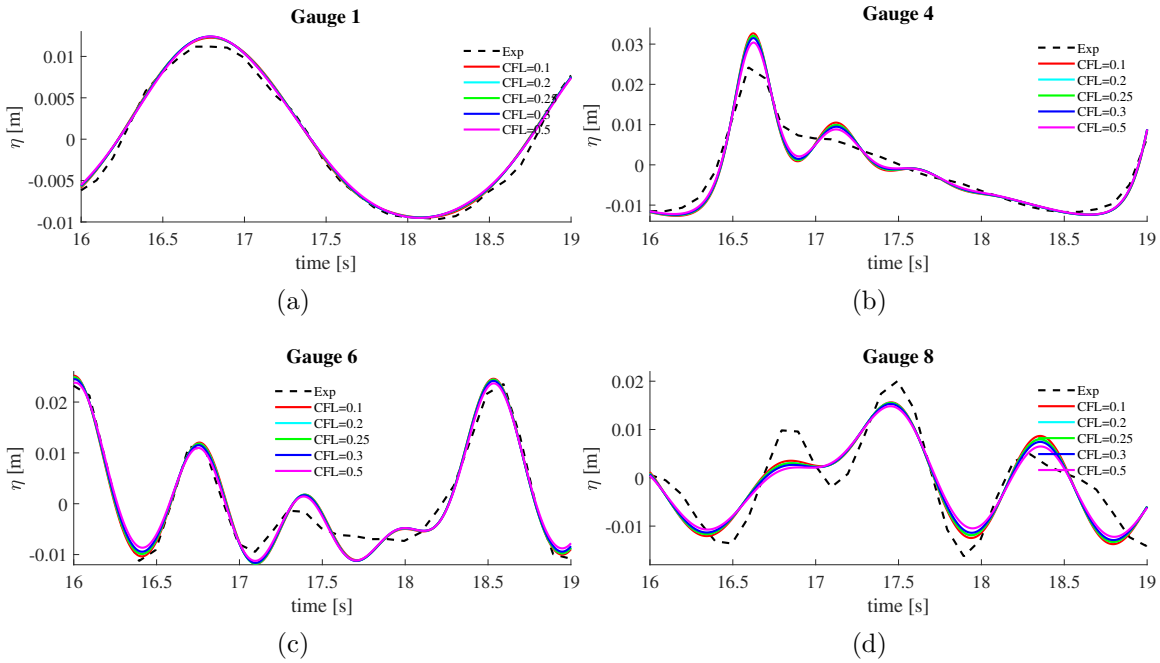

Figure 5.3: Time-step convergence study with H=0.022 m and dx= 0.01 m. Experimental data - Exp - is represented by the dash line. Five different time-steps - CFL - were simulated. (a) Waves without transformation due to the obstacle. (b)Waves already transformed due to the obstacle, located on the high and flat part of the obstacle. (c) Waves loosing height due to the presence of the second slope. (d) Waves completely transformed due to the obstacle.

Moreover, results obtained from mesh size Fig. 5.2 and time-step Fig. 5.3 studies, were used as the base for the depth convergence study applying the most suitable value from dx and CFL. As explained before this convergence method consists on only modify the same variable at the time as it is expressed on Table 5.1.

To complement the testing of the numerical wave tank, section 5.1.1, a depth convergence study was conducted. Numerical tank was set-up with 0.4 m depth. A total of 14 differences water depth values were used to find the depth limit of REEF3D::SFLOW model. Only seven depths presented good results, therefore, the rest were dismissed. Values greater than 0.5 on Table 5.1 were discarded. Thus, REEF3D::SFLOW approach is a numerical wave model ideal for shallow water theories were the ratio of d/λ is < 1.

The wave height, identify on Fig. 5.4, is not modified through all the wave tank in any moment. Waveforms were kept unmodified. This means that the wave generation zone and the working zone are working properly without transforming the waves during all their trajectory toward the numerical beach.

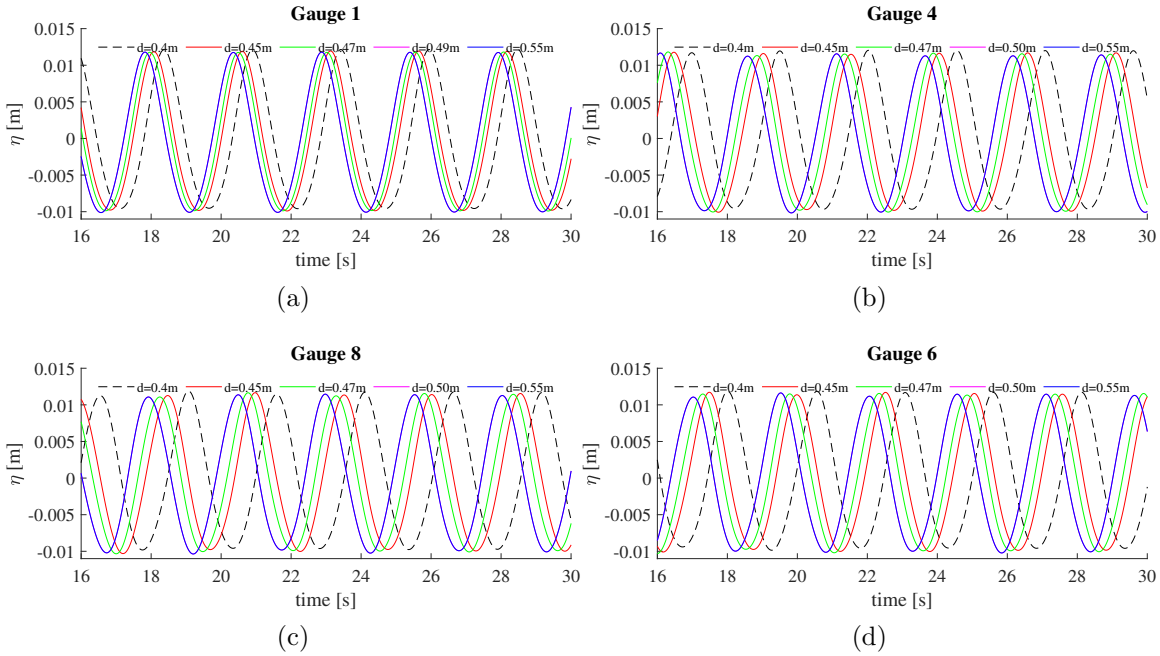

Figure 5.4: Convergence study testing the potential impact due to changes on water depth during different simulations using REEF3D::SFLOW approach. Five different water depths were tested and compared between each other. Only four time-series out of eight were placed here.

Table 5.1: Depth convergence study. Depths used during different simulations to find the limits of the model.

Water Depth [m]	***dx*** **[m]**	**Time-step (CFL)**	***H*** **[m]**	***T*** **[s]**
0.4	0.01	0.5	0.022	2.5
0.45	0.01	0.5	0.022	2.5
0.46	0.01	0.5	0.022	2.5
0.47	0.01	0.5	0.022	2.5
0.48	0.01	0.5	0.022	2.5
0.49	0.01	0.5	0.022	2.5
0.50	0.01	0.5	0.022	2.5
0.60	0.01	0.5	0.022	2.5
0.70	0.01	0.5	0.022	2.5
0.80	0.01	0.5	0.022	2.5
0.90	0.01	0.5	0.022	2.5
1.0	0.01	0.5	0.022	2.5
5.0	0.01	0.5	0.022	2.5
10.0	0.01	0.5	0.022	2.5

5.1.3 Submerged Bar case

Beji and Battjes in 1993 [5], reported results examining sinusoidal waves propagating over a submerged bar from a laboratory experiment. Nowadays, their contribution is one of the most used case studies on numerical wave models. It is considered a complex case and due to the reliability of their results, it had been widely applied to validate new models such as SWAN [26] [56], REEF3D::CFD [36] and NEOWAVE [74].

As was described above in section 5.1.2, and to summarise the findings of the different convergence studies applied: a grid refinement study was carried out to select the correct grid size - dx=0.01 m -; reliability of the wave tank was studied through several simulations analysing the accurate wave propagation and transformation, as well as, the performance of the numerical beach and the wave generation zone; and, determining the ideal time-step value - CFL= 0.5. Once all the parameters were tested and the most suitable found, wave propagation over a submerged bar was simulated for different incident wave heights. Numerical results obtained were compared with experimental data [5][36]. The wave transformation over the submerged bar was studied using the data obtained from the different wave gauges at diverse locations along the submerged bar described on Fig. 5.5.

This case study was carried out using a two-dimensional numerical wave tank - Fig.

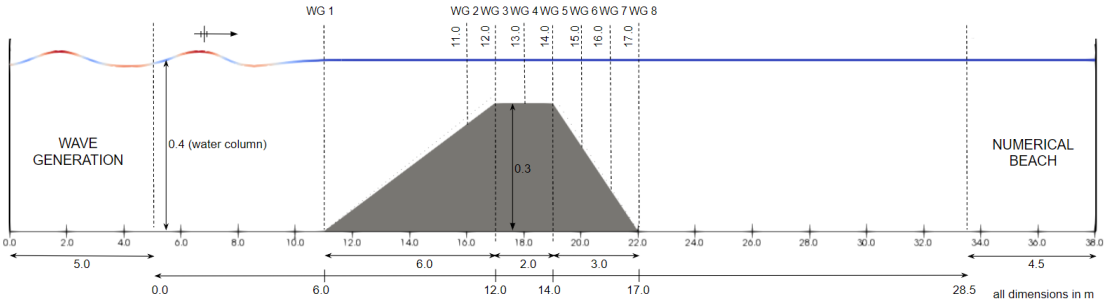

Figure 5.5: Numerical wave tank dimensions and submerged bar dimensions. Wave gauges - WG - distributed over the length of the numerical wave tank

5.5 - with 38 m of length and a maximum height of 0.8 m. During the simulations 2nd-order Stokes waves were generated with a wave period of - $T = 2.5$ s -, a wavelength - $\lambda = 4.74$ m - and three different wave heights - H= 0.022, 0.035 and 0.042 m -. A full description of the wave parameters used during the set-up of each simulation are located on Table 5.2. Dimensions of the submerged bar with a trapezium shape used during this validation are: 0.3 m on the higher point with a front slope of 1:20 and a lee slope of 1:10. The incident sinusoidal waves were generated at the left side of the numerical tank and the absorption system/numerical beach is imposed on the right side. The free-surface elevations were recorded using eight wave gauges located all over the submerged bar. Wave gauges - WG - present different locations as it is illustrated on Fig. 5.5. As mentioned above the total water depth of the numerical tanks was set-up on 0.4 m, thus, on the top of the submerged bar a resulting depth of 0.1 m is present. All this information was used following the dimensions reported from the laboratory experiment [5] and also from the validation of REEF3D::CFD [36]. Additionally, a wave generation zone with a length of 5 m - relaxation ZONE 1 - and a numerical beach of length 9.5 m - relaxation ZONE 3 - were set-up. More information regarding the relaxation zones can be found in section 3.6. A bigger extension of the relaxation ZONE 3, lays over the idea to have enough space where the wave energy can be fully dissipated.
During this study, results from Kamath et al. (2017) [36] using a REEF3D::CFD approach were used as a reference point. Thus, as they reported a grid size of dx = 0.005 m was found as the most suitable value obtained during the mesh size study. This small grid size offered simulations able to capture the full evolution of wave shoaling and breaking. Unfortunately, this small grid size had to be discarded due to the high computational demand and not reliable results described in section 5.1.2. The most relevant values found were dx= 0.01 and 0.05 m.

Table 5.2: Parameters considered during the different simulations using REEF3D::SFLOW approach on the benchmark case

Test	**T [s]**	**H [m]**	**Mesh size [m]**	**Time-step (CFL)**	**Breaking type**
1	2.5	0.022	0.01	0.1	Non-breaking
			0.015	0.2	
			0.02	0.3	
			0.03	0.4	
			0.05	0.5	
2	2.5	0.035	0.01	0.1	Non-breaking
			0.015	0.2	
			0.02	0.3	
			0.03	0.4	
			0.05	0.5	
3	2.5	0.042	0.01	0.1	Spilling
			0.015	0.2	
			0.02	0.3	
			0.03	0.4	
			0.05	0.5	

Fig. 5.6 represents the wave propagation and transformation during a 'N' simulation. Here it is possible to observe the wave evolution due to the presence of a front slope on the submerged bar and the results in the transfer of wave energy into higher frequency components on a lee slope. On the Fig. 5.6 (c), shoaling effect starts producing modifications on the waveform stacking the energy of the wave. The wave height simulated was not to high - H= 0.022 m -, thus, it is not expected to observe a breaking wave effect either. However, due to the presences of the lee slope a wave decomposition effect can be found together with a wave dissipation due to the rapid decrement on water depth. The subsequent plots - Fig. 5.6 (d), (e) and (f) - show the full transformation of the wave composed by multiple frequencies. Wave crest becomes steeper and secondary wave crest appears. The reminder wave energy from the higher frequencies was mitigated by the numerical beach.

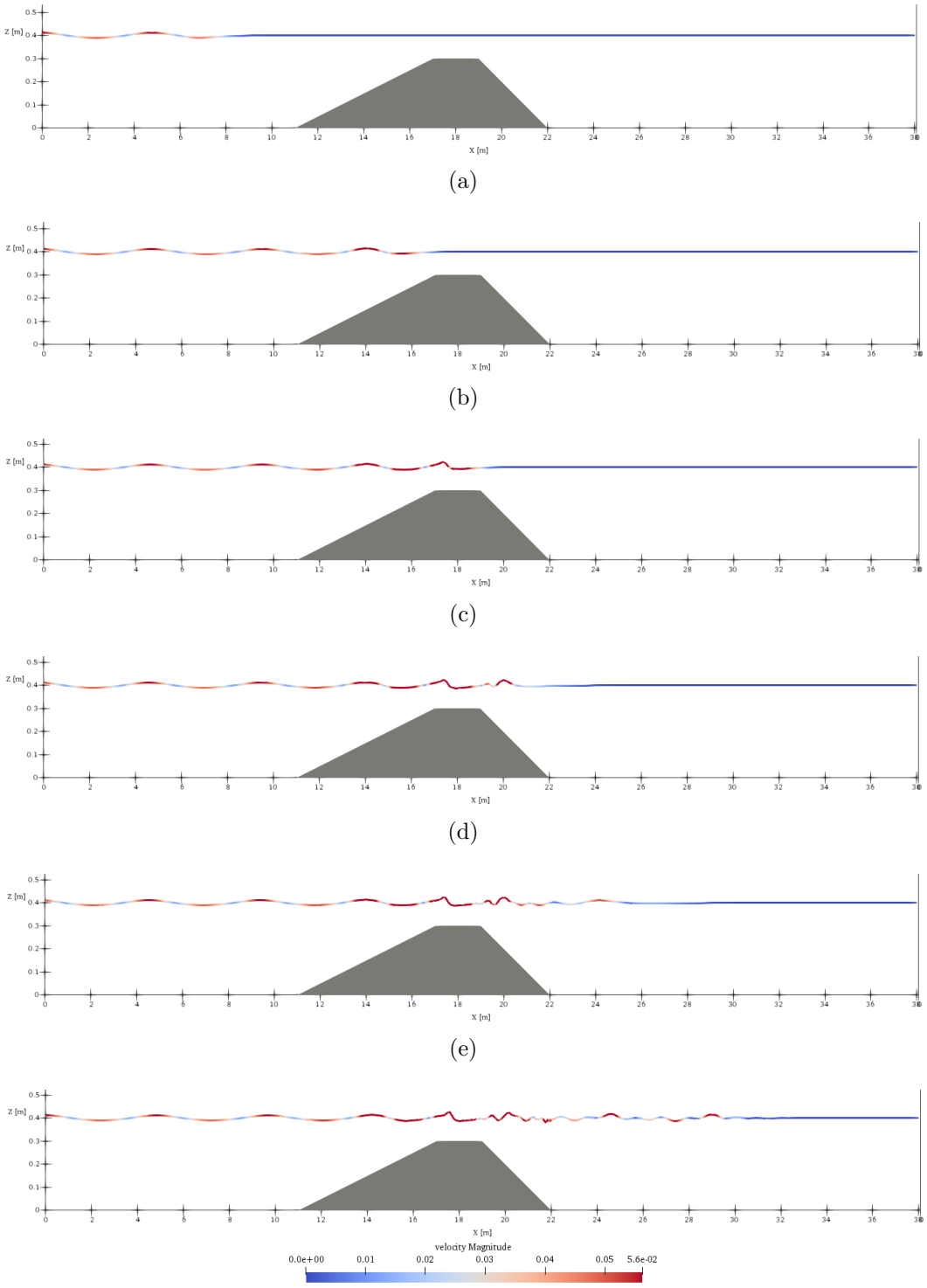

Figure 5.6: Wave evolution from the initial conditions in figure (a) until the full wave transformation in figure (f) by using REEF3D::SFLOW approach, with H=0.022 m, T= 2.5 s and CFL=0.5

Test 1 - H=0.022 m, dx= 0.01 m, T= 2.5 s

Validation process, as mentioned above, involves a comparison of two different data sets. In this case, experimental data from [5] was compared with the data set obtained from this study. Wave propagation using a wave height of H=0.022 m can be found on Fig. 5.7. Within the time-series plots of Fig. 5.7, η in the y-axis, represents the free surface elevation in meters and x-axis the time of the simulation in seconds.
The sinusoidal waves applied during the simulation seems to conserve their waveforms without any alteration along Fig.5.7 (a), with a good matching pattern - either on the wave amplitude and wave phase - between both datasets. Once the wave modification started due to the shoaling effect produced by the front slope - Fig 5.7 (b) and (c)- and on the upper part of the submerged bar - Fig 5.7 (d) and (e) - waveforms became sharper with wave crest steeper. The upper section of the submerged bar presents a higher amplitude value of η over 0.03 m - Gauge 4 and Gauge 5 - due to the wave energy been stacked. Notable decomposition into shorter waves occurs immediately after passage over the bar - higher frequency waves -. Gauge 4 recorded the first decomposition of the waves along the bar - Fig. 5.6 (d) - where secondary crests appear at the trailing side of the primary waves. The accumulation of the wave energy peaked the wave crest resulting in a direct increment of wave height H, as well as, a decrement on the wave T. The modification of these variables was produced instants before the wave energy was released into the water column due to an opposite shoaling effect - posteriorly referred as de-shoaling effect -. De-shoaling effect occurs straight after the water depth rapidly increase due to a steeper lee slope. Thus, the energy contained on a peaked wave crest was spread all over the water column, therefore, higher frequency wave components could be observed - Fig. 5.6 (e) and (f) - and the reminder energy was dissipated by the numerical beach. As mentioned above, the submerged bar has a steeper slope on its lee side. It produced an effect on the free surface elevations, Fig. 5.7 (f), (g) and (h), reducing wave height - η lower than 0.02 m - in comparison with the profiles showed on Fig. 5.7 (d) and (e). Fig. 5.7 (e) presented a wave height that increased more than twice the original value with $\eta < 0.03$ m. Reduction on wave height is attributed to the amount of energy dissipated during the de-shoaling effect. The limitations of the model - previously mentioned on section 5.1 - reduced the accuracy of the model at that section, therefore, it could not capture the full wave decomposition. Owing to de-shoaling effect, SFLOW - shallow water equations - faced issues dealing with the computation of the full physical phenomena occurring when the conditions of the water column changed abruptly. However, it had been considered to have a good agreement with the experimental data [5].

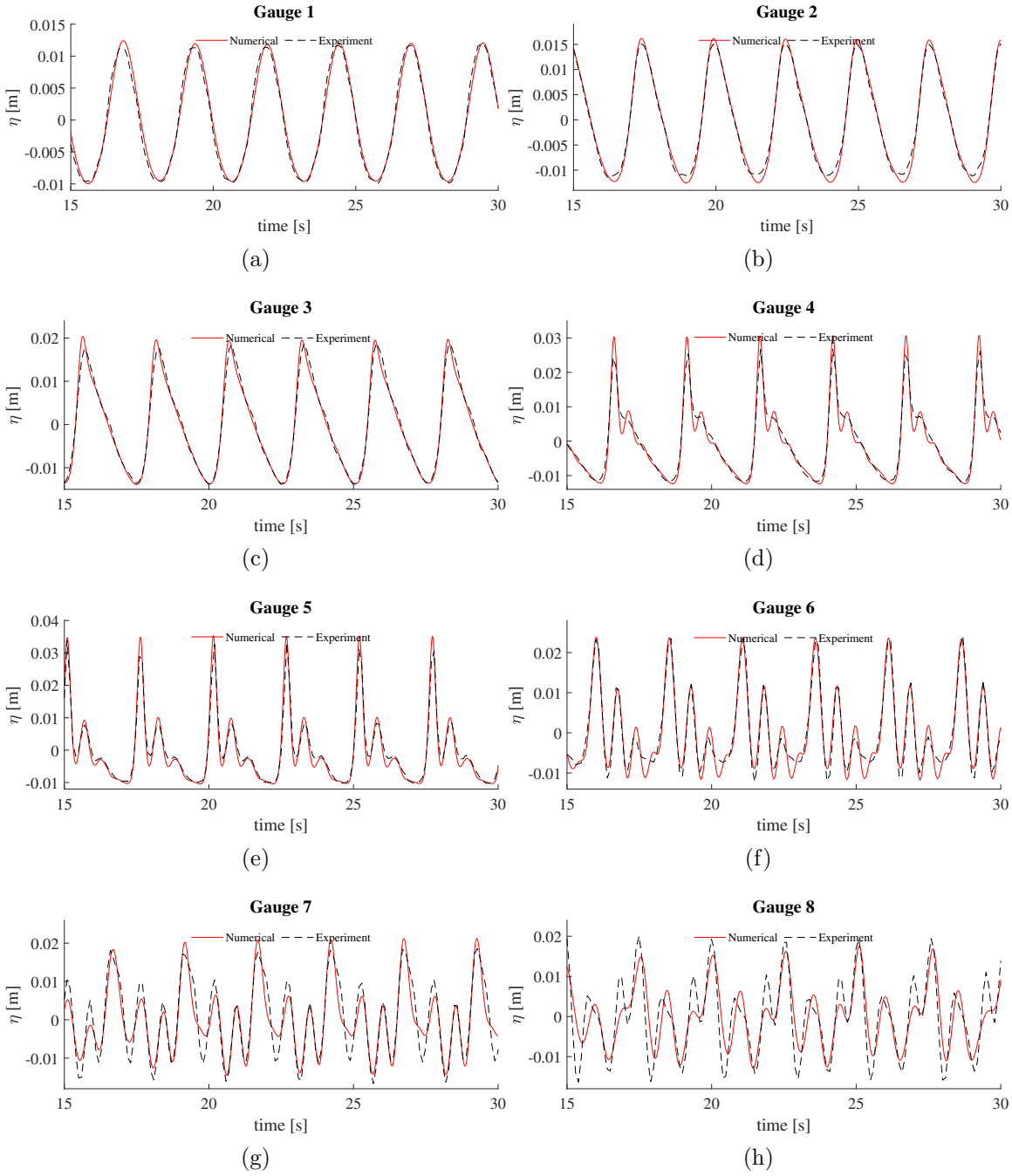

Figure 5.7: Time series comparing the numerical and experimental profiles from the eight different wave gauges starting in figure (a) until figure (h). Wave evolution using REEF3D::SFLOW approach, with H=0.022 m, T= 2.5 s and CFL=0.5

Test 2 - H=0.035 m, dx= 0.01 m, T= 2.5 s

The second test is considered a transition between a good approximation from Fig. 5.7 and a less accurate wave evolution capture at Fig. 5.9 - below explained. This is reflected on a good approximation including amplitude and wave phase until Fig. 5.8 (d). From this point of the simulation onward high frequency components - second and third wave crest - started presenting shaper crest and higher amplitudes a bit apart from the experimental data profiles. Profiles still showing good matching pattern, however, de-shoaling effect produced a greater effect on capturing process resulting on less accurate computations. The higher the wave, the higher the transformation of waves on the lee slope. Gauge 4 on Fig. 5.8 (d) also presented the highest wave with $\eta \approx 0.06$ m which represents an $\approx 80\%$ higher value than the set-up input value. As a contrast, Gauge 8 at Fig.5.8 (h), shows the greatest differences regarding matching profiles on Test 2. Even though patterns of the different crest - higher frequency components - are similar, the differences on amplitude are enormous. The highest crest of the experimental data - dash black line - reaches a free surface elevation value of ≈ 0.025 m. On the other hand, numerical data - red continuous line - barely pass η 0.015 m. As mentioned above, this big differences between experimental vs numerical data at the end of the submerged bar, might be attributed to de-shoaling effects and limitations of REEF3D::SFLOW approach regarding the principles of shallow water equations.

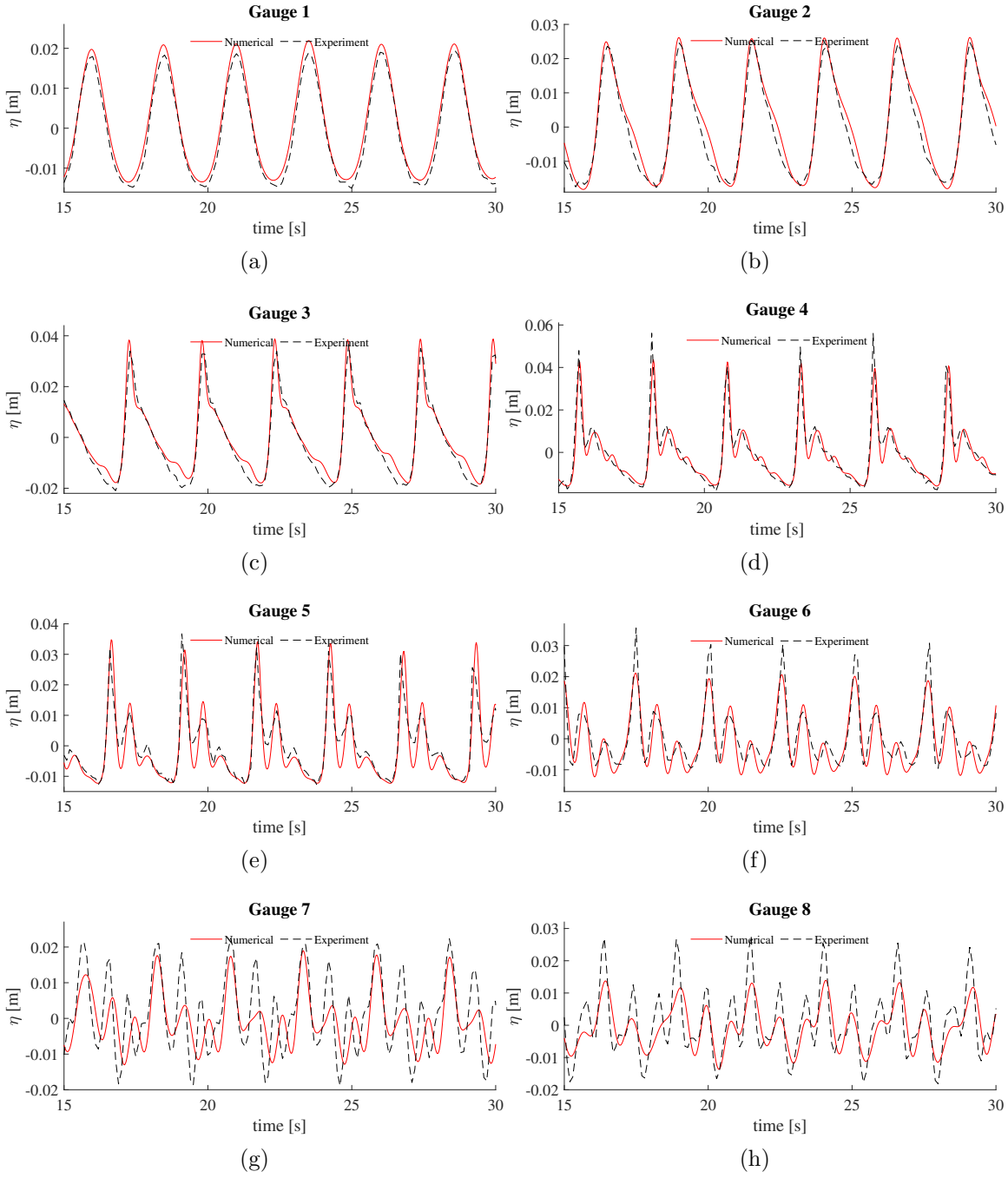

Figure 5.8: Time series comparing the numerical and experimental profiles from the eight different wave gauges starting in figure (a) until figure (h). Wave evolution using REEF3D::SFLOW approach, with H=0.035 m, T= 2.5 s and CFL=0.5

Test 3 - H=0.042 m, dx= 0.01 m, T= 2.5 s

In order to follow the wave variables described on Table 5.2 Test 3 was set-up with the highest wave - H= 0.042 m - chosen for this validation case. The sinusoidal wave then offered another type of wave breaking - plunging -, thus, it produced a different wave behaviour due to its wave height and the ratio d/λ. The wave propagation and transformation showed some differences on wave amplitude since the first section Fig.5.9 (a). Moreover, shoaling effects during Test 3 appeared before than on the two previous cases, as a result of a longer wavelength λ. The wave feels the bottom of the front slope before, therefore, the transformation of the waves occurred in an earlier stage Fig. 5.9 (c).

Waves reach their higher amplitude before the flat part of the submerged bar, on the edge between the flat top and the end of the front slope. Free surface elevation increased on a lower rate than on the previous case with $\eta \approx 0.06$ m. It represents an increment of wave height barely greater than 40% of the original value. Time series conserved similar patterns, however, second and third wave components presented sharper crests. High frequency components also presented differences on wave amplitude in comparison with experimental time series. In some cases -Fig.5.9 (f) and (h) - wave height was considerably reduced. Kamath et al. (2017) [36], reported also test 3 with same wave variables and as a plunging breaking type due to the wave amplitude. It was also mentioned the complexity to capture the free surface changes from the mixing process of air and water with REEF3D::CFD approach. Regarding REEF3D::SFLOW approach limitations, this model can deal with plunging breaking type, however, overturning process might be not fully taken into account.

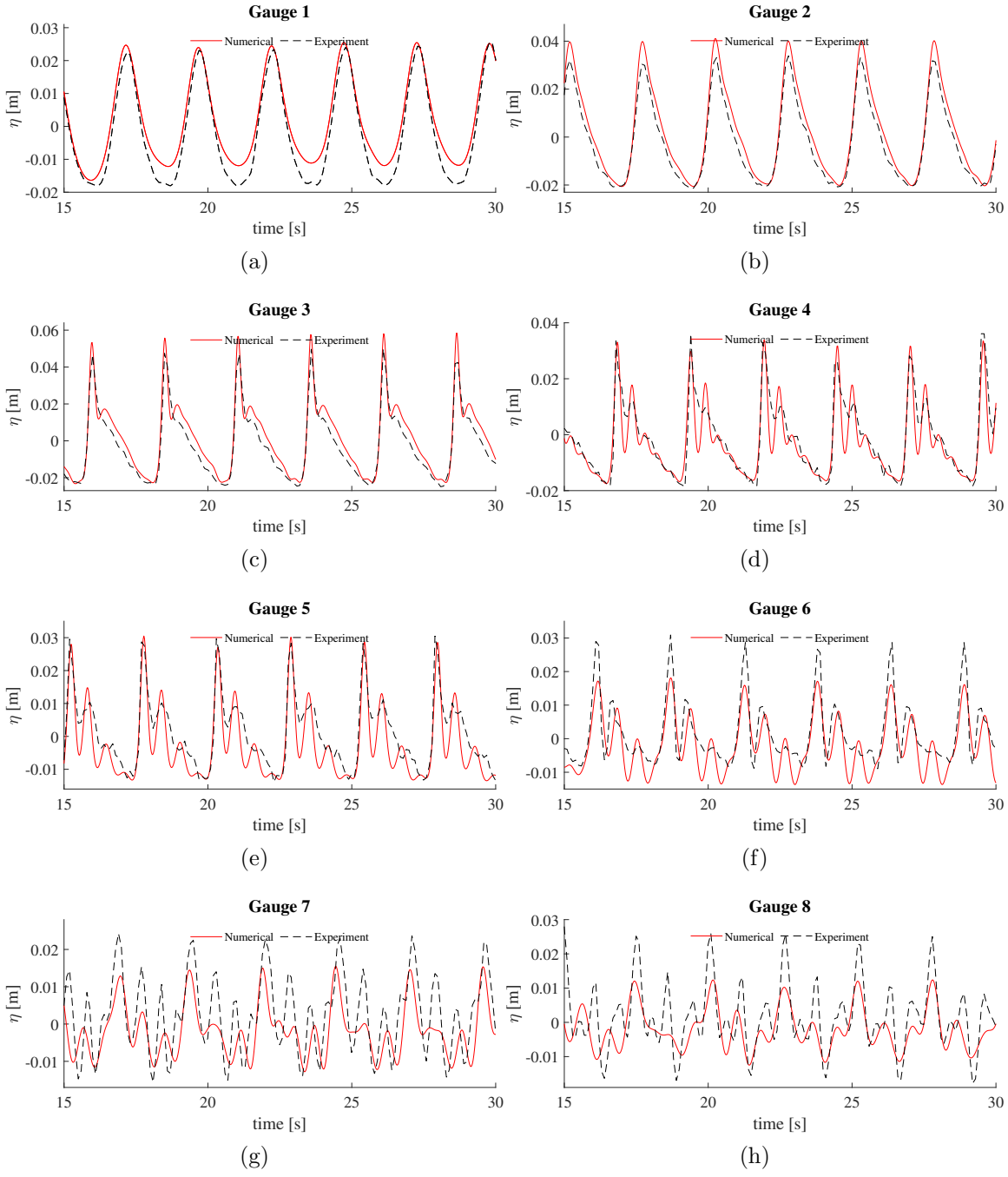

Figure 5.9: Time series comparing the numerical and experimental profiles from the eight different wave gauges starting in figure (a) until figure (h). Wave evolution using REEF3D::SFLOW approach, with H=0.042 m, T= 2.5 s and CFL=0.5

5.2 Case Study: Flatøya fish farm

As mentioned above, Norwegian authorities are pushing aquaculture industry to be located on the offshore part of the Norwegian coast. Notable positive impact over Norwegian economy had been produced by aquaculture industry during the last decades, contrasting with the huge negative environmental impact associated with the industry within the fjords. For more details regarding Norwegian coastline features reader could check section 1.1.
Fjords are considered a fragile environment and different aquaculture companies are taking a step forward to help on the conservation of those environments. It is planning to develop an offshore aquaculture site under the influence of the harsh ocean conditions of the Norwegian Sea.
Different wave models were applied to find to most suitable numerical model for the unique conditions at the Norwegian coastline.

5.2.1 Bathymetric map

A reliable bathymetric information is the key to obtain a trustworthy simulation while working with real case scenarios.
Two different bathymetry maps with different resolution - 2 and 10 m - were combined to obtain the most possible details of the bathymetric features. This bathymetric base map was provided by $NorConsultAS$. However, during the coupling process of the two different resolution maps some features and important details of the different islands were completely modified or lost. Therefore, a manual post-process to recover those several geographical points was carried out. This post-process consisted in localising the areas of interest on the big scale map - Fig. 5.12 - and compare them with the map on the website $a3.kystverket.no$. This website is part of the Norwegian Coastal Administration department, therefore, there is a high reliability on the amount of details and information regarding Norwegian coastline.
A raw data *.txt* file containing the combined maps data above mentioned was processed through SURFER software. First the file provided was opened as $GRID - Data$. A box popped out - Fig. 5.10 - where the X, Y and Z components have to be placed with their equivalent column from the data file loaded. A Kriging gridding method was chosen - interpolation method - and a grid size of ≈ 20 m was selected. Finally, the limits of the grid on X and Y directions had to be checked out. The maximum and minimum values placed there have to correspond with the limits of the domain of the raw data, otherwise, the grid generated will not correspond with the raw data.

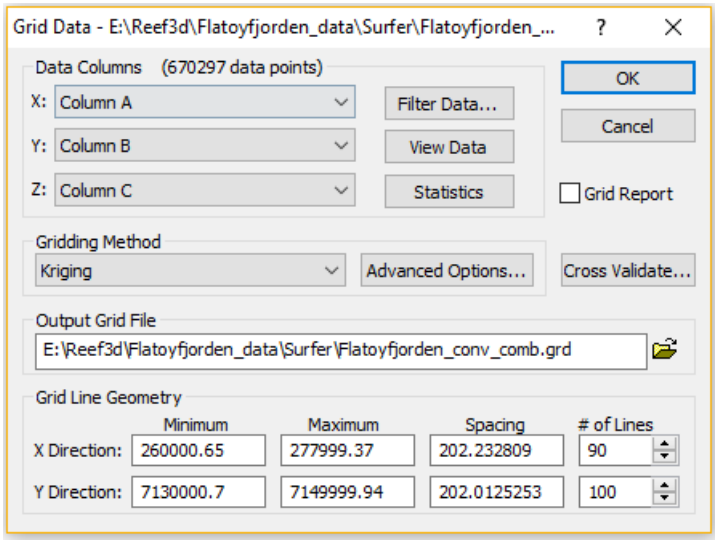

Figure 5.10: Step 1 on grid acquisition process by using SURFER software. Different varibales can be find here such as the limits of the domain and the grid spacing, also including the type of interpolation method applied among others variables.

Fig. 5.11 (a) shows a zoom in map from Flatøya Island obtained by using the Norwegian Coastal Administration department website. Through this thematic map is possible to get bathymetric information of a specific area, and the possibility to use it with several different coordinates systems available on the website. For this study WGS-84 / UTM zone 33N coordinate system was used. The information obtained from Fig. 5.11 (a) - latitude, longitude and depth - was used to identify and correct the wrong nodes contained on the raw grid map showed on Fig. 5.11 (b). Depth is referred on the software as Z column. Through the SURFER post-process it is possible to modify by hand only Z value of a single node at the time. It might be identified on the left-top corner at Fig. 5.11 (b). The red dot contained on the central part of Fig. 5.11 (b) was placed there to exemplify the amount of nodes contained on a single and small section of the raw grid. Therefore, readers could realise the amount of time that was needed to modify a single and small section of the raw grid data, considering also the scale located on the left-bottom corner of Fig. 5.11 (a) and the dimension of the island in comparison with the full map Fig. 5.13.
By changing the depth value we were re-designing contour 0. The contours represent Mean Sea Level - MSL - 0 m. Left side of Fig. 5.12 (a) and (c), show the raw data with sharper shapes on contour 0. Raw data contours might be identified by the red lines. Full sections were completely erased or added such as the top and central sections of Flatøya Island on Fig. 5.12 (c).

(a)

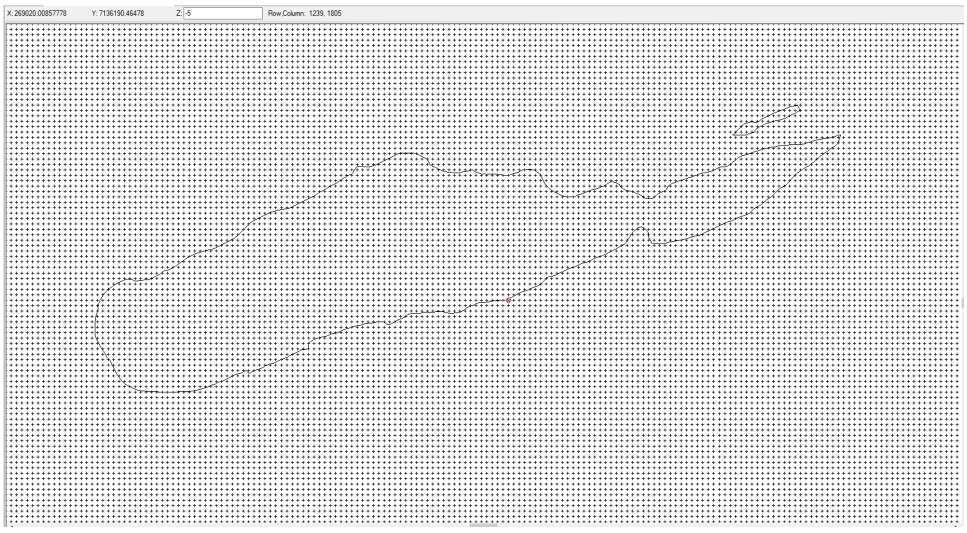

(b)

Figure 5.11: a) Thematic map showing geographical information. White box include: Latitude, Longitude and Depth. Source: a3.kystverket.no. b) SURFER grid map with nodes, showing the coordinates information from the node highlighted in red. The specific coordinates information from this single point can be found on the left-top corner. These figures are referred to 32633 - WGS 84 / UTM zone 33N N: 7136456 E: 268475.

As is possible to see in Fig. 5.12, the number of wrong nodes needed to be corrected was enormous. It is a long but very important process. The correction of the nodes

will determine the accuracy on the bathymetric map. This step resulted on a higher importance to obtain as much details as possible from the features of ocean bottom. As mentioned in section 1.1, a coastline covered by fjords produces an unique behaviour on the wave propagation and transformation. Therefore, there is a need to capture as much details as possible from the different channels and islands around the study area.

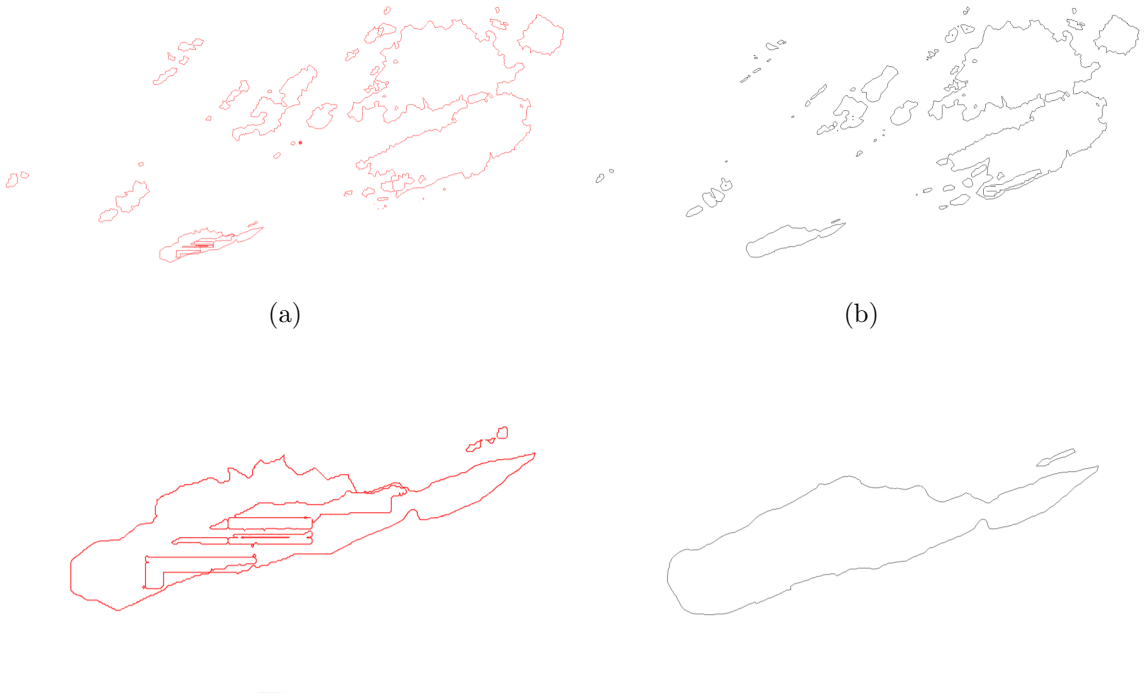

(a) (b)

(c) (d)

Figure 5.12: Comparison between raw data before SURFER post-process and the final data. These figures are referred to 32633 - WGS 84 / UTM zone 33N N: 7136456 E: 268475. Top part of each figure represent True North. a) Zoom out map raw data; b) Zoom out map processed data; c) Zoom in map of Flatøya Island raw data; and, d) Zoom in map of Flatøya Island processed data.

Once all the modifications of the nodes were finalised, a full-scale map was generated using SURFER software - Fig. 5.13 -. This process gave us a database map including a *.dat* dataset file with three different columns: longitude, latitude and depth. The file generated will be used as an input by REEF3D::CFD approach. It is necessary to modify its name to *geo.dat* before to be included on the numerical model.

Figure 5.13: Full scale map of study area generated through SURFER and used as an input for the fish farm case simulations. Black lines delimit the contour zero within the domain and the area of interest is locate in 32633 - WGS 84 / UTM zone 33N N: 7136456 E: 268475.

5.2.2 Fish farm grid

Cage array proposed for the fish farm can be observed in Fig. 5.14 (a). It is located on the relative protected Eastern part of Flatøya Island. The island itself together with the different islands in the surrounding area - Northern area - could produce a shadow effect where the rough ocean wave conditions could be diminished. This also could increase the time where the fish farm might be not exposed to those harsh ocean waves. The cage array is composed by five independent lines containing four squared fish cages each line.

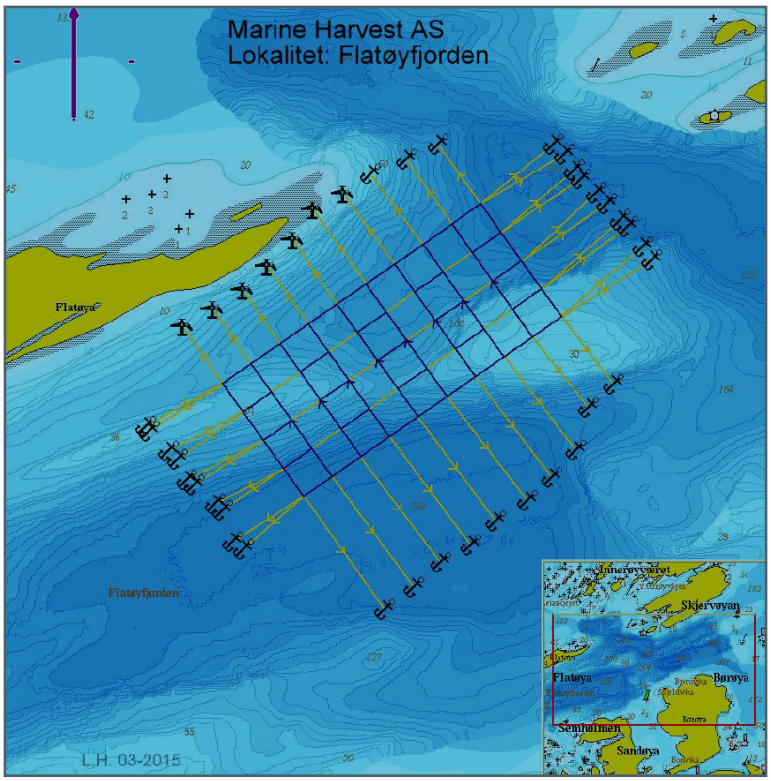

(a)

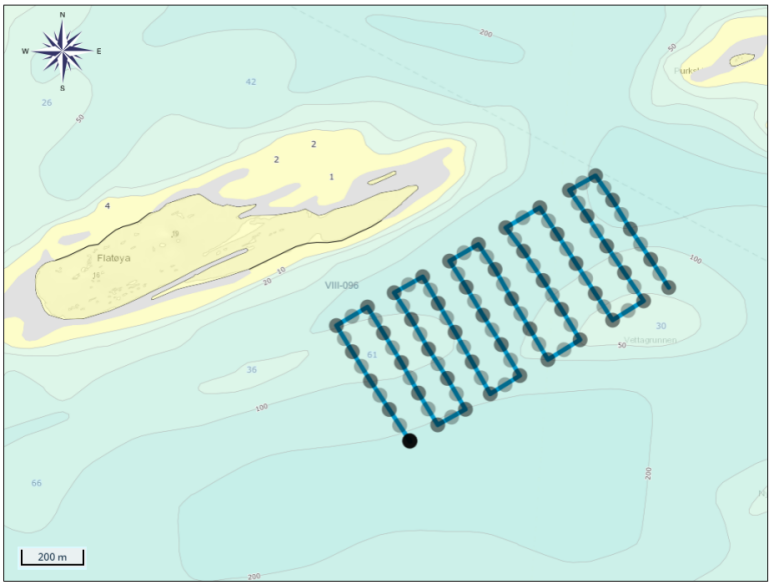

(b)

Figure 5.14: Fish farm grid location (32633 - WGS 84 / UTM zone 33N N: 7136456 E: 268475). a) Fish farm cage location proposed by Marine Harvest AS. Source: NorConsult. b) Wave gauges array locations determined through an on-line thematic map. Source: a3.kystverket.no

Therefore, 50 different wave gauges - WG - were proposed to be used during the simulations. The criterion used to choose the amount of WG and the location to place them was simply using the intersections of each line with the squared fish cages - Fig. 5.14 (b) and Fig. 5.15 -. The higher number of WG proposed obeys to the number of details required from the decomposition of the waves on this area and the extension of the total area $\approx$ 500,000 m^2.
The total of the fish farm is located on the main channel front of the Eastern part of Flatøya Island. Wave travelling through the Northern part of the island could be completely transformed and decomposed due to the depth water of the area, which is characterised by a rapid transition from deep water to shallow water - shoaling effect- and also areas where the transition occurs on the opposite way from shallow to deep waters - de-shoaling effect -. All this process will diminish the energy contained on a set of waves arriving on this area. However, it will also produce a n number of high frequency components after waves reaching shallow sections.
Through the use of the Norwegian Coastal Administration department website geographical coordinates for each WG were obtained. Dark grey dots - Fig. 5.15 - represent the locations of the points used as the inputs for the numerical wave gauges. Thus, WG coordinates - latitude and longitude - were obtained through the thematic map. The distribution of the wave gauges started from the Eastern point - WG 1 -, passing to the Northern point - WG 5 -, then to the Western - WG 46 - and finalising on the Southern point - WG 50 -.

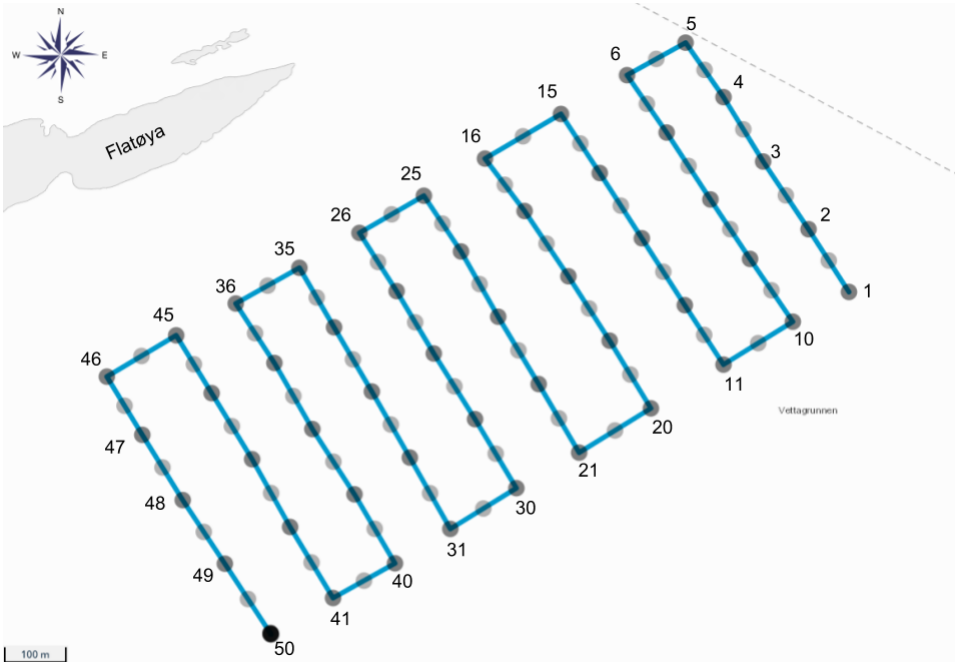

Figure 5.15: Wave gauge set-up, based on the fish farm grid scheme proposed by Marine Harvest AS. Located in 32633 - WGS 84 / UTM zone 33N N: 7136456 E: 268475. Grid built through an online thematic map. Source: a3.kystverket.no

5.2.3 Simulations Set-up

Once the bathymetric map was obtained - section 5.2.1 - and the wave gauges locations determined - section 5.2.2 -, wave parameters had to be defined. Through a collaboration with *NorconsultAS* it was possible to obtain the wave parameters from the central Western Norwegian Sea. The wave weather was extracted from an offshore numerical wave probe located nearby Flatøya Island on WGS-84 / UTM zone 33N N7138307; E266973. Numerical wave probe would be later described on STWAVE section.
The first step to set-up the simulations was to find the proper water level where the waves can propagate properly and the contour 0 is correctly set-up and kept during all the simulation.

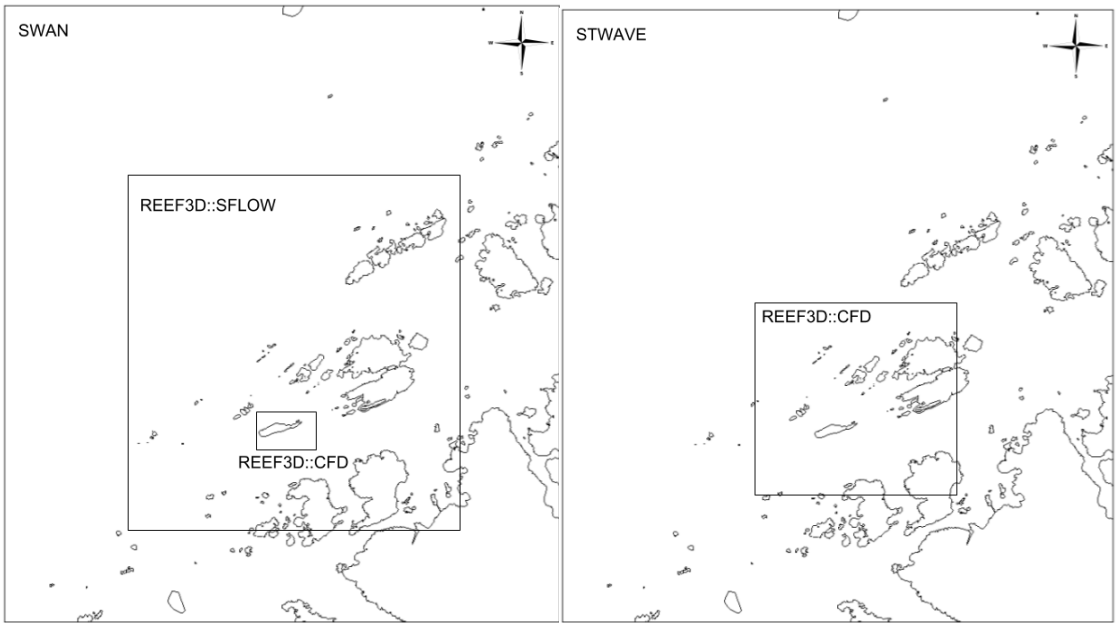

(a) (b)

Figure 5.16: Cascade of wave models methodology schemes. a) Original methodology applying three wave models. b) Modified Methodology applying two wave models. Rectangles on each figure represents the domain size of each numerical model.

There were some complications to find the correct water level due to the extension of the study area and also the characteristic features of the ocean bottom of a fjord system. Three different approaches were initially planned to be part of the cascade of the wave model method. This method consists of using the output of the coarse wave model with the biggest domain - spectral wave model SWAN - to feed in as input on the wave model of medium domain - REEF3D::SFLOW - and the final step was to use this last output data from the medium domain model to feed in the wave model with the smallest domain - REEF3D::CFD.

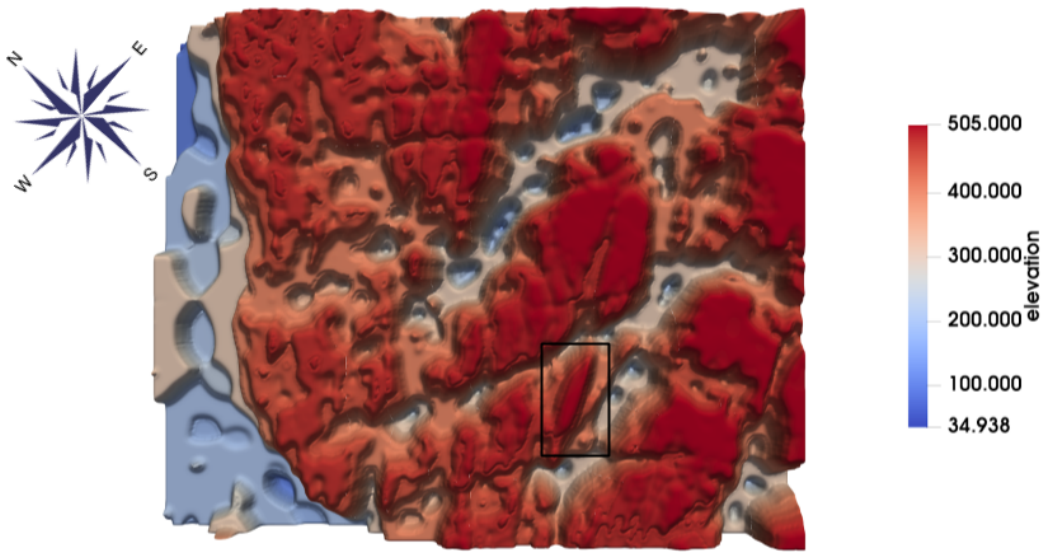

(a)

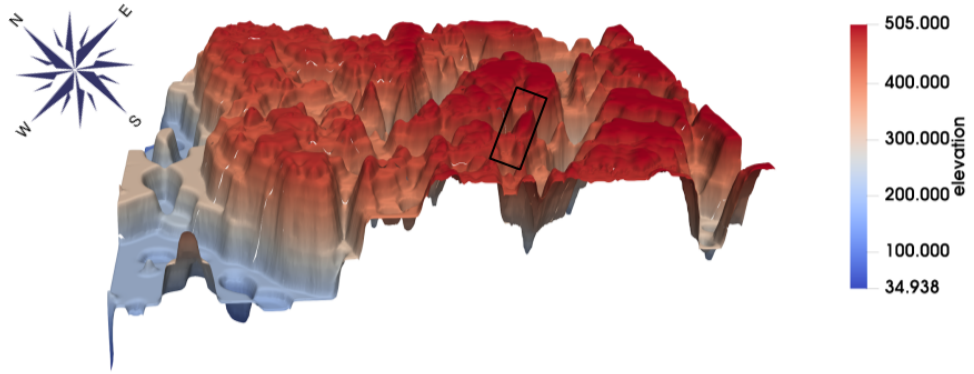

(b)

Figure 5.17: Initial full domain of the cascade of wave models methodology scheme. Bathymetric 3D map obtained through the simulations of REEF3D::CFD approach set-up from 0 to 305 m. Black rectangles highlight the location of Flatøya Island in both figures. a) Plan view. b) Side view.

In Fig. 5.16 (a) SWAN contains the full big domain with low resolution, followed by REEF3D::SFLOW with a medium resolution and the final step was the smallest domain with the highest resolution on REEF3D::CFD. Is important to clarify that the methodology applied during this study is base in a combined use of different wave

models, which differ considerably and might be confused with a coupling wave models methodology.
REEF3D::SFLOW approach was first tested, however, as was mentioned on the validation of this model - section 5.1 - it was not built to deal with abrupt changes of depth as the presences on Fig. 5.17 (a). Limitations of the wave model make the computation of the wave decomposition even harder. The presences of many deep channels all over the study area, in addition to several islands distributed around, enhance the complexity of Norwegian coast - Fig. 5.17 (a). As can be seen, the bathymetry can be rather deep near the fish farm and there are step-like dramatic changes of bathymetry near the shore, the impact of which also gets amplified due to the coarse resolution of the bathymetry data. Such situation introduces instability in the shallow water model REEF3D::SFLOW. An attractive alternative is REEF3D::NSEWAVE, which is under development for the improvement of computational speed in comparison to REEF3D. Since REEF3D::CFD has already been proven to be capable of simulating complex wave transformations [51] [36] [38], REEF3D::CFD is chosen to be used together with the spectral model STWAVE in this study because of their robustness. As CFD model demands relatively higher computational resources, a smaller computational domain is chosen for this case study. The key locations such as the fish farm site and the islands which have a direct influence on the wave behaviour near the fish farm are all included in the computational domain. The outer archipelago closer to the open sea is excluded for now. The resulting domain is shown in Fig. 5.18
Reduced REEF3D::CFD domain in Fig. 5.18 with a water level of 305 m, was find the simulation to well represent the shape of the islands and the mean sea level on contour 0, as well as, a realistic wave propagation pattern. Wave physical phenomena seem to follow regular distribution patterns with the wave crest adapting to the shape of the islands. The grid size dx was also fixed on 5 m and the wave generation zone was set-up with a length of 600 m and 800 m length of the numerical beach.

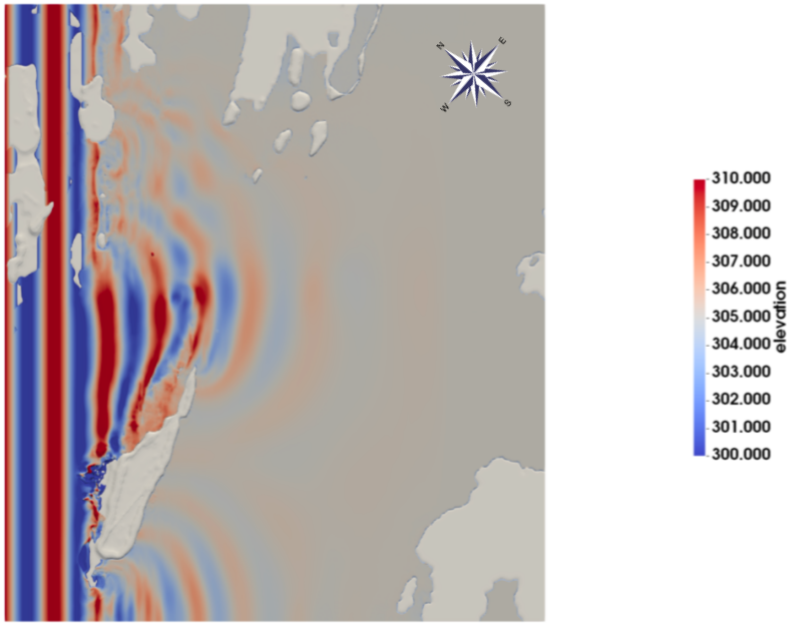

Figure 5.18: Final REEF3D::CFD approach domain. 3D map obtained through the simulations of REEF3D::CFD approach set-up from 0 to 305 m. The free surface elevation - η - changes are expressed on the colour palette as elevation in meters.

STWAVE

Spectral wave models as mentioned in section 2.1, are normally used with coarse grids on big domains. The inclusion of STWAVE as the spectral wave model from the large domain instead of SWAN, lies over the fact that *NorconsultAS* could provide the full wave weather of the Trøndelag region. It includes the surroundings of Flatøya Island. This action reduced one step within the methodology. It means that instead of using the output of STWAVE to feed in SWAN and then CFD, it could go straight from STWAVE to CFD. Thus, it reduces the amount of work and the time consumed in this first step of the simulation. Reliability of STWAVE was already proven [25]. STWAVE model was run with Cartesian grids of 750 x 750 m^2 resolution for the coastal region of Trøndelag. The parameters used during their simulations are included in Table 5.3. Here γ represents the peak enhancement factor for JONSWAP spectrum, nn being the directional spread. A significant wave height $Hm0$ of 5 m is chosen here as a conservative value to make the wave height coefficient only dependable on wave direction and period, and not dependent on wave breaking. The depth data is interpolated using a linear interpolation method to calculate the depths at unknown points.

Table 5.3: Parameters considered during the different simulations using the spectral weave model STWAVE.

Input parameter	**Value**
Offshore wave direction	240°, 270°, 300°, 330°, 360°
Significant wave height, $Hm0$	5 m
Peak spectral wave periods, Tp	10 s, 12 s, 14 s, 16 s, 18 s
Gamma for JONSWAP spectrum , γ	2.5
Standard deviation, nn	20
Number of rows	300
Number of columns	300
Cell size	750 m
Number of frequency distribution	30
Minimum frequency	0.04 Hz
Maximum frequency	0.33 Hz
Number of angle distribution	72
Minimum angle	0°
Maximum angle	360°

Each wave angle was run with each different Tp value from Table 5.3. From these simulations, a wave angle of 300° with a Tp=12.5 s resulted on the highest combination of wave heights observed outside Flatøya. The STWAVE simulations were run with a different objective than the one stipulated for this study.
Therefore, in Fig. 5.19 the probe location represents the grid points that are converted to numerical wave buoys to measure the wave spectra outside of Flatøya Island. Numerical wave station works in the same way as a meteorological buoy in the open ocean. Sensors placed inside the buoy will record any variations on the parameters previously set-up for the buoy. Likewise, a numerical probe was set-up to record the evolution of the wave spectrum passing over this specific point during the full simulation. Wave parameter values set-up for STWAVE simulations - $Hm0$ = 5 m, θ=300° and Tp=12.5 s - were slightly different from the parameter values recorded on the numerical probe. It is a result of the wave transformation effect during the propagation from the open ocean until waves reach the numerical probe. Physical phenomena such as refraction, diffraction and shoaling effects produced modifications on the wave parameters.

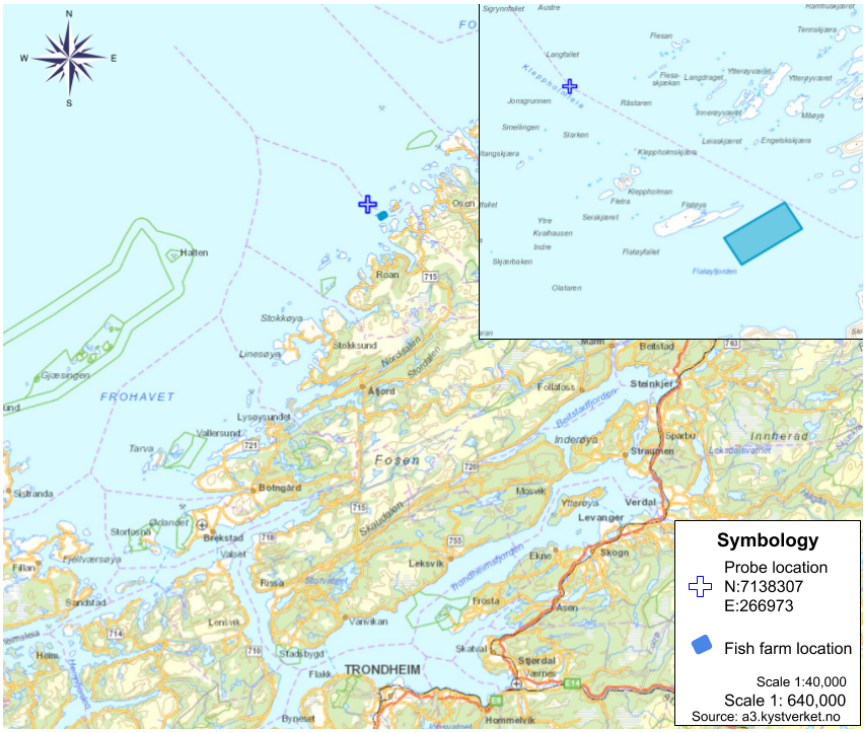

(a)

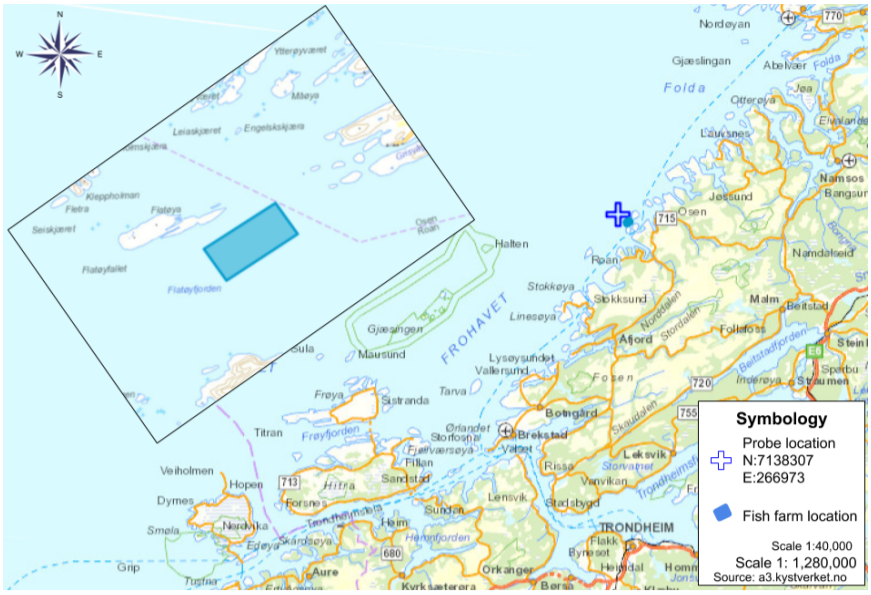

(b)

Figure 5.19: Trondelag coastal region. a) STWAVE probe and fish farm locations. b) Final dimensions and orientation of both domains used on the cascade of wave models methodology: STWAVE, with the big domain; and, CFD with the small domain. Base maps source: a3.kystverket.no

As mentioned above, wave refraction coupling with the shoaling effect will directly

modify the wave height, wave period and angle of approximation. Diffraction effect might also change the angle of approximation of the waves. The velocity of the waves decreases, when the water became shallower, therefore, a direct affection on the wave period was produced. Thus, the outputs from the STWAVE numerical station were $Hm0 = 5.7$, $Tp = 12.5$ s and $\theta = 325°$. This is the data used as an input for REEF3D::CFD approach.

REEF3D::CFD

Summarising, the pre-procedures followed to obtain the full parameters for REEF3D:: CFD approach simulations were: a bathymetric map was build and the correct domain size was set-up; position of wave gauges grid acquired to cover the total extension of the fish farm development; cascade of wave models including the number of numerical models and their domain size, and wave weather variables obtained from STWAVE model simulations. Simulations were run with a 2nd-order regular Stokes waves. The most relevant parameters used during the simulations were placed on Table 5.4.
Once the correct domain size was set-up - Fig. 5.20 -, the angle of the domain was rotated $\approx 50°$ to the left. The left side of Fig. 5.20 represents the full domain in its original position. The right side of Fig. 5.20 shows the domain in its final position applied on REEF3D::CFD approach. Thus, its rotation was carried out to make the propagation of the waves - generation zone - to start on the left side of the domain.
Before to continue with the explanation of the simulation results and to help the reader to follow the findings in Fig. 5.21 the colour scale presented was defined as: wave crest or higher point of the wave is defined by a red colour and the wave through with a blue. The more intense the colour on the wave front, the higher - red colour - or lower - blue colour - the wave height values. Patterns near to grey pattern are approaching to mean sea level / water level 0.
Moreover, the transformation of the waves from the STWAVE numerical probe to the REEF3D::CFD domain were unknown. However, the waves parameters were assumed to not have a considerable variation during this gap between the two numerical models.
Reliable wave propagation was finally achieved as it is possible to observe in Fig. 5.21. Left-top corner of Fig. 5.21 (a) presents few different islands straight on the left boundary of the domain. Those islands did not present any interaction with the wave front because the generation zone was extended to exclude them from the simulation. Due to the proximity of the islands with the domain boundary, in addition with the generation of the waves occurring straight in their location, these obstacles could also produce complications to capture the full wave transformation. Avoiding the interaction of these islands during the simulation helps to diminish the issues faced before, during the selection of the domain size.

Table 5.4: Parameters considered during the simulations using REEF3D::CFD approach.

Input parameter	**Value**
Wave direction, θ	310°
Significant wave height, $Hm0$	5 m, 5.7 m
Peak spectral wave periods, Tp	12.5 s
Cell size, dx	5 m
Simulation time, t	600 s
Time-step, CFL	0.25
Generation zone length	600 m
Numerical beach length	800 m
Water level	305 m
Total number of cells	46,480,000
Number of cores	1024
Real simulation time required	≈ 5 hours

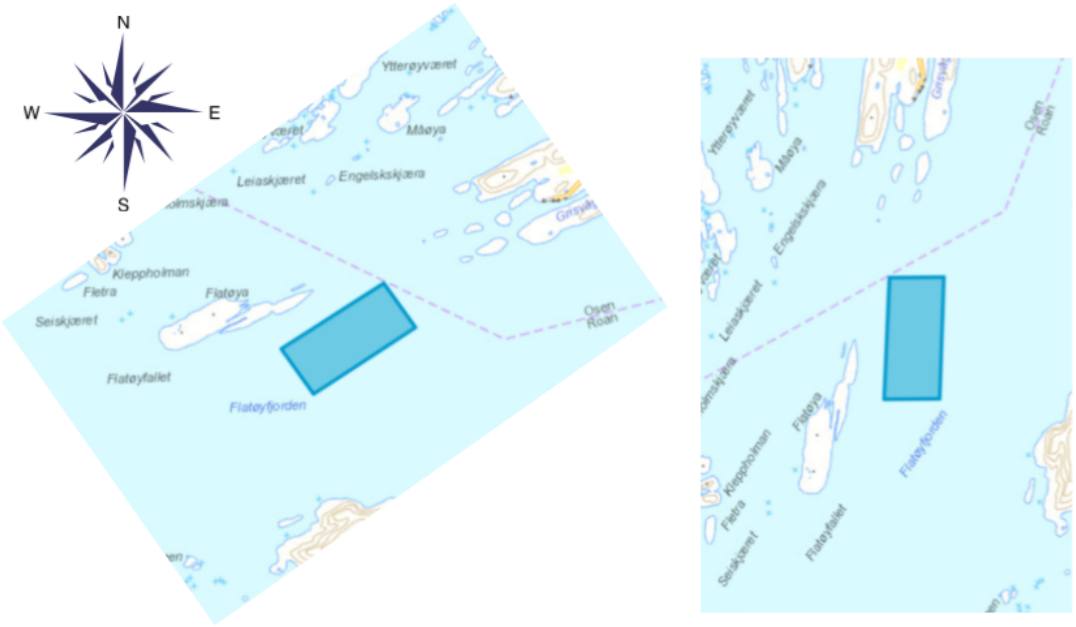

Figure 5.20: REEF3D::CFD approach final domain size located in 32633 - WGS 84 / UTM zone 33N N: 7136456 E: 268475.. Left side) Real orientation of the domain. Right side) Domain rotated ≈ 50° for simulations. Base map source: a3.kystverket.no

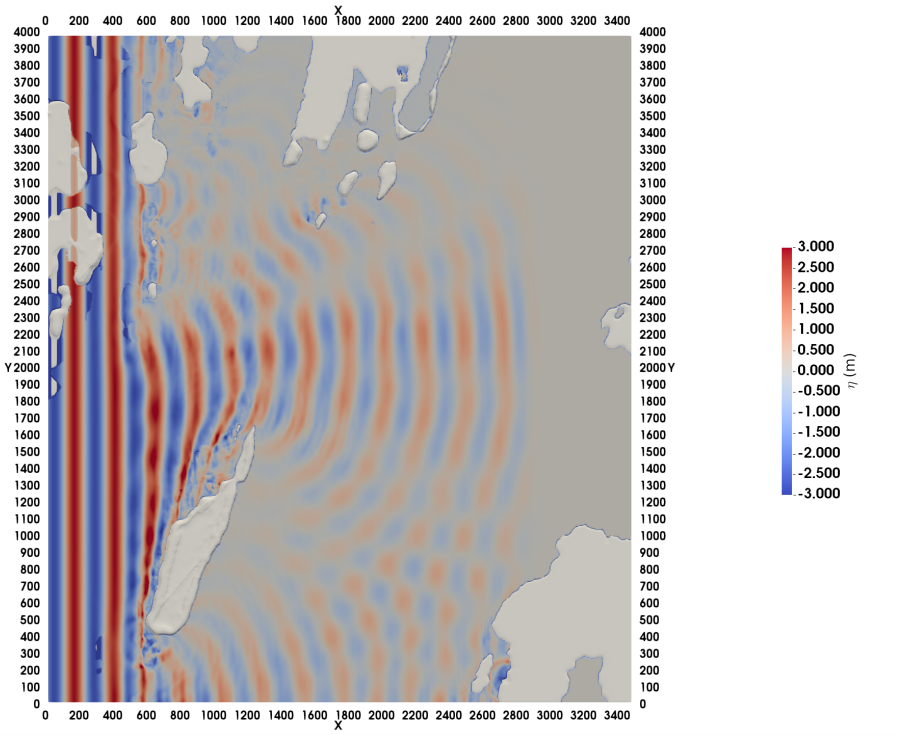

(a)

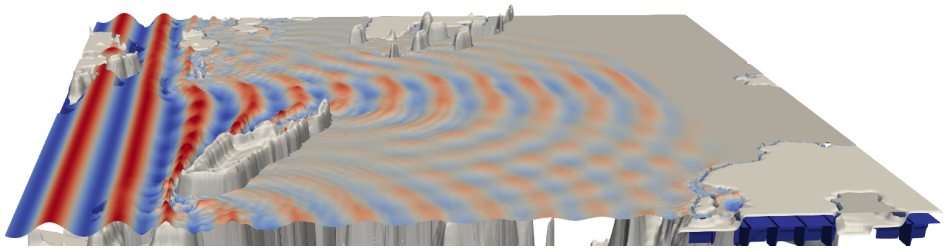

(b)

Figure 5.21: Full simulation showing the wave propagation and transformation by using REEF3D::CFD approach. a) Plan view. b) Side view. All the dimensions of the grid are in meters and it was set-up from 0 to 305 m.

The wave front presents an initial transformation firstly on the Southern part of Flatøya island in Fig. 5.21. The first wave transformation effect was the wave refraction phenomena identified with the wave crest tending to reach a parallel approximation with respect of the coastline. A second wave refraction effect is easily identified occurring almost at the same time on the Southwestern and Central regions of Flatøya island. Here, the wave front slowed down its velocity and impacted the beaches on the central part of the island while the rest of the wave front kept practically its original velocity an wave direction. The angle of propagation on the central region of the

island starts to be affected and the wave crest is tending to approach the beach at a close parallel angle. In the meantime, the waves slowed down its velocity at the central part of Flatøya island, as a result of the wave refraction and the shoaling effect, the topography in the Northern part of the island - deep channels in Fig. 5.22 (a) and (b) - allowed the wave front to continue propagating. As a consequence, waves present a high value on wave height determined by the strong red colour pattern in Fig. 5.21.

The increment on the wave height in the Northern part of Flatøya island might obey to the waves been channelised, by following the deep features of the topography. The channelised wave pattern could be related with the wave refraction effects. This means that the wave energy refracted from both sides - Northern and Southern parts of the channel - converge in this area. Therefore, the highest wave height parameter of all the simulation - after the waves left the generation zone - seems to be located in the middle of the Northern channel.

Afterwards the wave front crossed the physical obstacles - represented by Flatøya island and the Northern islands - two different phenomena occurred: the high energy value contained on the waves due to the convergence effect is released toward the coastline on a fan shape; and the wave diffraction effect can be also identified in both sides of the channel.

Wave diffraction phenomena can be also identified on the Southern part of Flatøya island. As mentioned within the section 4.4, the wave diffraction occurs when the energy contained on the wave front, in this case, the wave energy convergence on the central section of the channel, is transmitted laterally to cover out the shadow zone of Flatøya island in Fig. 5.21. Similar process occurred on the Southern region of the island. In this section, a small portion of the wave crest conserved its angle of propagation, however, it is also possible to observe the lateral distribution of the wave energy into the shadow zone due to the wave diffraction effect. Spreading out the energy contained on the wave into a larger area can be described as a divergence effect. Divergence as well as convergence are effects produced by the wave refraction and the shoaling effect due to changes on depth. Therefore, the energy contained on this diffracted waves seems to be low. It can be corroborated by observing the colour pattern of the wave crest, this means that the closer the wave crest to the coastline the lower the wave height. By following the elevation of the free surface in accordance with the colour scale, on the Southern region of the island, it seems to show that waves are decreasing in height. This effect is more evident on its central region, where the shadow zone is located - this area is also known as the protected area.

Wave diffraction on the Southern region produced a sharp angle of wave approximation heading to the island. The wave crest seems to reach the shoreline at an angle of $\approx 90^{\circ}$ with respect to the beach axis. The distance between the wave crest diffracted

near the South boundary and the shoreline seems to be to small. Thus, waves did not have enough time to be transformed by the ocean bottom.

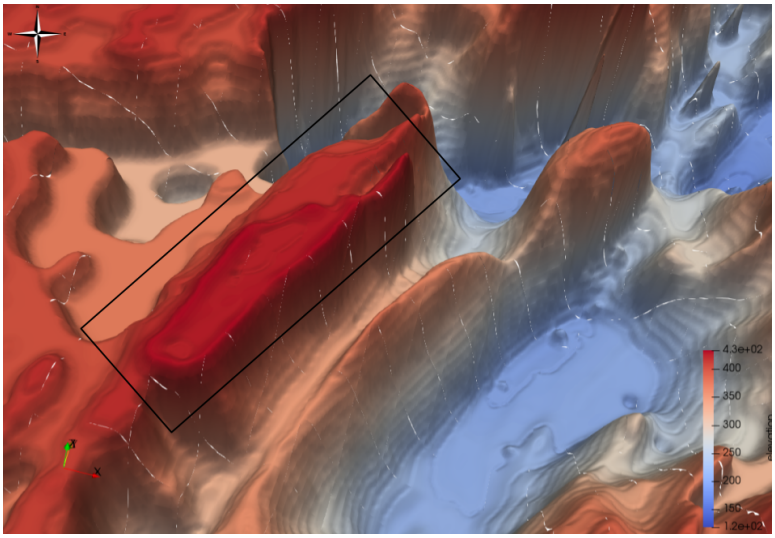

(a)

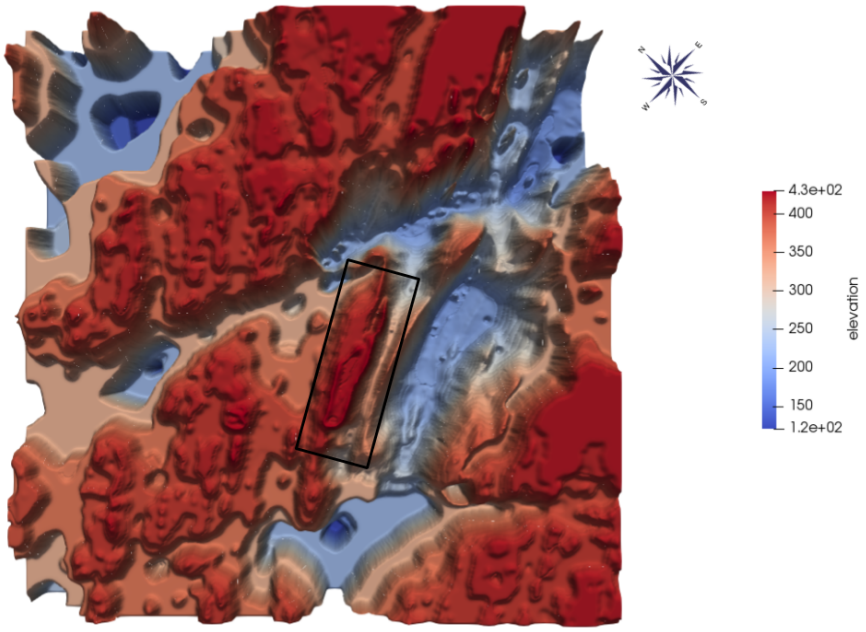

(b)

Figure 5.22: Maps on 3D obtained from REEF3D::CFD approach simulations. Black rectangles are used to highlight the presences of Flatøya island. Maps were set-up from 0 to 305 m. a) Zoom in of the main channel on the Southern part of Flatøya island. b) Two main channels surrounding Flatøya island identified in blue.

As a result of this angle, the refraction of the waves present a low effect at this

region. Similar occurs on the waves diffracted from the Northside. There the angle of approximation resulted higher than 90°, because when the wave front finish to cross the tip of the island, the waves are almost parallel to the shoreline and travelling toward the mainland.
The central region of the protected area of Flatøya island presents almost a total calm waters regarding the wave height. Here, wave fronts from both sides - Southern waves travelling toward the North-East and Northern waves travelling toward the South-East - collide toward the protected area in the central part of the island. In accordance with the colour scale in Fig. 5.21, this values seems to be close to 305.5 m in both cases. On the other hand, mean sea level - water level 0 - was set-up at 305 m. Thus, the shadow zone is having waves propagating there with a wave height of less than 1 m, from both directions of approximation. Therefore, the combined effect of wave refraction and diffraction phenomena offer a very calm zone. It seems to be an ideal area to place a fish farm development. However, this simulation only consider one single angle of approximation.
Wave reflection was clearly observed only in one spot, at the right-bottom corner of the domain. It occurs between Sandøya island and the mainland and presents a high reflection phenomena. This case seems to be important to be pointed out due to the wave height value observed. The wave reflected presents values - red wave crest - as big as the wave set approaching the exposed part of Sandøya island. In accordance with the wave height and the configuration of the topography between the island and mainland, this area could be acting as a resonance box, where the shorelines in both sides are not able to dissipate the energy of the waves.
The channelised waves as previously mentioned, present the highest wave height in open waters during all the simulation. Those waves were travelling through the main deeper channel, therefore, due to the de-shoaling effect the full wave front could be expected to decrease in high straight after Flatøya island. However, the results show that it did not happen and the waves conserved its height a bit longer in a small section of the wave front. This small section is located on the central part of the channel and can be attributed to an underwater ridge. The ridge is located right on the middle of the channel - Fig. 5.22 - and the wave front section with the high values travels straight on top of it. Once the waves passed the ridge the wave front seems to slowly decrease in wave height as a result of the de-shoaling effect.
REFF3D::CFD simulation also generates a dataset measuring the changes on the wave decomposition based on the location of the wave gauges described in section 5.2.2. As mentioned above, 50 different wave gauges were set-up, however, only 26 of them were analysed in accordance with its location in Fig. 5.23. Wave gauges were set-up only to measure free surface elevation - η. Wave gauges on the inner part of the grid illustrated on Fig. 5.23 were assumed to not show relevant differences with respect to those placed on the boundaries of the grid.

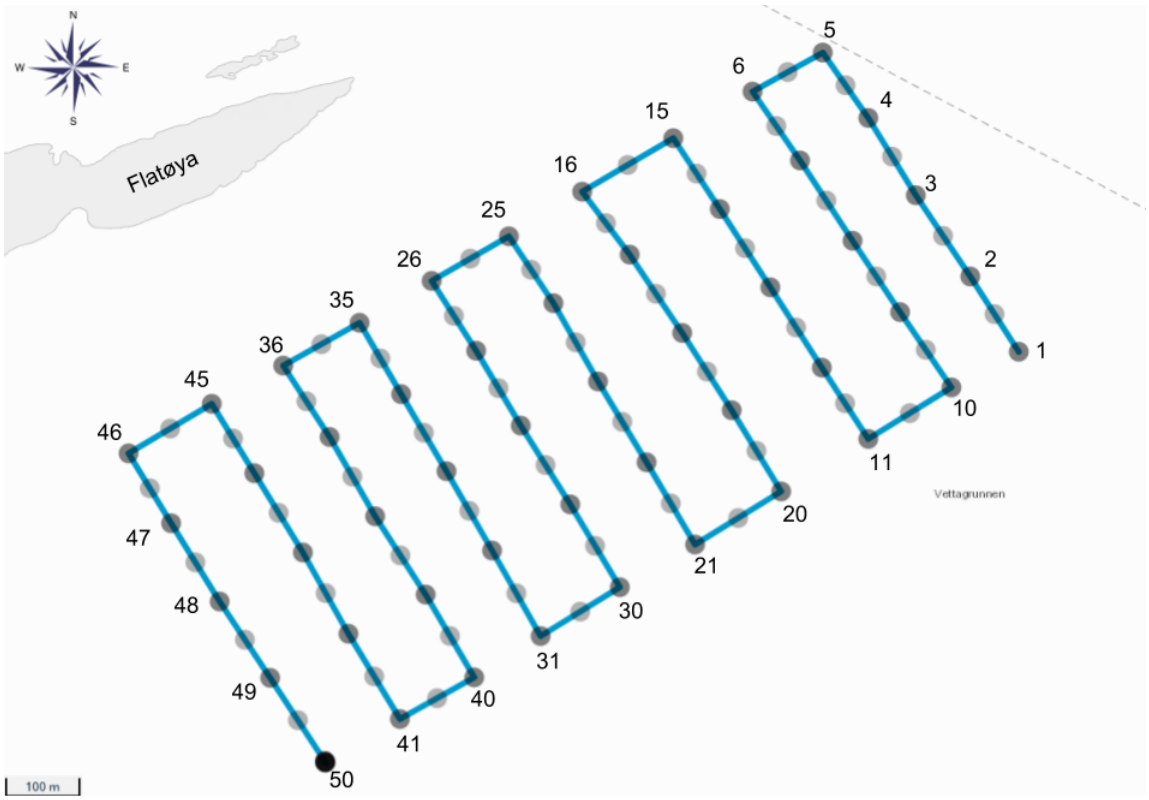

Figure 5.23: Wave gauges numerate were selected to be analysed through different time-series plots.

Fig. 5.24 shows the gauges line closer to Flatøya island - Fig. 5.23. Due to their high exposition to rough wave conditions, within this line of wave gauges is expected to find the highest η values. Above was already described the presence of a wave diffraction effect on this specific region, with an enormous affection due to the tip of the island. The modification the tip of the island produced on the wave propagation can be compared with a wave crest crossing a breakwater. The wave crest approaching the tip of the island can be observed orientated almost parallel to the shoreline axis. The section of the wave crest oriented straight in front of the island's tip was completely dissipated and the adjacent wave crest passed over. Once the wave crest crossed the island's tip the wave diffraction effect appears and the wave energy is distributed laterally. Thus, on Fig. 5.24 the evolution of the wave diffraction is observed from the highest wave height value - over 3.0 m - on Fig. 5.24 (a) to the lower wave height value - less than 1.0 m - on Fig. 5.24 (j).

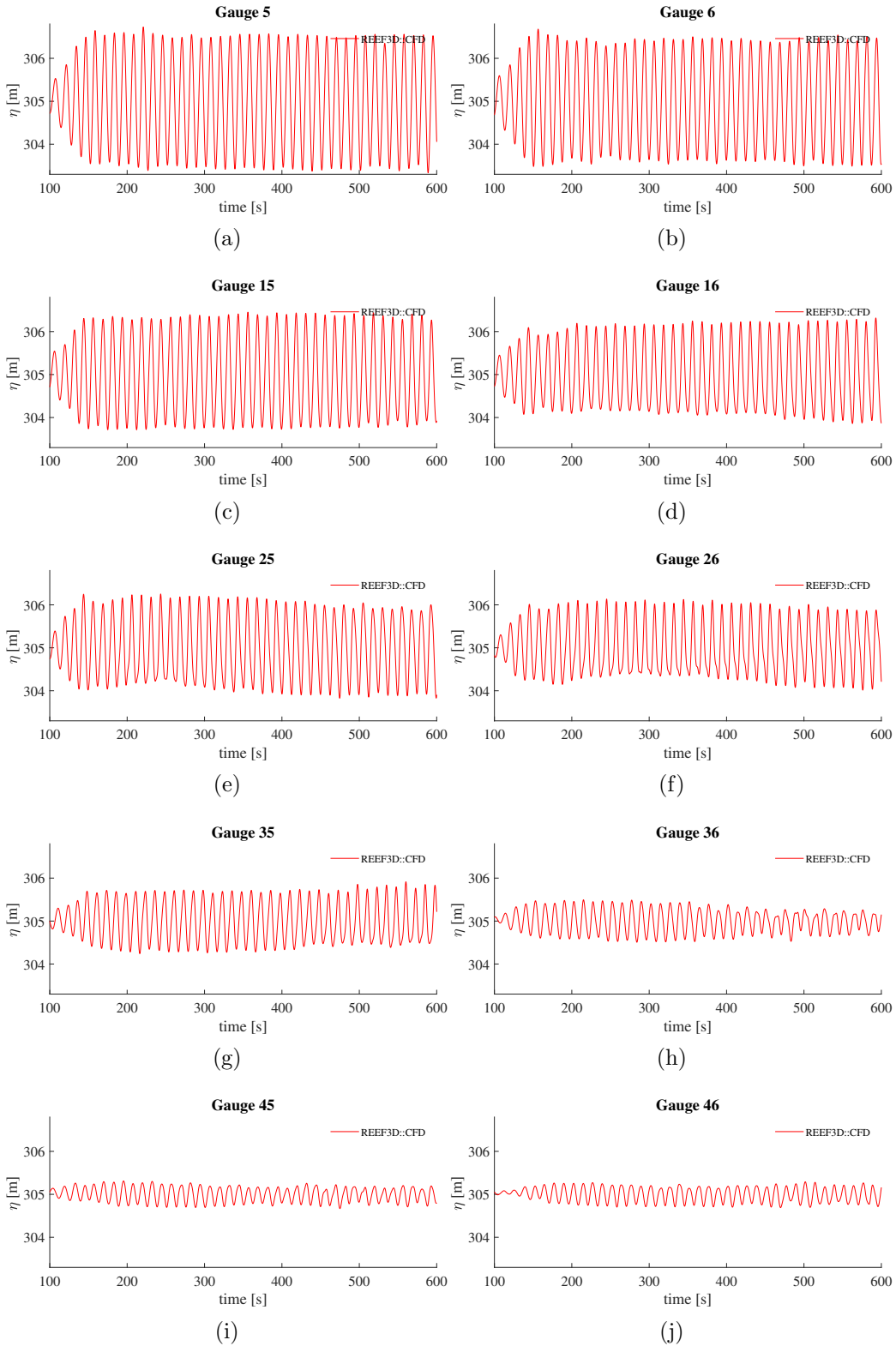

Figure 5.24: First section of the front line of the wave gauges arrangement showing the time-series from the plot (a) within the exposed area until the plot (j). Free surface elevation changes - η - through REEF3D::CFD approach, with $Hm0$=5.7 m, Tp= 12.5 s and θ=310°.

The elevation of the free surface can be observed to decrease gradually from the exposed area represented in Fig. 5.24 (a) toward the protected area represented in Fig. 5.24 (j). Closer the wave gauges to the shadow zone higher the variations on wave height. On the other hand, in the three first plots in Fig. 5.24 (a), (b) and (c), time series does not show changes on wave amplitude as it reminds almost constant. However, there is an evident inflection on the wave height tendency after the wave gauge 26 in Fig. 5.24 (f). Wave gauge 26 can be labelled as the last point of the wave gauges grid of the exposed area. From this point onwards the wave amplitude decreases dramatically.

A similar tendency can be observed in Fig. 5.25, with the highest values - ≈ 3.0 m - on the most exposed part and the gradually diminish on wave height. The pattern of the free surface elevation within these plots resulted a bit different due to the location of the wave gauges. These wave gauges are mainly located in the exposed region, and they were expected to record high values around the majority of the gauges than in Fig. 5.24. It did not occur as a result of the complex topography. Straight in front of the Eastern part of Flatøya island a deep channel was identified followed by an underwater ridge - Fig. 5.22. Waves partially transform passing from a shallow area to a deeper area will face a de-shoaling effect. There the energy contained on the wave crest is once again spread, however, de-shoaling effect produces the wave energy to be transmited vertically all over the water column. De-shoaling effects affecting the wave height does not produce a huge impact on its amplitude in this region. Wave height values recorded on this group of wave gauges varied from ≈ 3 m in Fig. 5.25 (a) to ≈ 2 m in Fig. 5.25 (h).

The group of wave gauges in Fig. 5.26 recorded the lowest wave height range differences. These gauges are also located straight on top of the channel above mentioned and identified in Fig. 5.22. The wave energy in this section is transmitted laterally by wave diffraction effect and vertically due to the de-shoaling effect. This two wave phenomena combined produce a huge impact on the wave crest reducing the wave height significantly. Fig. 5.26 shows wave height values <2 m in average and the lowest values in gauges 40 and 47 ≈ 1 m - Fig. 5.26. There was also possible to identify some high-frequency wave components in Fig. 5.26 (c). The presence of those few secundary waves is not possible to be associate with either of the wave phenomena already described and neither with topography features, due to the location of the wave gauge and how isolated this event happened.

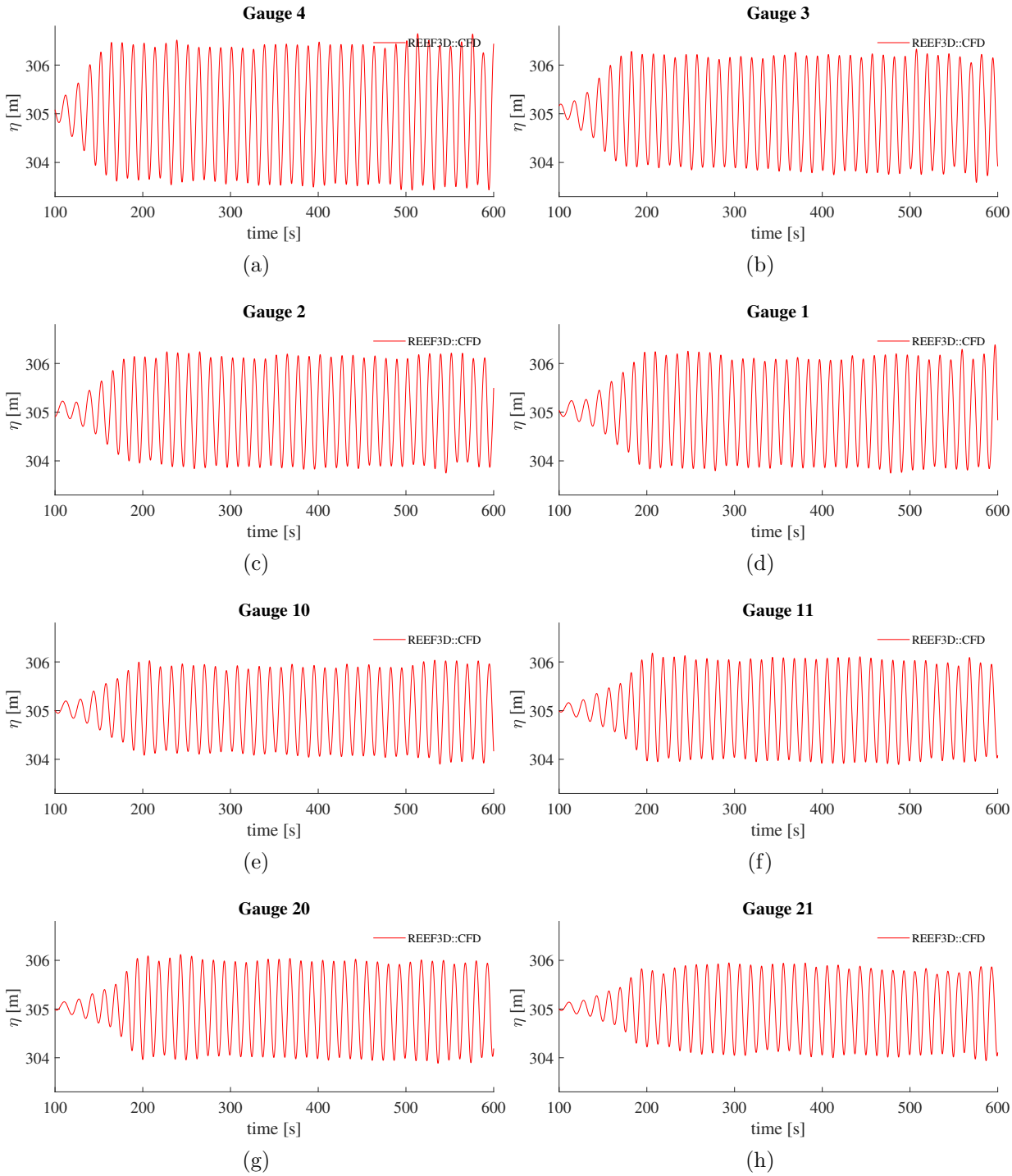

Figure 5.25: Second section include the exposed East line (external right-top section) of wave gauges arrangement showing the time-series from the plot (a) within the exposed area until the plot (h). Free surface elevation changes - η - through REEF3D::CFD approach, with $Hm0$=5.7 m, Tp= 12.5 s and θ=310°.

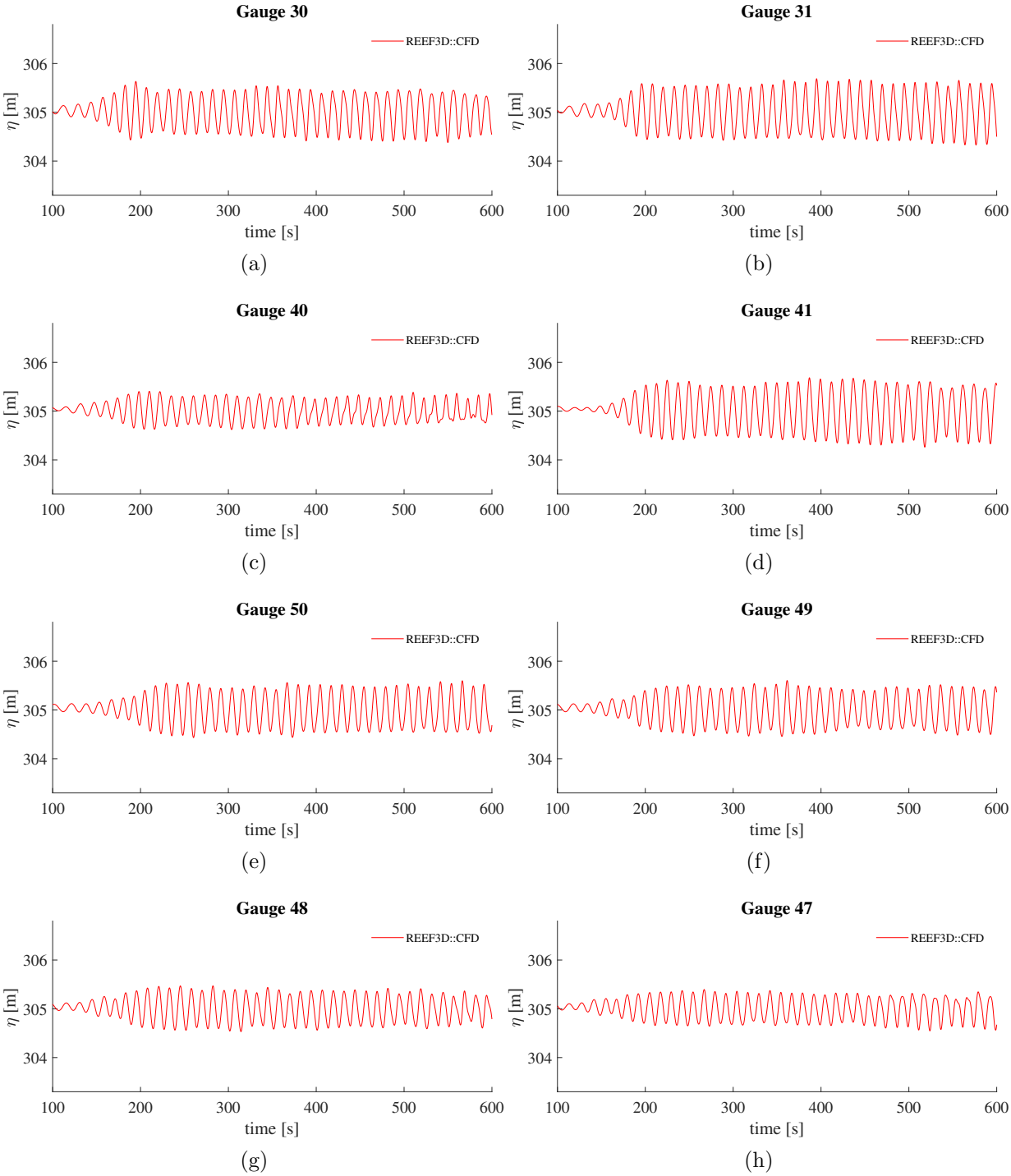

Figure 5.26: Third section include the Southern line (external left-bottom section) of the wave gauges arrangement showing the time-series from the plot (a) in the central region until the plot (j). Free surface elevation changes - η - through REEF3D::CFD approach, with $Hm0$=5.7 m, Tp= 12.5 s and θ=310°.

Chapter 6

Conclusions

This study was focused on the reliability while implementing more than one different numerical model to determining the evolution of the ocean waves in a complex system. Through the cascade of wave model methodology three different numerical models were proposed - SWAN, REEF3D::SFLOW and REEF3D::CFD . The combined use of them attempted to enhance the strengths of the models while reducing their disadvantages. Basic concept and foundations of these numerical models were also addressed. As a first step validation of the 2D numerical wave model REEF3D::SFLOW was carried out. This validation includes testing the performance of its numerical wave tank.

During the evolution of the different steps to properly set-up a simulation, few complications popped out while implementing the combined methodology. As a response, new approaches were added and some were discarded. The new adjustments consist of the combined use of only two different numerical models: the spectral wave model STWAVE and the high-resolution REEF3D::CFD approach.

A submerged bar case widely known was used to find the limits and advantages of REEF3D::SFLOW approach. During the three different tests the compute of the free surface elevation along the submerged bar were compare with experimental data, and the numerical results present generally a good agreement. Shoaling effects occurring on the lee slope seems to match well the experimental data both in terms of phase and wave amplitude. However, after the wave front passed the submerged bar, the numerical results start to show mismatch patterns in both terms of phase and wave amplitude. This demonstrates that the shallow water equation is capable of simulation waves with milder slope variations. However, when the ratio d/λ becomes too big, there will be numerical instability and the model becomes sensitive to de-shoaling effect.

REEF3D::SFLOW approach is an ideal tool to work with shallow water region. However, the user should examine the water conditions and apply this numerical model in the right region according to its limitations.

Norwegian coastline offered a great challenge due to its complexity regarding the topography features and the unique wave behaviour occurring through their interactions. Capturing the full wave decomposition by applying the cascade of wave model presented different adjustments. It could confirm that REEF3D::SFLOW is a numerical model suitable for shallow water conditions without dramatic bathymetry changes. If applied to a suitable location, REEF3D::SFLOW requires less computational resources and is less time-consuming. However, for complicated wave transformation over dramatic bathymetry changes, a high-resolution model such as REEF3D::CFD is more suitable. The new REEF3D::NSEWAVE is designed to fill the gap between accuracy and computational cost in the future.

The re-arrangement of the cascade of wave models seems to be a good option to analysis the wave conditions on complex scenarios as a fjord system represents. STWAVE model offer a reliable simulation of wave weather conditions in the open ocean with a coarse domain. Its limitations have the focus regarding the size of the domain and the accuracy to capture physical phenomena in coastal regions.

REEF3D::CFD approach seems to be the ideal numerical model to compute the full transformation of the wave field within the Norwegian coast. The high accuracy that this model can offers also became its own limitation, due to the high cost of computational demand required and the high time-consuming. The size of its original domain was increased to cover as much extension of the study area as possible without compromising its accuracy. The simulation shows how even a high-resolution numerical model could struggle to represent the wave decomposition properly if the set-up of the model was not carefully chosen.

The simulation applying REEF3D::CFD approach shows that Flatøya island and its surrounding area presents a complex interaction between the wave front and the local topography. As mentioned many times, the complexity of the system plays an enormous role on the wave decomposition patterns, thus, it should be the most relevant variable to consider during the simulation. This complexity made a wave front travelling toward mainland on the Northern part of Flatøya island, to change its direction, due to the wave refraction and shoaling effects, and made it cross completely the front part of the island and collide with the wave front on the Southern part of the island.

Due to the proximity between the different islands and the well know complexity of the system, wave reflection could be expected to has a greater impact on the region than the found it here.

The locations of the fish farm in the vicinity of the shadow zone product of Flatøya island seems to be accurate, in accordance with only one wave of approximation simulated. The Northern part of the fish farm could be exposed to the harsh wave front crossing over that channel. This asseveration is based on the wave height results found through the time series plots. Where closer the fish farm grid approach to the

shadow zone, the lowest the wave height was recorded. It could be diminished to around 1/4 - ≈0.7 m - than the wave height found it on the Northern section - over 3.0 m. The tendency of the wave height values seems to decrease toward the central part of the shadow zone due to the wave diffraction and the de-shoaling effect. The wave approximation range used during the simulation is limited to only one angle, therefore, is necessary to simulate a wider variety of angles on the wave approximation. During the description of the simulation in the previous chapter it was mentioned that the transformation of the waves from the STWAVE numerical probe to the REEF3D::CFD domain boundary was unknown. Therefore, it was assumed that waves parameters do not have considerable variations during the gap between the two numerical models. However, due to the findings as a result of the simulation applying REEF3D::CFD approach it is evident that the complexity of a fjord system resulted in a bigger challenge than the expected. The topography features could modify dramatically the wave propagation and transformation in a short extension by passing for one section of the fjord to another.

The combined use of STWAVE and REEF3D::CFD approach produced a general good agreement computing the wave propagation and transformation. The findings of this study could be used as a base to improve the use of the cascade of wave models methodology. This methodology proved that it is reliable to apply the output of a coarse numerical model as a input for the finer numerical model. Limitations regarding the domain size could be approached in a different way. The evolution of the waves could be fully tracked from the STWAVE numerical probe location until the shoreline of the mainland in front of Flatøya island, by applying a higher number of smaller REEF3D::CFD approach domains. Smaller the domain size set-up with a smaller cell size could reduce the time-consuming and it will offer much greater details of the wave decomposition.

Bibliography

[1] D. Adalsteinsson and J. A. Sethian. A fast level set method for propagating interfaces. *Journal of computational physics*, 118(2):269–277, 1995.

[2] E. B. Agamloh, A. K. Wallace, and A. von Jouanne. Application of fluid-structure interaction simulation of an ocean wave energy extraction device. *Renewable Energy*, 33(4):748–757, apr 2008.

[3] V. Babovic, S. A. Sannasiraj, and E. S. Chan. Error correction of a predictive ocean wave model using local model approximation. *Journal of Marine Systems*, 53(1-4):1–17, 2005.

[4] J. A. Battjes. Shallow water wave modelling. In *International Symposium on Waves - Physical and Numerical Modelling*, pages 1–24Battjes, J.A., 1994. Shallow water wave modell. University of British Columbia, 1994.

[5] S. Beji and J. Battjes. Experimental investigation of wave propagation over a bar. *Coastal Engineering*, 19(1-2):151–162, 1993.

[6] A. Bergheim, H. Hustveit, A. Kittelsen, and A. Selmer-Olsen. Estimated pollution loadings from norwegian fish farms. ii. investigations 1980–1981. *Aquaculture*, 36(1-2):157–168, 1984.

[7] J. C. W. Berkhoff. *Computation of combined refraction-diffraction*. Delft Hydraulics Laboratory, 1974.

[8] H. Bihs, A. Kamath, M. Alagan Chella, A. Aggarwal, and Ø. A. Arntsen. A new level set numerical wave tank with improved density interpolation for complex wave hydrodynamics. *Computers and Fluids*, 140:191–208, 2016.

[9] J. L. Bona and R. L. Sachs. Global existence of smooth solutions and stability of solitary waves for a generalized boussinesq equation. *Communications in Mathematical Physics*, 118(1):15–29, 1988.

[10] N. Booij and L. H. Holthuijsen. Propagation of ocean waves in discrete spectral wave models. *Journal of Computational Physics*, 68(2):307–326, 1987.

[11] N. Booij, R. C. Ris, and L. H. Holthuijsen. A third-generation wave model for coastal regions: 1. Model description and validation. *Journal of Geophysical Research: Oceans*, 104(C4):7649–7666, apr 1999.

[12] W. Boone, S. Rysgaard, S. Kirillov, I. Dmitrenko, J. Bendtsen, J. Mortensen, L. Meire, V. Petrusevich, and D. Barber. Circulation and fjord-shelf exchange during the ice-covered period in young sound-tyrolerfjord, northeast greenland (74 n). *Estuarine, Coastal and Shelf Science*, 194:205–216, 2017.

[13] T. Bunnik and R. Huijsmans. Validation of wave propagation in numerical wave tanks. In *ASME 2005 24th International Conference on Offshore Mechanics and Arctic Engineering*, pages 875–883. American Society of Mechanical Engineers, 2005.

[14] E. Caetano and V. Innocentini. An improved second generation wave model. *Brazilian Journal of Oceanography*, 51(unico):1–21, 2003.

[15] T. Campbell, J. Cazes, and E. Rogers. Implementation of an important wave model on parallel architectures. *Oceans '02 MTS/IEEE*, pages 1509–1514, 2002.

[16] L. Cavaleri, J.-H. Alves, F. Ardhuin, A. Babanin, M. Banner, K. Belibassakis, M. Benoit, M. Donelan, J. Groeneweg, T. Herbers, P. Hwang, P. Janssen, T. Janssen, I. Lavrenov, R. Magne, J. Monbaliu, M. Onorato, V. Polnikov, D. Resio, W. Rogers, A. Sheremet, J. McKee Smith, H. Tolman, G. van Vledder, J. Wolf, and I. Young. Wave modelling The state of the art. *Progress in Oceanography*, 75(4):603–674, 2007.

[17] Q. Chen, J. T. Kirby, R. A. Dalrymple, A. B. Kennedy, and A. Chawla. Boussinesq modeling of wave transformation, breaking, and runup. ii: 2d. *Journal of Waterway, Port, Coastal, and Ocean Engineering*, 126(1):48–56, 2000.

[18] A. J. Chorin. Numerical solution of the navier-stokes equations. *Mathematics of computation*, 22(104):745–762, 1968.

[19] C. o. E. Department of the Army Waterways Experiment station. Shore protection manual. *Coastal engineering researcher center*, 2, 1984.

[20] D. Enright, R. Fedkiw, J. Ferziger, and I. Mitchell. A hybrid particle level set method for improved interface capturing. *Journal of Computational physics*, 183(1):83–116, 2002.

[21] J. Fenton. Nonlinear wave theories. *The Sea -Ocean Engineering Science*, 9:3–25, 1990.

[22] J. D. Fenton. A FifthOrder Stokes Theory for Steady Waves. *Journal of Waterway, Port, Coastal, and Ocean Engineering*, 111(2):216–234, 1985.

[23] G. Ferentinos, G. Papatheodorou, M. Geraga, M. Iatrou, E. Fakiris, D. Christodoulou, E. Dimitriou, and C. Koutsikopoulos. Fjord water circulation patterns and dysoxic/anoxic conditions in a mediterranean semi-enclosed embayment in the amvrakikos gulf, greece. *Estuarine, Coastal and Shelf Science*, 88(4):473 – 481, 2010.

[24] O. Fredin, B. Bergstrøm, R. Eilertsen, L. Hansen, O. Longva, A. Nesje, and H. Sveian. Glacial landforms and Quaternary landscape development in Norway. *Quaternary Geology of Norway Geological Survey of Norway Special Publication*, 13:5–25, 2013.

[25] M. Gonçalves, E. Rusu, and C. Soares. Evaluation of the wave models SWAN and STWAVE in shallow water using nested schemes. *Maritime Engineering and Technology*, (January):481–485, 2012.

[26] W. Group. The WAM ModelA Third Generation Ocean Wave Prediction Model. *Journal of Physical Oceanography*, 18(12):1775–1810, dec 1988.

[27] A. Harten. High resolution schemes for hyperbolic conservation laws. *Journal of computational physics*, 49(3):357–393, 1983.

[28] A. Harten, B. Engquist, S. Osher, and S. R. Chakravarthy. Uniformly high order accurate essentially non-oscillatory schemes, iii. In *Upwind and high-resolution schemes*, pages 218–290. Springer, 1987.

[29] K. Hasselmann, T. P. Barnett, E. Bouws, H. Carlson, D. E. Cartwright, K. Enke, J. A. Ewing, H. Gienapp, D. E. Hasselmann, P. Kruseman, A. Meerburg, P. Muller, D. J. Olbers, K. Richter, W. Sell, and H. Walden. Measurements of Wind-Wave Growth and Swell Decay during the Joint North Sea Wave Project (JONSWAP). *Ergnzungsheft zur Deutschen Hydrographischen Zeitschrift Reihe*, A(8)(8 0):p.95, 1973.

[30] S. Hasselmann, K. Hasselmann, J. Allender, and T. Barnett. Computations and parameterizations of the nonlinear energy transfer in a gravity-wave specturm. part ii: Parameterizations of the nonlinear energy transfer for application in wave models. *Journal of Physical Oceanography*, 15(11):1378–1391, 1985.

[31] C. W. Hirt and B. D. Nichols. Volume of fluid (vof) method for the dynamics of free boundaries. *Journal of computational physics*, 39(1):201–225, 1981.

[32] J. A. Howe, W. E. Austin, M. Forwick, M. Paetzel, R. Harland, and A. G. Cage. Fjord systems and archives: a review. *Geological Society, London, Special Publications*, 344(1):5–15, 2010.

[33] J. Jakacki, A. Przyborska, S. Kosecki, A. Sundfjord, and J. Albretsen. Modelling of the Svalbard fjord Hornsund. *Oceanologia*, 59(4):473–495, oct 2017.

[34] A. Jeschke, G. K. Pedersen, S. Vater, and J. Behrens. Depth-averaged non-hydrostatic extension for shallow water equations with quadratic vertical pressure profile: equivalence to Boussinesq-type equations. *International Journal for Numerical Methods in Fluids*, 84(10):569–583, 2017.

[35] A. Kamath. *CFD based Investigation of Wave-Structure Interaction and Hydrodynamics of an Oscillating Water Column Device*. PhD thesis, 2015.

[36] A. Kamath, M. Alagan Chella, H. Bihs, and Ø. A. Arntsen. Energy transfer due to shoaling and decomposition of breaking and non-breaking waves over a submerged bar. *Engineering Applications of Computational Fluid Mechanics*, 11(1):450–466, jan 2017.

[37] A. Kamath, H. Bihs, M. Alagan Chella, and Ø. A. Arntsen. Upstream-cylinder and downstream-cylinder influence on the hydrodynamics of a four-cylinder group. *Journal of Waterway, Port, Coastal, and Ocean Engineering*, 142(4):04016002, 2016.

[38] A. Kamath, H. Bihs, M. A. Alagan Chella, and Ø. A. Arntsen. Cfd simulations of wave propagation and shoaling over a submerged bar. *Aquatic Procedia*, 4:308–316, 2015.

[39] J. T. Kirby. Chapter 1 Boussinesq models and applications to nearshore wave propagation, surf zone processes and wave-induced currents, 2003.

[40] J. M. Klinck, J. J. O'Brien, and H. Svendsen. A Simple Model of Fjord and Coastal Circulation Interaction. *Journal of Physical Oceanography*, 11(12):1612–1626, 1981.

[41] H. E. Krogstad and Ø. A. Arntsen. LINEAR WAVE THEORY Part A: Regular waves. Technical Report February, 2000.

[42] J. Larsen and H. Dancy. Open boundaries in short wave simulationsa new approach. *Coastal Engineering*, 7(3):285–297, 1983.

[43] M. A. Maâtoug and M. Ayadi. Numerical simulation of the second-order Stokes theory using finite difference method. *Alexandria Engineering Journal*, 55(3):3005–3013, 2016.

[44] P. A. Madsen and O. R. Sørensen. A new form of the boussinesq equations with improved linear dispersion characteristics. part 2. a slowly-varying bathymetry. *Coastal engineering*, 18(3-4):183–204, 1992.

[45] P. J. Martínez-Ferrer, L. Qian, Z. Ma, D. M. Causon, and C. G. Mingham. Improved numerical wave generation for modelling ocean and coastal engineering problems. 2018.

[46] T. C. Massey, M. E. Anderson, J. M. Smith, J. Gomez, and R. Jones. STWAVE : Steady-State Spectral Wave Model User ' s Manual for STWAVE , Version 6.0. Technical Report September, 2011.

[47] J. W. Miles. Hamiltonian formulations for surface waves. *Applied Scientific Research*, 37(1-2):103–110, 1981.

[48] W. H. MUNK. THE SOLITARY WAVE THEORY AND ITS APPLICATION TO SURF PROBLEMS. *Annals of the New York Academy of Sciences*, 51(3):376–424, may 1949.

[49] W. H. Munk and M. A. Traylor. Refraction of ocean waves: a process linking underwater topography to beach erosion. *The Journal of Geology*, 55(1):1–26, 1947.

[50] L. Olsen, O. Fredin, and O. Olesen. Quaternary geology of norway. 2013.

[51] M. C. Ong, A. Kamath, H. Bihs, and M. S. Afzal. Numerical simulation of free-surface waves past two semi-submerged horizontal circular cylinders in tandem. *Marine Structures*, 52:1–14, 2017.

[52] R. Padilla-Hernández. Numerical modelling of wind wave energy dissipation at the bottom including ambient currents. *PhD Katholieke Universiteit Leuven*, 2002.

[53] O. M. Phillips. The Equilibrium Range in the Spectrum of Wind Generated Waves. *Journal of Fluid Mechanics*, 4(4):426–434, 1958.

[54] W. J. Pierson and W. Marks. The power spectrum analysis of ocean-wave records. *Transactions, American Geophysical Union*, 33(6):834, 1952.

[55] A. A. Pires-Silva, J. Monbaliu, O. Makarynskyy, C. Ventura-Soares, and E. Coelho. WAM/SWAN Simulations in an open coast: Comparisons with ADCP measurements. In *Littoral 2002, The Changing Coast. EUROCOAST / EUCC, Porto Portugal Ed. EUROCOAST Portugal, ISBN 972-8558-09-0*, pages 169–173, 2002.

[56] R. C. Ris, L. H. Holthuijsen, and N. Booij. A third-generation wave model for coastal regions: Verification. *Journal of Geophysical Research*, 104:7667, 1999.

[57] W. E. Rogers, J. M. Kaihatu, L. Hsu, R. E. Jensen, J. D. Dykes, and K. T. Holland. Forecasting and hindcasting waves with the SWAN model in the Southern California Bight. *Coastal Engineering*, 54(1):1–15, 2007.

[58] J. S. Russell. Report on waves. In *14th meeting of the British Association for the Advancement of Science*, volume 311, page 1844, 1844.

[59] O. Saelen. Temperature variations and heat transport in the Nordfjord. 1947.

[60] R. G. Sargent. Verification and validation of simulation models. *Journal of Simulation*, 7(1):12–24, feb 2013.

[61] C.-W. Shu and S. Osher. Efficient implementation of essentially non-oscillatory shock-capturing schemes. *Journal of computational physics*, 77(2):439–471, 1988.

[62] L. Skjerbreia and J. Hendrickson. Fifth order gravity wave theory. *Wave theory*, 1(7):184–196, 1960.

[63] M. D. Skogen, M. Eknes, L. C. Asplin, and A. D. Sandvik. Modelling the environmental effects of fish farming in a norwegian fjord. *Aquaculture*, 298(1-2):70–75, 2009.

[64] J. M. Smith, A. R. Sherlock, and D. T. Resio. STWAVE : Steady-State Spectral Wave Model User 's Manual for STWAVE , Version 3.0, 2001.

[65] J. Sodja. Turbulence models in CFD. (March), 2007.

[66] A. Stigebrandt. Hydrodynamics and circulation of fjords. In *Encyclopedia of lakes and reservoirs*, pages 327–344. Springer, 2012.

[67] J. E. Stopa, F. Ardhuin, A. Babanin, and S. Zieger. Comparison and validation of physical wave parameterizations in spectral wave models. *Ocean Modelling*, 103:2–17, 2015.

[68] H. U. Sverdrup and W. H. Munk. Empirical and theoretical relations between wind, sea, and swell. *Eos, Transactions American Geophysical Union*, 27(6):823–827, 1946.

[69] S. team et al. Swan user manual. *Delft University of Technology. The Netherlands*, 2007.

[70] T. J. Thomas and G. Dwarakish. Numerical Wave Modelling A Review. *Aquatic Procedia*, 4:443–448, 2015.

[71] D. Vasileska. Poisson equation solvers. 2010.

[72] W. Wang, H. Bihs, A. Kamath, and Ø. Arntsen. Large Scale Cfd Modelling of Wave Propagation in Sulafjord for the E39 Project. In *9th National Conference on Computational Mechanic MekIT'17*, pages 1–13, 2017.

[73] M. Wary, F. Eynaud, L. Rossignol, J. Lapuyade, M.-C. Gasparotto, L. Londeix, B. Malaizé, M.-H. Castéra, and K. Charlier. Norwegian sea warm pulses during dansgaard-oeschger stadials: Zooming in on these anomalies over the 35–41 ka cal bp interval and their impacts on proximal european ice-sheet dynamics. *Quaternary Science Reviews*, 151:255–272, 2016.

[74] Y. Yamazaki, Z. Kowalik, and K. F. Cheung. Depth-integrated, non-hydrostatic model for wave breaking and run-up. *International Journal for Numerical Methods in Fluids*, 61(5):473–497, oct 2009.

[75] M. Zabihi, S. Mazaheri, and A. R. Mazyak. Wave Generation in a Numerical Wave Tank. In *The 17th Marine Industries Conference (MIC2015) 22-25 December2015 Kish Island*, page 11, 2015.

[76] Y. Zerihun. A Non-Hydrostatic Depth-Averaged Model for Hydraulically Steep Free-Surface Flows. *Fluids*, 2(4):49, sep 2017.

[77] M. Zijlema and G. Stelling. Efficient computation of surf zone waves using the nonlinear shallow water equations with non-hydrostatic pressure. *Coastal Engineering*, 55(10):780–790, oct 2008.

[78] M. Zijlema and G. S. Stelling. Further experiences with computing non-hydrostatic free-surface flows involving water waves. *International journal for numerical methods in fluids*, 48(2):169–197, 2005.